

LOW WATER UPTAKE ANION EXCHANGE MEMBRANES UTILIZING POLY(1,1- DIPHENYLETHYLENE-*ALT*-BUTADIENE) BACKBONES

Musashi Briem

Submitted in Partial Fulfillment of the Requirements
for the Degree of

DOCTOR OF PHILOSOPHY

Approved by:

Dr. Sangwoo Lee, Chair

Dr. Chulsung Bae

Dr. Georges Belfort

Dr. Chaitanya Ullal



Department of Chemical and Biological Engineering
Rensselaer Polytechnic Institute
Troy, New York

[December 2022]
Submitted October 2022

© Copyright 2022
By
Musashi Briem
All Rights Reserved

Table of Contents

Table of Contents	iii
List of Tables	vi
List of Figures	vii
Acknowledgements	xii
Abstract	xiv
1. Introduction	1
1.1 Polymers and Polymer Systems	1
1.1.1 Introduction to Polymers	1
1.1.2 Homopolymer Blends	2
1.1.3 Functional Polymers	4
1.2 Ionomers	4
1.2.1 Ionomer Properties	4
1.2.2 Impact of Small Molecules on Ion-Containing Polymers' Phase Behavior	6
1.3 Swelling	8
1.4 Polymer-Based Ion Exchange Membranes in Fuel Cell Applications	12
1.5 Ion Exchange Membrane Devices for Clean Energy	17
1.6 Donnan Exclusion Effect	19
1.7 Outline of Thesis Research	20
2. Introduction of Experimental Techniques	21
2.1 Introduction	21
2.2 Anionic Polymerization	21
2.3 Hydrogenation	27
2.4 Backbone Cyclization with Intramolecular Friedel-Crafts Cyclization	28
2.5 Acid-Catalyzed Friedel-Crafts Bromoalkylation	29
2.6 Nuclear Magnetic Resonance (NMR)	30
2.7 Size Exclusion Chromatography (SEC)	32
2.8 Differential Scanning Calorimetry (DSC)	34
2.9 Ion Exchange Capacity (IEC)	34
2.10 Ion Conductivity	36
3. Anion Exchange Membranes Based on Poly(1,1-diphenylethylene- <i>alt</i> -butadiene)	38
3.1 Introduction	38
3.2 Experimental Details	39
3.2.1 Materials	39

3.2.2 Potassium Naphthalenide.....	39
3.2.3 Polymerization	40
3.2.4 Selective Hydrogenation	40
3.2.5 Synthesis of Brominating Agent	41
3.2.6 Acid-Catalyzed Friedel-Crafts Bromoalkylation of DPE/E and PS.....	41
3.2.7 Homogeneous Quaternization.....	42
3.2.8 Size Exclusion Chromatography (SEC).....	42
3.2.9 ¹ H Nuclear Magnetic Resonance (¹ H NMR).....	43
3.2.10 Differential Scanning Calorimetry	43
3.2.11 Ion Exchange Capacity (IEC) Measurements	43
3.2.12 Chloride Conductivity Measurements.....	43
3.2.13 Chloride Water Uptake	43
3.2.14 Hydroxide Counterion Exchange.....	44
3.2.15 Hydroxide Water Uptake	44
3.2.16 Hydroxide Conductivity.....	45
3.3. Results.....	45
3.3.1 Polymerization of Poly(1,1-diphenylethylene- <i>alt</i> -butadiene).....	45
3.3.2 Selective Hydrogenation of Poly(1,1-diphenylethylene- <i>alt</i> -butadiene).....	47
3.3.3 Acid Catalyzed Friedel-Crafts Bromoalkylation	48
3.3.4 Quaternization.....	56
3.3.5 Film Casting.....	57
3.3.6 Differential Scanning Calorimetry.....	58
3.3.7 Conductivity.....	60
3.3.8 Water Uptake	69
3.4 Conclusions.....	74
4. Cyclized Poly(1,1-diphenylethylene- <i>alt</i> -butadiene) with Glass Transition Temperature Above 200°C	76
4.1 Introduction.....	76
4.2. Experimental Details.....	79
4.2.1 Materials	79
4.2.2 Potassium Naphthalenide	79
4.2.3 Polymerization	79
4.2.4 Cyclization of DPE/B.....	80
4.2.5 Synthesis of Brominating Agent	81
4.2.6 Acid-Catalyzed Friedel-Crafts Bromoalkylation of DPE/B-C.....	81
4.2.7 Homogeneous Quaternization.....	82

4.2.8 Size Exclusion Chromatography (SEC).....	82
4.2.9 ¹ H Nuclear Magnetic Resonance (¹ H NMR).....	82
4.2.10 Differential Scanning Calorimetry.....	83
4.2.11 Ion Exchange Capacity (IEC) Measurements.....	83
4.2.12 Chloride Conductivity Measurements.....	83
4.2.13 Chloride Water Uptake.....	83
4.2.14 Hydroxide Counterion Exchange.....	83
4.2.15 Hydroxide Water Uptake.....	84
4.2.16 Hydroxide Conductivity.....	84
4.2.17 Mechanical Testing.....	85
4.3 Results.....	85
4.3.1 Cyclization of Poly(1,1-diphenylethylene- <i>alt</i> -butadiene).....	85
4.3.2 Acid Catalyzed Friedel-Crafts Bromoalkylation.....	94
4.3.3 Quaternization.....	96
4.3.4 Film Casting.....	97
4.3.5 Differential Scanning Calorimetry.....	98
4.3.6 Conductivity.....	100
4.3.7 Water Uptake.....	103
4.3.8 Mechanical Strength.....	106
4.4 Conclusions.....	106
5. Thesis Summary.....	108
References.....	110

List of Tables

Table 1. T_g 's of DPE/E-Br at various degree of functionalizations	59
Table 2. T_g 's of PS-Br at various degrees of functionalizations.....	59
Table 3. Cl^- conductivity of DPE/E(QA).....	61
Table 4. Cl^- conductivity of PS(QA).....	61
Table 5. OH^- conductivity of DPE/E(QA).....	66
Table 6. OH^- conductivity of PS(QA).....	66
Table 7. Properties of functionalized DPE/tBS copolymer, adapted from ¹⁵⁸	73
Table 8. Some reaction conditions tested in the optimization of the cyclization of DPE/B. Run DPE/B-028 was diluted with trifluoroacetic acid to reach a Hammett acidity function of -11.3, detailed in section 4.2.4., and was ultimately used as the optimized procedure.	90
Table 9. T_g 's of DPE/B-C-Br at various degree of functionalizations	98
Table 10. Cl^- conductivity of DPE/B-C(QA).....	101

List of Figures

Figure 1. Schematics of PEM and AEM fuel cells.....	14
Figure 2. Global temperature anomaly since 1880, higher positive anomaly means warmer weather. The sharp increase is indicative of a rapidly warming earth. Adapted from ¹²⁸	17
Figure 3. Measurement of historic carbon dioxide levels, showing the immense spike in CO ₂ from recent human activity. Adapted from ¹²⁹	18
Figure 4. Energy production from a solar cell in one day, showing intermittent energy production depending on time of day and weather conditions. Adapted from ¹³⁰	19
Figure 5. Anionic polymerization of polystyrene.	22
Figure 6. Anionic polymerization of polybutadiene in different solvents.	24
Figure 7. Selective hydrogenation of DPE/B backbone, saturating the backbone alkenes while leaving the pendant phenyl groups untouched.....	28
Figure 8. Triflic acid catalyzed intramolecular Friedel-Crafts cyclization of DPE/B.....	29
Figure 9. Friedel-Crafts bromoalkylation of DPE/E and PS, utilizing triflic acid as a Brønsted acid to generate <i>tert</i> -carbocation.	29
Figure 10. a) Polymerization, selective hydrogenation, bromoalkylation, and quaternization of DPE/B. b) Bromoalkylation and quaternization of PS.	46
Figure 11. ¹ H NMR of DPE/B and DPE/E. Selective hydrogenation of DPE/B was confirmed by the lack of alkene peaks (b) and the aromatic peaks (a) remaining.	47
Figure 12. SEC chromatograph of DPE/B and DPE/E, showing no increase in dispersity after selective hydrogenation.	48
Figure 13. ¹ H NMR of DPE/E-Br of varying degrees of functionalization.....	49

Figure 14. Representative ^1H NMR of DPE/E-Br, the arrow points to the peak from the hydrogens on the carbon adjacent to the bromine. The degree of functionalization was determined by the integration of this peak vs. the integration of the aromatic region.	50
Figure 15. Representative SEC chromatogram of DPE/E-Br, showing a shift in the main peak to higher molecular weight as alkyl chains are added and an increase in lower molecular weight chains from unwanted degradation.	51
Figure 16. ^1H NMR of PS-Br of varying degrees of functionalization.	51
Figure 17. Representative ^1H NMR of PS-Br, the arrow points to the peak from the hydrogens on the carbon adjacent to the bromine. The degree of functionalization was determined by the integration of this peak vs. the integration of the aromatic region.	52
Figure 18. SEC chromatogram of PS-Br, showing a shift in the main peak to higher molecular weight as alkyl chains are added.	53
Figure 19. SEC chromatogram of bimodal DPE/E-Br, indicative of two different polymer species being present, a functionalized species and an unfunctionalized species.	54
Figure 20. SEC chromatogram of monomodal DPE/E-Br, indicative of uniform functionalization across all chains.	55
Figure 21. Mechanism of Friedel-Crafts bromoalkylation of DPE/E showing possible degradation mechanism of tertiary carbocation on polymer backbone stabilized by aromatic group.	55
Figure 22. Quaternization of PS-Br and DPE/E-Br.	56
Figure 23. Glass transition temperatures (T_g 's) of PS-Br and DPE/E-Br, showing a decrease in T_g with increasing degree of functionalization.	60
Figure 24. Cl^- conductivity of DPE/E(QA)-IEC.	62
Figure 25. Cl^- conductivity of PS(QA)-IEC.	63
Figure 26. Cl^- conductivity of DPE/E(QA) and PS(QA) at IEC ~ 1.5 meq./g, showing nearly identical conductivity.	64

Figure 27. Cl ⁻ conductivity of DPE/E(QA) and PS(QA) at IEC~2.0 meq./g, PS(QA)-2.08 conductivity drops to 0 mS/cm at high temperature (80°C) while DPE/E(QA)-1.99 maintains conductivity of 40 mS/cm.	65
Figure 28. PS(QA)-2.08 after Cl ⁻ conductivity measurement at 80°C, the film does not maintain its form, is very gel like, and is impossible to collect in one piece.	66
Figure 29. OH ⁻ conductivity of DPE/E(QA) and PS(QA) at IEC~1.5 meq./g, showing no significant differences between the two species.	67
Figure 30. OH ⁻ conductivity of DPE/E(QA) and PS(QA) at IEC~2.0 meq./g, PS(QA)-2.02 conductivity drops to 9 mS/cm at high temperature (80°C) while DPE/E(QA)-1.94 maintains conductivity of 46 mS/cm.	68
Figure 31. PS(QA)-2.02 after OH ⁻ conductivity measurement at 80°C, the film does not maintain its form, is very gel like, and is impossible to collect in one piece.	68
Figure 32. DPE/E(QA)-1.94 after OH ⁻ conductivity measurement at 80°C, the film maintains its form with no noticeable difference after the measurement.	69
Figure 33. Water uptake of DPE/E(QA) and PS(QA) with Cl ⁻ counterion, PS(QA) water uptake increases significantly with IEC while DPE/E(QA) maintains a water uptake of ~15% regardless of IEC.	70
Figure 34. Water uptake of DPE/E(QA) and PS(QA) with OH ⁻ counterion, PS(QA) water uptake increases significantly with IEC while DPE/E(QA) maintains a water uptake of ~50% regardless of IEC.	71
Figure 35. Potential backbone segments of DPE/E(QA) and PS(QA), both segments have functionalization of 50% and 3 consecutive repeat units without functionalization, DPE/E(QA), however has a much longer chain segment between functionalized phenyls.	72
Figure 36. 100% functionalized DPE/tBS(QA), adapted from ¹⁵⁸	74
Figure 37. Various polymers with T_g 's around 200°C.	78
Figure 38. Anionic polymerization of DPE/B, followed by triflic acid catalyzed intramolecular Friedel-Crafts cyclization, Friedel-Crafts bromoalkylation, and quaternization.....	86

Figure 39. ¹ H NMR of DPE/B and DPE/B-C from monodisperse DPE/B, cyclization was determined to have occurred by the loss of the alkene peaks (b) and the broadening of the aromatic region (a and d) and aliphatic region (c).....	87
Figure 40. DSC of DPE/B-C from monodisperse DPE/B, compared to DPE/B.....	88
Figure 41. SEC chromatograms of DPE/B-C from monodisperse DPE/B, showing a shift in the molecular weight peak due to a change in hydrodynamic volume of the polymer backbone as well as an increase in dispersity from an increase in low molecular chains due to degradation.....	89
Figure 42. Cyclization mechanism and possible degradation mechanism of DPE/B. Reaction was optimized to get the cyclized product and avoid chain scission.....	89
Figure 43. ¹ H NMR of DPE/B and DPE/B-C from bimodal DPE/B, the loss of the alkene peaks (b) is indicative of cyclization but the expected broadening of the aromatic region (a and d) is not observed, while there is some broadening of the aliphatic region (c).	91
Figure 44. DSC of DPE/B-C from bimodal DPE/B, compared to DPE/B-C from monodisperse DPE/B-C, showing bimodal DPE/B-C has slightly lower <i>T_g</i>	92
Figure 45. SEC chromatograms of DPE/B-C from monodisperse DPE/B, showing no shift in molecular weight, despite expecting one due to a change in the hydrodynamic volume of the polymer backbone.....	93
Figure 46. ¹ H NMR of the cyclization product of different DPE/B precursors with the same reaction conditions, both precursors saw the disappearance of the alkene peaks (b), monodisperse DPE/B-C gave the expected ¹ H NMR, seen in the broadening of the aromatic region (a and d) and in the aliphatic region (c), while bimodal DPE/B-C did not.	94
Figure 47. SEC chromatogram of bromofunctionalized DPE/B-C, showing an increase in molecular weight from the alkyl chains added as well as an increase in low molecular weight chains due to degradation.....	95
Figure 48. ¹ H NMR of DPE/B-C-Br, the arrow points to the peak from the hydrogens on the carbon adjacent to the bromine. The degree of functionalization was determined by the integration of this peak vs. the integration of the aromatic region.	96

Figure 49. Functionalization mechanism of DPE/B-C, the ability to form a tertiary carbocation stabilized by an aromatic ring allows for easier degradation of the backbone.	96
Figure 50. Quaternization of DPE/B-C-Br.	97
Figure 51. Glass transition temperatures (T_g 's) of DPE/B-C-Br and DPE/E-Br, each decrease with increasing degree of functionalization. DPE/B-C maintains $\sim 100^\circ\text{C}$ higher T_g than its DPE/E counterpart.	99
Figure 52. Example DSC of bromofunctionalized DPE/B-C.	100
Figure 53. Cl^- conductivity of DPE/B-C(QA).	101
Figure 54. Cl^- conductivity of DPE/B-C(QA) and DPE/E(QA) at IEC ~ 1 , showing no significant difference in conductivity.	102
Figure 55. Cl^- conductivity of DPE/B-C(QA) and DPE/E(QA) at IEC ~ 2 , showing no significant difference in conductivity despite an elevated T_g for DPE/B-C(QA)-2.06.	103
Figure 56. Water uptake of DPE/B-C(QA) and DPE/E(QA) in Cl^- form, DPE/B-C(QA) shows a higher water uptake than DPE/E(QA) despite having a higher T_g	104
Figure 57. Water uptake of DPE/B-C(QA), DPE/E(QA), and PS(QA) in Cl^- form, DPE/B-C(QA) shows a higher water uptake than DPE/E(QA) despite having a higher T_g but still has a significantly lower water uptake than PS(QA).	105
Figure 58. DMA characterization of DPE/B-C(QA) and DPE/E(QA) at IEC ~ 2.0 at 50°C and 50% R.H., no significant difference is observed in the mechanical properties with both polymers being brittle.	106

Acknowledgements

I thank my advisors, Dr. Sangwoo Lee and Dr. Chulsung Bae, for their confidence in me to undertake this multidisciplinary project. Thank you for challenging me to think deeper and wider. Thank you for mentoring me through the ups and downs of the Ph.D. program. Thank you for your patience when I needed it. Thank you for all your help in my journey to hone my skills as a researcher and growing as a person throughout that journey.

Thank you to my committee members, Dr. Geroges Belfort and Dr. Chaitanya Ullal, for their support and for taking the time to offer advice on my thesis work.

I would not have made it to this point without the help, support, and friendship of my colleagues, both past and present. From both the Bae Group and the Lee Group: Dr. Gagan Kangovi, Dr. Liwen Chen, Dr. Sungmin Park, Dr. Carrie Trant, Dr. Toluwanimi Bello, Erik Zimmerman, Juhong Ahn, Melissa Nelson, Henry Hua, Seungbae Jeon, Dr. Stefan Turan, Dr. Junyoung Han, Dr. Sangtaik Noh, Dr. Kihyun Kim, Dr. Asheesh Singh, Dr. Santosh Adhikari, Dr. Gregory Kline, Dr. Jong Yeob (Jay) Jeon, Dr. Ding Tian, Dr. Xiaofeng Wang, Dr. Heemin Park, Dr. Joseph Jang, Dr. Mike Pagels, Dr. Chandula Walgama, Dr. Pothana Gandhi Nallepalli, Zongwei Ma, Sariah Marth, Linda Cortes, and Natalie Fifield. Thank you for your perspectives, collaboration, and friendship. I truly would not have been able to succeed without you.

Thank you to my funding sources: RPI Isermann Fellowship and NSF PIRE. Thank you to RPI's Center for Materials, Devices, and Integrated Systems (cMDIS) and Polymer Center.

Thank you to William Flaherty, Ken Beckley, Dr. Scott McCallum, Sandra Annan, Marylouise Dowd, Lisa McGill, Lisa Martin, Sharon Gardner, Yasin Brown, Jeffery Raway, and Blake Cimo. None of this would have been possible without your hard work.

Finally, thank you to my family. A lifetime of support from my parents, Karl and Kimie Briem, and my brother, Shingen. Having you in my corner makes anything possible. Thank you to Erin Steele, life with you was truly special and I wish you nothing but the best in your next chapter. Thank you to Rebecca Maggiano for years of friendship. Finally, thank you to Cameron Boyd and Tré Cooper for always having my back since day one.

Abstract

This research seeks to explore the relationship between polymer backbone composition, water uptake, and conductivity to contribute to the development of high-performance, yet inexpensive, ion exchange membranes. The goal of the projects described, including future work, is to work towards a structure-property understanding that enables the design of ionomers which self-assemble hydrated ion-conducting channels. Any such materials must also have good mechanical integrity, as well as properties that prevent excessive swelling from water uptake, which is known to lead to the failure of membrane materials. This will enable electrochemical energy devices, such as fuel cells and electrolyzers, that utilize ion-transporting membranes to become more economically viable routes for the production of cleaner and more sustainable energy.

In this work, novel polymer backbones were designed, synthesized by anionic polymerization, functionalized by the post-polymerization addition of alkyl side chains with terminal ionic groups, and characterized as anion exchange membranes. Characterization techniques included differential scanning calorimetry, ion conductivity, and water uptake.

In the first project, the backbone investigated was poly(1,1-diphenylethylene-*alt*-butadiene) (DPE/B). The bulky DPE monomer cannot self-polymerize, which lends itself to the precisely tailored synthesis of alternating copolymer backbones. The DPE/B alternating copolymer was selectively hydrogenated to saturate the polymer backbone (DPE/E), then functionalized *via* an acid-catalyzed Friedel-Crafts reaction to attach alkyl side chains containing bromofunctional groups for subsequent quaternization. The anion exchange membrane properties, including ion conductivity and water uptake, of the quaternized polymer was then compared to

quaternized polystyrene controls of similar ion content for a baseline comparison to a well-known and used polymer for anion exchange membranes.

Additionally, the DPE/B polymer was cyclized *via* an acid-catalyzed Friedel-Crafts reaction to increase the glass transition of the precursor polymer backbone. The cyclized DPE/B (DPE/B-C) had a glass transition temperature of 205°C, up from 103°C for DPE/E. Benefits of the increased glass transition temperature of the polymer backbone are explored.

1. Introduction

1.1 Polymers and Polymer Systems

Much in the same way that stone, iron, and bronze were defining materials of their respective ages, polymers are a defining material of our current age. Polymers have a high strength to weight ratio, are easy to process, are cost efficient, and are tunable, making them useful as either stand-alone materials or as additives or composites with existing materials. Polymer applications are ubiquitous: plastic packaging, synthetic clothing fabrics, coating for non-stick pans, adhesives, rubber tires, medical devices, functional biomaterials, fuel cells, airplanes, and countless other uses.¹⁻⁶ Plastic production has seen an astronomical 20,000% increase globally since 1950, increasing from 2 million metric tons to nearly 400 million tons in 2015.⁷⁻⁸ In this time, six polymers have separated themselves from the pack, accounting for nearly 90% of all the plastics synthesized: polyethylene (PE), polyethylene terephthalate (PET), polypropylene (PP), polystyrene (PS), polyurethane (PUR), and polyvinylchloride (PVC).⁸ Polymers, with their myriad of unique characteristics, are easily utilized as advanced materials, as they can be functionalized and tailored for specific applications.

1.1.1 Introduction to Polymers

Polymers are large molecules comprised over 1,000 repeat units (monomers) covalently bonded together. Like proteins, polymers are categorized as macromolecules and have lengths on the order of micrometers.¹ The degree of polymerization (N) is the number of repeat units within a polymer and is defined as the ratio of the polymer's molecular weight (M) to the individual monomer's molecular weight (M_0):

$$N = \frac{M}{M_0} \quad (1.1)$$

Two attributes of polymers are used to characterize them, the average molecular weight (M) and dispersity (\mathcal{D}). The average molecular weight can be found a number of ways; two common ways are number-averaged molecular weight (M_n) and weight-averaged molecular weight (M_w), and the dispersity is the distribution of molecular weights and is defined as $\mathcal{D} = M_w/M_n$. The polymerization reaction dictates the dispersity; lower dispersities, $\mathcal{D} < 1.1$, are possible with living anionic polymerization, whereas other polymerization reactions like condensation and free-radical polymerizations (statistical polymerizations), lead to higher dispersities, $\mathcal{D} > 2$.^{1,9}

A material's phase behavior, the temperatures at which it is a solid and temperatures at which it is a fluid (liquid or gas), dictates its use cases. Due to their large size, polymers do not have a gas phase. The temperature at which a polymer undergoes solid to liquid phase transition is called the glass transition temperature (T_g) and dictates how polymers are used and processed. Above its T_g , the polymer is rubbery; the polymer has the kinetic energy needed for the chains to flow, a liquid state. Below its T_g , the polymer is glassy; chains are kinetically trapped and the polymer does not flow over observable time scales, a solid state. In this glassy solid state, the polymer is an amorphous solid that looks like a liquid in terms of molecular organization due to its lack of long-range order. For use as a solid, a polymer should be below its T_g ; above its T_g , a polymer can be processed as a liquid.¹ Many factors affect a polymer's T_g , but the monomers in a given polymer have the most direct impact. Linear 1,4-polybutadiene is a rubber at room temperature with a T_g of -107°C , but polystyrene, with its pendant phenyl groups, is a glass at room temperature with a T_g of 100°C .¹⁰

1.1.2 Homopolymer Blends

Tough materials, materials that hold their shape but are also elastic enough to resist brittle fracture, are desired in many polymer applications.¹¹ However, these properties often come at the

expense of the other; increasing a material's strength at break often hurts its elasticity, leaving a material that is stronger, yet more brittle.¹² By blending homopolymers, polymer properties can be modulated and tuned. Blending a soft and elastic polymer with a brittle but stiff polymer can yield a final product that is tougher than the individual starting materials but less brittle.¹²

A balance between the enthalpic drive to phase separate and the entropic drive to mix drives a blend of homopolymers to an equilibrium, whether the components be mixed (one phase) or unmixed (phase separated). This balance is represented by the Gibbs free energy; for a binary mixture of two polymers, the free energy of mixing can be written as:¹

$$\Delta G_m = kT \left[\frac{\phi_A}{N_A} \ln \phi_A + \frac{\phi_B}{N_B} \ln \phi_B + \chi \phi_A \phi_B \right] \quad (1.2)$$

Where χ is the Flory-Huggins interaction parameter, N is the degree of polymerization, and ϕ is the volume fraction for polymers A and B, respectively. The Flory-Huggins interaction parameter is a temperature dependent empirical measure of the relative incompatibility of the components:^{1, 13}

$$\chi = \frac{\alpha}{T} + \beta \quad (1.3)$$

Where α and β are constants and $\alpha > 0$. The first two terms of the Gibbs free energy equation are entropic while the third term is enthalpic. Phase separation is favored by lowering T, which increases χ , and by increasing N , which decreases the entropic contribution to the free energy. Polymers generally have large N , as molecular weights are typically between 10^3 - 10^7 g/mol, leading to very small entropy of mixing contribution due to the $1/N$ dependence.¹ This reveals a fundamental problems when blending two homopolymers: there is a strong driving force for them to macrophase separate, like oil and water.¹⁴⁻¹⁵ This drive to macrophase separate is extremely

useful for some applications, including risers and down-hole plugs in the oil industry, but can be detrimental for others, including ion exchange membranes.¹⁶⁻¹⁷

1.1.3 Functional Polymers

To obtain unique properties, polymers can be synthesized with functional groups, either by polymerizing monomers with functional groups to make a functionalized polymer backbone or post polymerization functionalization to attach functional groups to a polymer.¹⁸⁻²⁰ Functionalized monomer polymerization is frequently hampered by the functional groups: increased steric hindrance from the functional group inhibiting polymerization, reduced activity of the polymerization reaction due to electron withdrawing effect from functional groups, or the functional groups participating in side reactions.²¹ Post-polymerization functionalization adds a synthetic step, but it avoids those pitfalls of functionalized monomers, expanding the types of functionality possible.^{18, 20} Post-polymerization functionalization requires ready sites for functionalizing; pendant aromatic rings provide ready sites. Polystyrene is an excellent polymer for post-polymerization functionalization; it has a saturated hydrocarbon backbone that is resistant to chemical scission during post-polymerization functionalization.²² Functionalized polymers have a variety of uses, including ion exchange membranes.²³

1.2 Ionomers

1.2.1 Ionomer Properties

Low dielectric constant polymers functionalized with a covalently bonded ionic group are known as ionomers.²⁴⁻²⁵ Only a small quantity of ionic groups, approximately 10%, is needed to greatly alter the physical properties of a polymer, as hydrogen bonding between acid groups or dipole-dipole interactions between salt neutralized acid groups form physical crosslinks that greatly improves the toughness of a polymer.²⁴ Ionic crosslinks are thermally reversible, unlike

chemical crosslinks; the thermal reversibility preserves the melt-processability of the polymer.²⁶ The ionic crosslinking in ionomers is comparable to physical crosslinking of block copolymers.²⁷

The Eisenberg-Hird-Moore model describes ionomers: within ionomer materials, ions aggregate, often forming “multiplets” of four or more ion groups within the bulk media of lower dielectric constant.²⁸ The strength of electrostatic interactions between ion pairs must be strong enough to overcome elastic forces of the non-ionic polymer chains that they are tethered to in order to form multiplets. With high enough ion content, ion rich clusters can form, resulting in aggregated regions where the mobility of polymer chains is restricted, causing these regions to have different phase behavior than the bulk material.²⁸⁻²⁹ Clustering is contingent on reaching a critical ion concentration, which depends on the molecular weights of the polymers and the distribution, evenly spaced or concentrated near one another, of ions along the polymer backbone chain.²⁸⁻²⁹ If clustering behavior is not observed in an ionomer, either multiplets do not form, or multiplets form but are too spaced out to form a cluster region (> 2 persistence lengths apart), or the multiplets are unstable and dissociate at the matrix T_g , or the ion content is high enough for the entire material to exhibit clustered behavior at the expense of the bulk.^{25, 29}

Polymer electrolytes, or polyelectrolytes, are ionomers that are highly functionalized, approaching one charged species per monomer repeat unit. Although the transition from an ionomer to a polyelectrolyte is murky, but the properties on either side of the transition are vastly different.³⁰ Ions are dissociated in polymer electrolytes, forming a continuous medium where electronic interactions span distances longer than the polymer chains.³⁰ Dissociated counter ions move, transporting charge, through the solid polyelectrolyte.^{24, 31} Higher ion conductivity is attained by soft, rubbery polymers, since ion transport through polyelectrolytes is facilitated by the segmental motion of polymer chains.³²⁻³⁴ Unlike ionomers, polymer electrolytes are usually

unable to be melt processed due to the high ion content and ionic aggregation; instead polyelectrolytes are processed in solution.³⁰

Polymer electrolytes may contain a low-molecular weight solvent, like water, to solvate ions; this boosts the conductivity of the mobile ions and allows ionic polymers with low ion content to function as polyelectrolytes.²⁴ An example of ionic polymers functioning as polyelectrolytes with the help of a low-molecular weight solvent is ion exchange membranes, discussed in depth in a following section.

1.2.2 Impact of Small Molecules on Ion-Containing Polymers' Phase Behavior

Ion containing polymers used for ion exchange membrane applications contend with the presence of small molecules. Fuel cells, a specific application of ion exchange membranes discussed in detail later, have these small molecules in water and fuels. Water is an unavoidable component of the fuel cell system, as it is a byproduct of the chemical reaction of fuel cells.³⁵

Water is required for effective ion transport in most ion exchange membranes, as ion conductivity is facilitated by water adsorbed to acid or base functional groups that forms a continuous network of hydrated channels through which ions can easily travel.³⁶⁻³⁷ Due to this, hydrated polymer electrolytes have much higher conductivity than dry polymer electrolytes.³¹ Increasing water uptake correlates to increasing conductivity, up to a point, after which increasing water uptake does not further increase conductivity.³⁸⁻³⁹

Ion exchange membranes can only contain continuous water channels, rather than mere ion aggregates, if there are enough ion functional groups in said membrane and sufficient water to hydrate channels; there is a critical transition point known as the percolation threshold.⁴⁰ Nafion and other proton exchange membranes exhibited a positive correlation between temperature and

conductivity, in addition to a positive correlation between the number of water molecules per ion in the membrane, known as the hydration number, and the self-diffusion coefficient and, more importantly, conductivity.⁴¹⁻⁴² In Nafion's case, low activation energy for ion movement by diffusion and large self-diffusion coefficients for the ions are symptomatic of efficient ion transport.⁴³ This is attributable to the amount of water present in the channels. Water uptake into Nafion is promoted by hydrophilic cations, like H^+ , which further expands hydrated ion conducting channels, which lessens the resistance to ion conductivity.⁴⁴

Nafion's well-defined phase separation is attributable to the large hydrophilic/hydrophobic difference between its phases. Nafion's backbone is perfluorinated and extremely hydrophobic; its sulfonic acid functional groups are extremely hydrophilic. These differences lead to the self-assembly of strongly segregated phases.³⁷ When Nafion phase separates, a well-connected, bicontinuous phase is formed from the hydrophilic domain and provides a continuous network of water channels which allows protons facile movement with minimal resistance.³⁷

It is important to understand the mechanism driving water uptake, as well as water uptake's effect of conductivity and dimensional swelling. Membranes that swell excessively with water are highly undesirable in fuel cells, because the shrink-swell dimensional changes can deplete the membrane and cause failure.⁴⁵ Furthermore, when a minimum level of humidification is necessary to prevent membranes from drying out and losing conductivity, humidification is required in fuel cell fuel streams, which add costs and complexity.⁴⁶

Ion exchange membranes in fuel cells should allow low or preferably no fuel crossover, fuel being the feeds for the electricity producing electrochemical reactions, as unreacted fuels that crossover do not contribute to the production of useful electrical work.⁴⁷⁻⁴⁸ Furthermore, gas crossover leads to the formation of hydrogen peroxide and oxygen radicals, contributing to

membrane deterioration.⁴⁹ Methanol and other polar organics considered for fuels are hydrophilic and are transported through hydrated channels by diffusion; thus high water uptake and wide hydrated channels can lead to increased fuel crossover and be detrimental to membrane performance.^{47, 50-51} Fuel crossover can be reduced with narrower water channels, due to their increased electroosmotic drag, that is, their reduced diffusion transport coefficients.^{37, 44}

1.3 Swelling

A careful balance must be struck between enough water uptake to boost ion conductivity and not too much water uptake to diminish the physical properties of an ion-exchange membrane. Physical properties of ion-exchange membranes are diminished with too much water uptake, as adsorbed water has a plasticizing effect, which softens the ionomer domain.⁵²⁻⁵³ When a polymer membrane becomes too soft, it can begin to creep. Severe dimensional swelling from excessive water uptake compromises a membrane's mechanical integrity.^{45, 54-57}

Polymer gels, that is, crosslinked, rubbery polymer networks known for imbibing and retaining significant amount of solvent, may hold the key to understanding the relationship between water uptake, dimensional swelling, and mechanical properties of ion-exchange membranes.^{1, 58-59} Understanding the thermodynamics of gel swelling and the implications of the reduced modulus of a plasticized, or solvent-swollen, gel gives a reference point for evaluating these phenomena in ion-exchange membranes, despite the fact that the thermodynamics of gel swelling by the Flory-Rehner theory is not directly applicable to polyelectrolyte gels; in the Flory-Rehner theory, rubbery polymers form a covalent network with well-defined junction points from chemical crosslinks, but in polyelectrolyte gels, glassy polymer backbones have physical crosslinks from microscopic glassy domains.^{1, 59}

The balance of a polymer network's elasticity and a chemical potential gradient that drives solvent uptake governs the amount of solvent taken up by a polymer network and the equilibrium volume of a gel. A polymer network's elasticity limits the stretching of polymer chains. Solvent is driven to enter the network, due to the favorable mixing entropy to dilute the polymer chains with a compatible solvent, like water with a hydrophilic polymer, and the concentration gradient in polyelectrolytes created by the fixed charges covalently bonded to the polymer.^{1, 59-61}

The Gibbs free energy of a liquid is given by:

$$dG = -SdT + VdP + \mu dN \quad (1.4)$$

Where G is the Gibbs free energy, S is the entropy, T is the temperature, V is the volume, P is the pressure, μ is the chemical potential and N is the number of particles in the fluid.⁵⁹

The polymer network is semi-permeable in a polymer gel system, that is, solvent can enter or egress the polymer network. With the assumption that the solvent-swollen polymer gel is in temperature, pressure, and chemical equilibria in a bath of excess solvent, the chemical potential of the solvent in the gel, $\mu(T, P)$, equals the chemical potential of the bulk solvent, $\mu_0(T, P)$, plus the chemical potential contribution from interacting with the polymer network, $\Delta\mu$.⁵⁹

$$\mu(T, P) = \mu_0(T, P) + \Delta\mu \quad (1.5)$$

Equilibrium occurs when the osmotic pressure (Π) within the swollen polymer, which comes about from the uptake of solvent, balances the chemical potential imbalance resulting from the concentration gradient:⁵⁹

$$\mu(T, P + \Pi) = \mu_0(T, P) \quad (1.6)$$

Polymer chains, when stretched, experience a reduction in conformational entropy, like springs. The elasticity of a rubber results from the favorable restoring force experienced by chain relaxation. In a polymer network, the restoring force is proportional to the elastic shear modulus (G'), which is dependent on the crosslink density:^{1,53}

$$G' = \frac{k_B T}{N\nu} \quad (1.7)$$

Where k_B is the Boltzmann constant, T is temperature, N is the number of monomers between crosslinks, and ν is the molecular volume of the solvent.^{1,53}

The volume fraction, ϕ , where $\phi = 1$ for pure polymer network and $\phi = 0$ for a pure solvent, of the polymer decreases when a network is swollen by a solvent. This decreases the tensile stress experienced by the network as well as the elastic shear modulus of a gel as, for an ‘ideal’ non-deformed network case, such:^{1,53}

$$G' = \frac{k_B T}{N\nu} (\phi^{1/3}) \quad (1.8)$$

Finding the equilibrium solvation state of a polyelectrolyte gel is complicated by the covalently bonded charges and their counterions.

A one-dimensional bead-spring model is helpful to envision; a polyelectrolyte can be visualized as a single chain where charged “beads” are connected by Hookian springs.⁶⁰ The elasticity of the polymer network act as the “springs” that resists stretching that counters the Coulombic repulsion between the like-charged “beads”, which is mediated by the associated counterions and the solvent.⁶⁰ This model describes the free energy, g , per “bead”, in units of thermal energy $k_B T$:

$$g = \frac{1}{2} ab^2 - \frac{l_B}{b} \ln(1 - e^{-\kappa b}) \quad (1.9)$$

The first term is the mechanical spring energy, where a is the spring constant and b is the spring length, or the distance between charges. The second term is the electrostatic free energy, which includes how the repulsion between the “bead” ions can be altered by the solvating solvent, the charge of the ion, and the temperature. The Bjerrum length, l_B , is the distance between two charges at which the electrostatic interaction between the charges is equal to the thermal energy $k_B T$.⁶⁰

$$l_B = \frac{e^2}{4\pi\epsilon_0\epsilon k_B T} \quad (1.10)$$

Where e is the charge of the “bead” ion, ϵ_0 is the permittivity of a vacuum, ϵ is the temperature-dependent dielectric constant of the solvent, k_B is the Boltzmann constant, and T is the temperature. The inverse Debye screening length, κ , describes the radius of influence of a charge:⁶⁰

$$\kappa^2 = 4\pi l_B \sum_i c_i z_i^2 \quad (1.11)$$

Where c_i is the bulk ion concentration, the number of ions per volume, and z_i is the valence of the ion, for ion species i .⁶⁰

The importance of the local chemical environment on the overall swelling of a polymer gel is highlighted by the bead-spring model. The swelling of polyelectrolyte gels changes as a function of salt concentration, polymer crosslink density, polymer backbone hydrophobicity (χ) and the ionizability of the charge pairs.⁵³

Relative humidity and temperature are typically cited as the parameters that drive water uptake and ion conductivity in ionomer membranes. This approach fails to recognize the role of

the membrane itself in resisting swelling. Investigating the thermodynamic drivers behind water uptake shows that the hydration of Nafion can be described by:⁶²

$$\lambda = \lambda^L + \lambda^O \quad (1.12)$$

Where λ^L is the hydration of an ionic group by the thermodynamically-favored, exothermic solvation of an ionic species, and λ^O is the entropy driven hydration by osmosis. The heat of hydration, temperature, relative humidity, and internal pressure all contribute to λ^L . The internal pressure and relative humidity are the primary contributors to λ^O , with a small contribution from temperature.⁶² At low relative humidities, the hydration of Nafion decreases with increasing temperature, at 65% relative humidity, hydration is virtually independent of temperature, and at high relative humidities, hydration increases with temperature due to osmosis.⁶²

Some gel systems, with changing temperature or solvent character, exhibit a phase transition characterized by a discontinuous change in volume, known as gel collapse, where the gel spontaneously phase separates to a two phase system, a polymer-rich and a solvent-rich phase, from a homogeneous one phase system.⁶³⁻⁶⁴

1.4 Polymer-Based Ion Exchange Membranes in Fuel Cell Applications

Ion transportation is the critical function of polymer-based ion exchange membranes for electrochemical applications, which include batteries, electrolyzers, and fuel cells.⁶⁵⁻⁶⁹ This section discusses fuel cells as an example of an energy system that utilizes ion-transporting membranes to highlight the importance of this technology as well as point out important design criteria and considerations for ion-transport membranes.

The overall fuel cell device is based on two half reactions separated by a membrane. The two half reactions can only proceed simultaneously when counterions are exchanged through the

ion exchange membrane and electrons flow through an external circuit, which are harnessed to perform electrical work. The solid polymer membrane also acts as the electrolyte, eliminating the need for corrosive working fluids. A perk of fuel cells is that their low operational temperatures can enable quick startup.^{31, 65, 70}

If there is mixing between the two sides of the membrane, or if the membrane is not an electronic insulator and electrons can pass through the membrane, the system will short, wasting the chemical potential as heat. To ensure the success of the system, the polymer ion exchange membrane must reliably and selectively transport ions with minimal resistance for optimal performance, meaning there is low over potential and low waste heat production. The cost of the polymer ion exchange membrane must also be low enough to maintain economic viability; the durability and integrity are vital to this.

There are various commercial uses for proton exchange membrane fuel cells, including fuel cell electric vehicles, combined heat and power systems, and mobile power sources for both computers and military equipment.^{65, 70-71} Fuel cells differ from traditional gasoline engines in that they convert fuels to electric energy without moving mechanical parts using electrochemical reactions. Since fuel cells operate at lower temperatures, they have much lower heat loss, making them very efficient.⁷²

When pure hydrogen and oxygen gases are used as the fuels in a fuel cell, the only byproduct of the electricity generating electrochemical reactions is environmentally benign water; this makes fuel cells a promising sustainable energy technology.³⁵ Ideally, hydrogen fuel will be produced sustainably (possibly by electrolyzers, or fuel cells operated in reverse), enabling a greener energy supply.⁷³⁻⁷⁶ Fuel cells have high current densities to go along with low weight and volume, and fuel cells are extremely reliable.⁷⁷

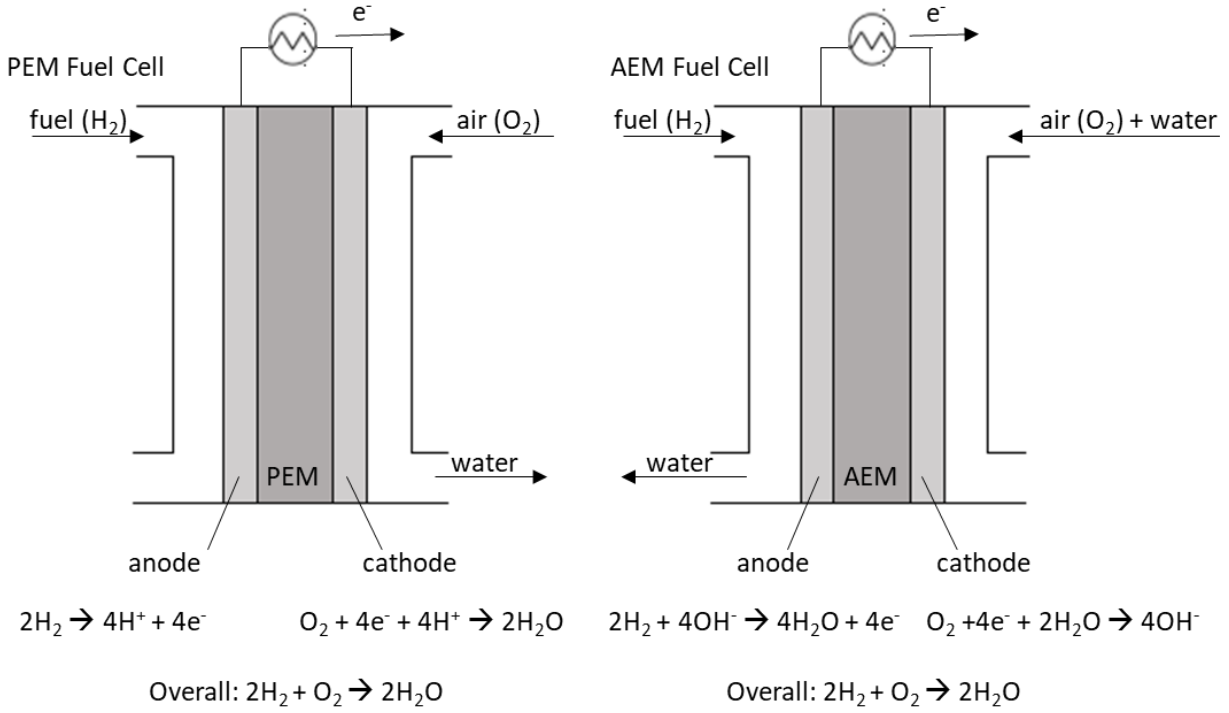
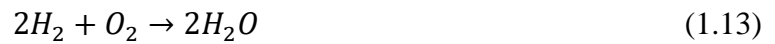
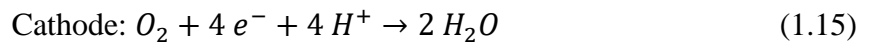


Figure 1. Schematics of PEM and AEM fuel cells.

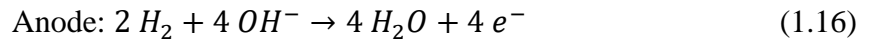
When using pure hydrogen and oxygen as fuels, the overall chemical reaction in a fuel cell is:

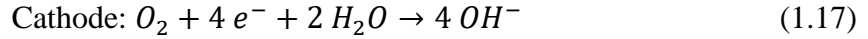


The overall chemical reaction is separated into two half reactions, one at each electrode, in order to induce the flow of electrons to do electrical work outside of the fuel cell. In a proton exchange membrane (PEM) fuel cell, the two half reactions are:



In an anion exchange membrane (AEM) fuel cell, the two half reactions are:





In a proton exchange membrane, the proton must pass through the polymer membrane from the anode to the cathode. In an anion exchange membrane, the hydroxide anion must pass through the polymer membrane from the cathode to the anion.

To speed the reactions taking place on the electrodes to a useful pace, the electrodes are coated with catalyst. Platinum is required as the electrocatalyst, along with corrosion resistant bipolar plates or graphite-coated stainless steel that can withstand the acidic environment of PEM fuel cells, due to the mobile ions being protons.⁷⁸⁻⁷⁹ This places inherent limitations on the ability to lower the cost of PEM fuel cells.

In an alkaline electrolyte, the oxygen has a lower activation energy and faster electrochemical kinetics, demonstrated by the lower reaction overvoltage and lower Tafel slopes, that is, cell potential divided by current density; enabling AEM fuel cells to use non-precious metal catalysts like nickel or silver, getting around the scarcity and subsequent high cost of platinum.⁸⁰⁻⁸² Further cost reduction is possible because nickel and stainless steel are candidates for bipolar plates and housing in AEM fuel cells, due to their low corrosion in alkaline environments; therefore there has been a recent uptick in interest in AEM fuel cells.^{54, 56, 81, 83-87}

Standard stable, high-performance, and economically viable AEMs are not established yet, despite the community having explored diverse polymer classes for AEM materials; these polymer classes include: poly(arylene ether),⁸⁸⁻⁹⁰ polyphenylene,⁹¹⁻⁹⁴ poly(phenylene oxide),⁹⁵⁻⁹⁷ polyvinyl,⁹⁸⁻¹⁰¹ and block copolymers.¹⁰²⁻¹⁰⁸ Furthermore, fundamental design factors for stable, both chemically and mechanically, and highly ion conductive AEMs are not yet well understood.⁵⁴⁻

The state-of-the-art PEM, Nafion, a perfluorinated PEM with randomly attached sulfonic acid groups along its Teflon backbone, has demonstrated that water content management and the formation of ion conducting channels are crucial for high ion conductivity.³⁶⁻³⁷ Microphase separation is driven by strong ionic association and water adsorbed to the hydrophilic acid functional groups separating from the hydrophobic, fluorinated backbone, forming a network of continuous, hydrated channels on a length scale of a few nanometers for the transportation of protons.³⁶⁻³⁷ Effective water channel network formation is contingent upon several factors, including: polymer chain architectures,¹⁰⁹⁻¹¹⁵ types of and density of ionic groups,^{106, 116} and operating conditions, like humidity.¹¹⁷⁻¹¹⁹ The exact mechanism of ion transport is yet unknown; however, it is proposed to be a combination of diffusion, convection, and the Grotthus mechanism, where ions “hop” through a network of hydrogen bonds by breaking and re-forming new hydrogen bonds.^{36, 83, 120-123}

Not all water within hydrated, ion-conducting channels is equal; water molecules are either tightly associated, or “bound”, with an ionic group, or they are in a bulk-like “free” state.¹²⁴ The state of water within the hydrated, ion-conducting channels can be determined by DSC: free water is freezable whereas bound water is not.¹²⁵⁻¹²⁶ Free water content has been found to drive ionic conductivity, membrane swelling, and water mobility within the membrane.^{124, 148} Bound water remains while free water evaporates at lower relative humidities; here, bound water remains effective at conducting ions.¹²⁴⁻¹²⁵ Confinement of the ion-conducting channels leads to the increase in bound water, altering the balance between free and bound water, leaving another knob to turn in membrane design.¹²⁵

To design high-performance polyelectrolyte membranes, it is critical to understand the impact that the polymer backbone architecture and the ionic groups, both in type and density, have

on the thermodynamic states, kinetics, and microstructures of solvated ion-containing polymers.³⁹

127

1.5 Ion Exchange Membrane Devices for Clean Energy

The earth is warming at an unprecedented clip. Record high temperatures are recorded with alarming frequency.¹²⁸ These trends in temperature are caused in part by carbon dioxide in the atmosphere at unprecedented levels, which is attributable to human behavior, specifically from the extraction and burning of fossil fuels, such as coal, oil, and natural gas.¹²⁹

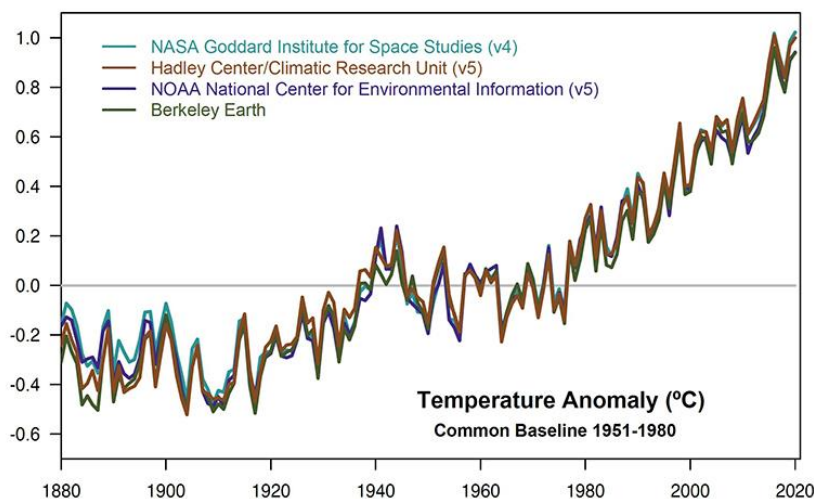


Figure 2. Global temperature anomaly since 1880, higher positive anomaly means warmer weather. The sharp increase is indicative of a rapidly warming earth. Adapted from ¹²⁸.

PROXY (INDIRECT) MEASUREMENTS

Data source: Reconstruction from ice cores.

Credit: NOAA

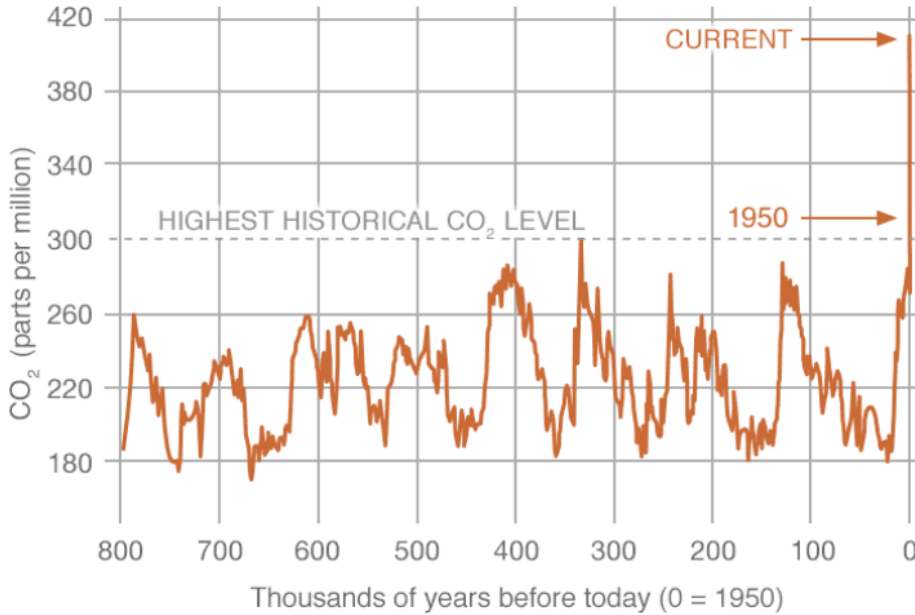


Figure 3. Measurement of historic carbon dioxide levels, showing the immense spike in CO₂ from recent human activity. Adapted from ¹²⁹.

Lowering atmospheric carbon dioxide can slow the rate of warming worldwide, making carbon emission free electricity generation highly desirable. Renewable energy sources like solar and wind, while clean, suffer from intermittency; the resource availability is weather dependent. The intermittent nature of these renewables makes them unreliable in some form. Energy storage, either in batteries or in fuels, addresses the intermittency and allows for energy to be consumed on demand.¹³⁰

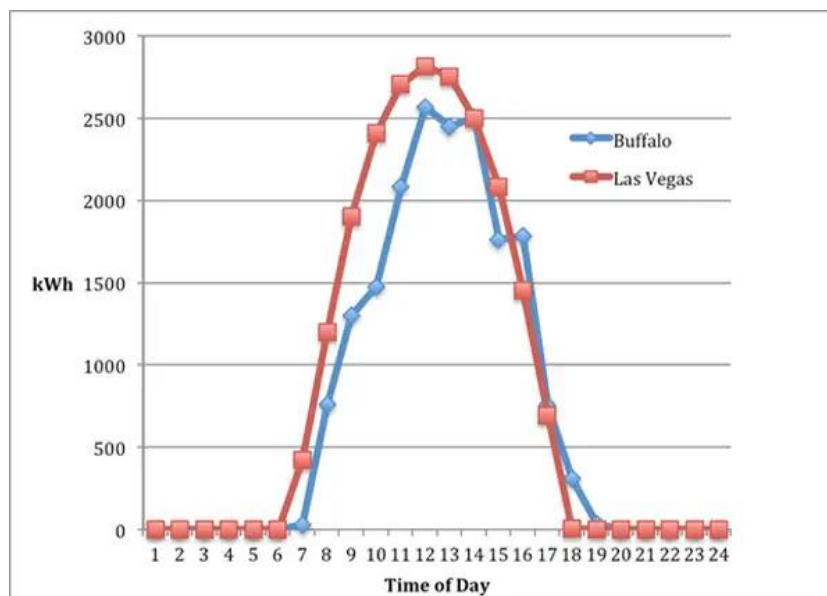


Figure 4. Energy production from a solar cell in one day, showing intermittent energy production depending on time of day and weather conditions. Adapted from ¹³⁰.

Hydrogen gas can be a fuel that allows for clean, carbon emission free energy to be produced on demand. Fuel cells are electrochemical devices that utilize hydrogen gas to produce electricity with only byproducts of environmentally benign water and heat.⁵⁴ Electrolyzers are essentially fuel cells in reverse, taking energy to split water into pure hydrogen and oxygen gases.¹³¹ With a clean source of energy for electrolyzers, hydrogen can be produced without carbon emissions, which can in turn be consumed in fuel cells without carbon emissions.⁵⁴ Fuel cells and, by proxy, electrolyzers are discussed in more depth in 1.4 Ion Exchange Membranes in Fuel Cell Applications.

1.6 Donnan Exclusion Effect

The Donnan membrane principle is essentially a specific domain of the second law of thermodynamics dealing exclusively with electrolytes that are completely ionized.¹³² The inability of certain ions to diffuse from one phase or region to the other in systems involving water or polar solvents give rise to the Donnan membrane equilibrium. Fixed charges, which are nondiffusible,

in contact with water, can be utilized to modulate the distribution of ions, creating ion rich and ion poor phases, leading to efficient separation.¹³² The Donnan exclusion effect inhibits the transfer of electroactive species of the same charge (positive charge for AEMs). This inhibits fuel crossover in exchange membranes, boosting performance.¹³³

1.7 Outline of Thesis Research

This research seeks to explore the relationship between polymer backbone architecture and ion transport to contribute to the development of inexpensive and high-performance anion exchange membranes. The goal of the projects is to work towards a structure-property understanding that will enable the design of ionomers that self-assemble efficient hydrated ion-conducting channels. The materials must also prevent excessive swelling and water uptake that is known to lead to the failure of membrane materials, contributing to good mechanical integrity. This will enable electrochemical energy devices that utilize ion-transporting membranes, like fuel cells and electrolyzers, to become more economically viable solutions for cleaner and more sustainable energy production.

Chapter 2 provides an overview of the synthetic and characterization techniques used in this research.

Chapter 3 describes the synthesis and characterization of anion exchange membranes based on poly(1,1-diphenylethylene-*alt*-butadiene).

Chapter 4 describes the synthesis and characterization of anion exchange membranes based on higher glass transition temperature polymer backbone, cyclized poly(1,1-diphenylethylene-*alt*-butadiene), with a glass transition temperature over 200°C.

2. Introduction of Experimental Techniques

2.1 Introduction

This chapter introduces key synthetic and characterization techniques utilized in this research. Synthetic techniques include: anionic polymerization, hydrogenation of diene containing polymers, and acid-catalyzed Friedel-Crafts bromoalkylation for post-polymerization functionalization. Characterization techniques include: size-exclusion chromatography (SEC), nuclear magnetic resonance (NMR), differential scanning calorimetry (DSC), ion conductivity, and ion exchange capacity (IEC). This chapter focuses on providing a general background about each technique as well as the relevance to the research.

2.2 Anionic Polymerization

Anionic polymerization is a living addition polymerization technique.¹³⁴ The value of this polymerization technique comes from the ability to synthesize polymers with highly uniform chain length and molecular weights, as well as block copolymers by the sequential addition of unique monomers.¹³⁵⁻¹³⁶ The number of polymer chains is set by the amount of initiator, and, unlike typical chain-growth polymerizations, living anionic polymerization does not contain chain transfer or termination steps. This means that the degree of polymerization of the polymer can be controlled by the molar ratio of initiator to monomer:

$$N = \frac{[\text{monomer}]}{[\text{initiator}]} \quad (2.1)$$

The anionic polymerization process is displayed in Figure 5, showing the polymerization of polystyrene initiated by *sec*-butyllithium.

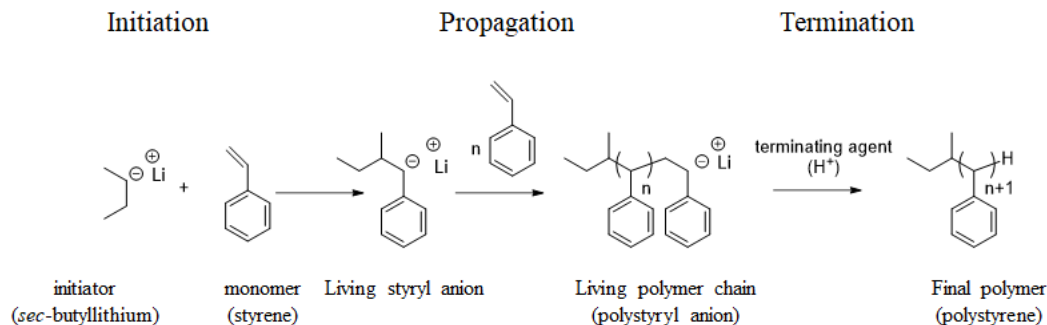


Figure 5. Anionic polymerization of polystyrene.

Upon initiation, anionic polymerization proceeds continuously by an active anion at the end of a growing polymer chain that continuously adds monomer units to the end of the polymer chain. This proceeds until thermodynamic equilibrium is achieved between the free monomer and the polymer chains. Ideally, termination only occurs when a reagent is added to quench the chain-end anions; impurities like oxygen gas, however, can prematurely terminate the living chain ends.¹³⁴

Polymerization is initiated by a carbanion initiator that attacks a more electropositive double bond of a monomer unit, forming the beginning of a chain with a carbanion end, and propagates through the successive attack of this carbanion on the double bond of additional monomer units.^{1, 134} To stabilize the resulting end carbanion and enable continued propagation, monomers that have an electron withdrawing group adjacent to the attacked double bond are needed. To avoid premature termination, the reaction environment must be free of protic impurities and electrophilic functional groups (e.g. water, oxygen, and carbon dioxide) that will complex with the carbanion.^{134, 137} To induce termination, acidic protons are introduced in excess of the living carbanions (i.e. adding methanol) that complex with carbanions.¹

Statistical polymerization (i.e. condensation polymerization and free-radical polymerizations) yield polydispersities that approach 2; however, the living nature of anionic polymerization produces polymers with mono-modal and low dispersity (<1.1), due to the unique aspect of well-controlled polymer chain growth.¹

The initiator and solvent choices are critical for successful polymerization of the selected monomer into the desired polymer. For example, the configuration of polymer chains in the polymerization of butadiene to polybutadiene is significantly influenced by the counterion and the solvent polarity; the solvent and initiator determines the microstructure of the resulting polymer as shown in Figure 6: cyclohexane solvent with a lithium counterion promotes the polymerization of 1,4-polybutadiene while tetrahydrofuran solvent and lithium counterion encourages the polymerization of 1,2-polybutadiene.^{134, 138} Electron transfer agents like potassium naphthalenide have been shown to initiate polymerization of conjugated olefinic hydrocarbons; the electron transfer agent allow for the formation of difunctional carbanion living chain that can propagate from both ends¹³⁹. The difunctional carbanion living chain allows for the formation of multiple blocks of copolymers of equal length with the sequential addition of monomers¹³⁹.

Of equal importance for the successful polymerization of a designed polymer is the temperature of the polymerization solution. Polymerizations in tetrahydrofuran with butyllithium initiator must be done at reduced temperatures, shown in Figure 6, because butyllithium reagents react with tetrahydrofuran and the reaction rate increases with temperature; for example, *n*-butyllithium has a half-life of 1.8 hours and polystyryl anions are quenched within 4 hours.^{137, 140-}

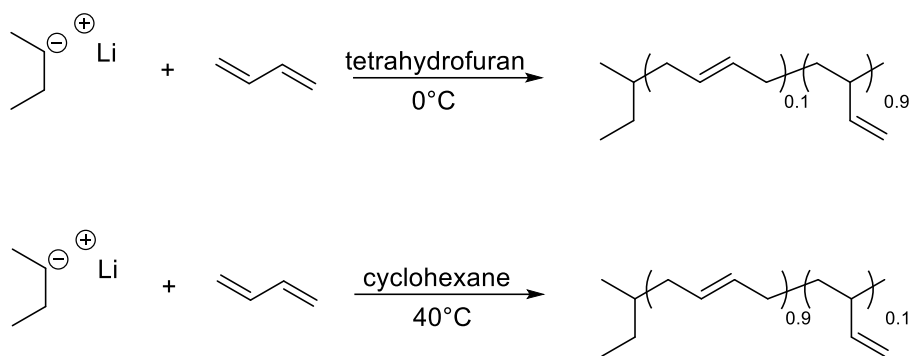


Figure 6. Anionic polymerization of polybutadiene in different solvents.

In this thesis, anionic polymerization is used to synthesize poly(1,1-diphenylethylene-*alt*-butadiene) (DPE/B) and polystyrene (PS).

Initiator: For polystyrene polymerization, commercially available sec-butyllithium in cyclohexane (1.4 M) was used as the initiator. For poly(1,1-diphenylethylene-*alt*-butadiene), potassium naphthalenide was synthesized. Potassium metal was collected in a Chemglass Airfree flask and dried. Naphthalene was added under positive argon pressure. Tetrahydrofuran was cannulated in, and the reaction mixture was stirred overnight. The potassium naphthalenide solution was used within two weeks to preserve the integrity of the electron transfer agent.

Solvent and monomer purification: To mitigate premature termination of polymer chains, special care in the reaction setup to exclude impurities (e.g. water, oxygen, and carbon dioxide) that can react and quench the living anion at the polymer chain end must be taken.¹⁴²⁻¹⁴³

Cyclohexane (Sigma-Aldrich) was purified by passing through activated alumina (BASF F-200) and activated copper catalyst (BASF Q-5). Tetrahydrofuran (Sigma-Aldrich) was purified by passing through activated alumina (BASF F-200).

Different monomers, due to their respective boiling points and reactivity with purification agents, require different purification procedures.

Styrene monomer (Acros, bp = 145 °C) was collected in a round bottom flask with a sidearm fitted with a CHEM-VAC™ high vacuum valve. The monomer was then degassed by performing three freeze-pump-thaw cycles: freezing with liquid nitrogen, pulling vacuum (gradually at first to reduce losses) while the monomer freezes until baseline is reached, then thawing in a 40 °C water bath. The degassed styrene monomer was transferred via vacuum distillation into a purification flask (a round bottom flask fitted with two side arms with CHEM-VAC™ high vacuum valves) containing vacuum dried di-*n*-butylmagnesium (purification agent, 4 mL of di-*n*-butylmagnesium for the first 10 g of styrene and 2 mL for each additional 10 g) and stirred at 40 °C for 1 hour. This purification was repeated a second time for further purification. After the second purification, the styrene monomer was vacuum distilled into a flame-dried monomer burette (a burette fitted with a CHEM-VAC™ high vacuum valve). The purified styrene monomer was stored at room temperature covered with aluminum foil (to mitigate photopolymerization) until use.

Butadiene (Sigma-Aldrich, bp = -4 °C) with its low boiling point is a gas at room temperature and requires special care to handle, always cooled in an ice water bath or in liquid nitrogen to keep butadiene as a liquid and avoid over-pressurizing the glass vessels. Butadiene monomer was collected from the gas cylinder and condensed, with liquid nitrogen, into a purification flask with two sidearms: one sidearm fitted with a CHEM-VAC™ high vacuum valve and the other sidearm fitted with a pressure-relief valve for safety. The butadiene was degassed by performing three freeze-pump-thaw cycles: freezing with liquid nitrogen, pulling vacuum (gradually at first to reduce losses) while the monomer freezes until baseline is reached, then thawing in a 0 °C ice water bath. The degassed butadiene was vacuum distilled twice over *n*-butyllithium (Aldrich, 1.6 M in hexanes) (2 mL *n*-butyllithium for each 10 g of monomer)

following the same procedure as for styrene, except the purification was conducted at 0 °C in an ice water bath for 30 minutes. After the second purification, the butadiene monomer was vacuum distilled into a flame-dried monomer burette containing dry tetrahydrofuran and then kept at room temperature until used.

1,1-diphenylethylene (DPE) (Tokyo Chemical Industry Co (TCI), bp = 277 °C) was purified over *n*-butyllithium (Aldrich, 1.6 M in hexanes) (1 mL *n*-butyllithium for each 15 g of monomer). After pulling vacuum on the DPE until baseline was reached, the *n*-butyllithium was added at room temperature while purging argon. The DPE plus *n*-butyllithium was gradually heated by 10 °C increments to 70 °C while pulling vacuum, held at there until baseline was reached, and then heated to 90 °C (in 10 °C steps) to distill via short-pass distillation. The purified DPE monomer was stored in the dry box freezer until used.

Polymerization: 1,1-Diphenylethylene (DPE) cannot self-polymerize, as the addition of two sequential DPE monomers is sterically prohibited. Alternating copolymers of DPE with butadiene comonomer can be produced under proper reaction conditions.¹⁴⁴ Previous reports show the appropriate reaction conditions to produce a 1:1 alternating copolymer involve a molar excess of DPE monomer in relation to butadiene in tetrahydrofuran at 0 °C.

Depending on the amount of polymer desired, two different reaction procedures were used. For smaller scales, in a flame-dried 150 mL pressure vessel, potassium naphthalenide is added to purified 1,1-diphenylethylene monomer. The solution is cooled to 0 °C. Purified butadiene in dry, purified tetrahydrofuran is added to the pressure vessel. After at least 14 hours, the anionic polymerization was terminated with argon-purged methanol. The synthesized polymer was precipitated in methanol, recovered, and freeze-dried in benzene under vacuum. For larger scales, a flame-dried 1000 mL 5 neck reactor is used. Purified tetrahydrofuran is added to purified 1,1-

diphenylethylene monomer, then potassium naphthalenide is added. The rest of the procedure mirrors the procedure for smaller scales.

2.3 Hydrogenation

Selective hydrogenation of the butadiene portion of DPE/B copolymer is crucial for this work, as unsaturated double bonds in the polymer backbone are susceptible to reaction with acid catalysts used for post-polymerization functionalization. Hydrogenation *via* a nickel-aluminum catalyst was used to selectively hydrogenate DPE/B polymer and leave a fully saturated backbone.¹⁴⁵

Hydrogenation with nickel-aluminum catalyst:¹⁴⁵ Nickel 2-ethylhexanoate was dried under dynamic vacuum at room temperature; anhydrous cyclohexane was added to make a 0.1 M solution. Triethylaluminum in a 3:1 molar ratio (triethylaluminum : nickel 2-ethylhexanoate) slowly to the 0.1 M nickel 2-ethylhexanoate solution in cyclohexane at 0 °C under argon, and then the solution was slowly warmed up to room temperature with stirring for 2 hours before use of the nickel-aluminum catalyst. Selective hydrogenation was conducted in a Parr reactor under 600 psi of hydrogen at 90 °C for 48 hours. After hydrogenation, the reactor was cooled down to room temperature. The hydrogenated polymer solution in cyclohexane was washed with an 8 wt% aqueous citric acid solution to neutralize the catalyst (stirred until the catalyst color disappeared), washed with a saturated sodium bicarbonate solution to neutralize the citric acid, and finally washed with distilled water to remove all salts from the hydrogenated polymer / cyclohexane solution, all at room temperature. The washed polymer solution was filtered with a 0.22 µm Millipore Durapore® membrane filter at room temperature. The filtered polymer solution was precipitated in methanol, and the hydrogenated polymer was recovered and fully dried under dynamic vacuum.

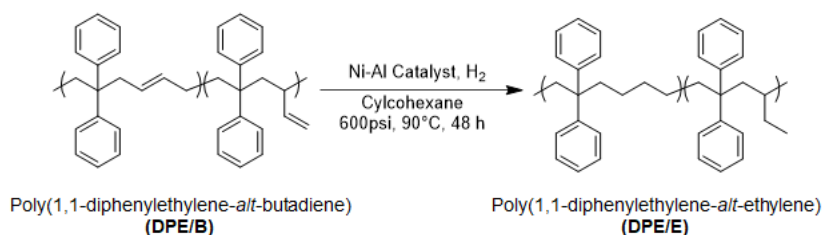


Figure 7. Selective hydrogenation of DPE/B backbone, saturating the backbone alkenes while leaving the pendant phenyl groups untouched.

2.4 Backbone Cyclization with Intramolecular Friedel-Crafts Cyclization

Intramolecular Friedel-Crafts cyclization of DPE/B leaves a polymer backbone with a 6 member ring and no alkene carbons; this backbone structure is appealing for AEM applications due to its increased glass transition temperature relative to DPE/B and DPE/E.¹⁴⁶

DPE/B was dried under dynamic vacuum at room temperature; anhydrous dichloromethane was added to make a 1.5 wt% solution. Diluted (10% in anhydrous dichloromethane) trifluoromethanesulfonic acid (triflic acid) was added in a 1:10 molar ratio (triflic acid:DPE/B) to the 1.5 wt% DPE/B in dichloromethane at 0 °C under argon. The reaction was quenched with methanol after 10 minutes. The polymer was dissolved in dichloromethane, washed with saturated sodium bicarbonate solution to neutralize any residual triflic acid, then washed with distilled water to remove all salts from the hydrogenated polymer/dichloromethane solution, all at room temperature. The washed polymer solution was filtered with a 0.22 μm Millipore Durapore® membrane filter at room temperature. The filtered polymer solution was precipitated in methanol, and the hydrogenated polymer was recovered and fully dried under dynamic vacuum.

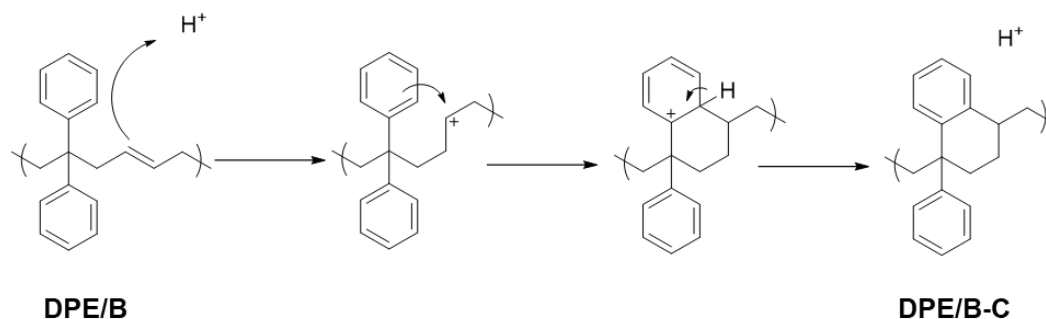


Figure 8. Triflic acid catalyzed intramolecular Friedel-Crafts cyclization of DPE/B.

2.5 Acid-Catalyzed Friedel-Crafts Bromoalkylation

Phenyl rings that are electron rich offer excellent sites for post-polymerization functionalization by electrophilic substitution reactions.²⁰ In this work, post-polymerization functionalization was achieved by an acid catalyzed Friedel-Crafts bromoalkylation reaction.^{23, 147-148} Figure 9 shows the mechanism, with DPE/E and PS as example polymers; triflic acid protonates the tertiary alcohol (2-methyl-7-bromo-2-heptanol) to generate a carbocation, which in turn attacks the electrophilic phenyl ring, attaching the alkyl sidechain.

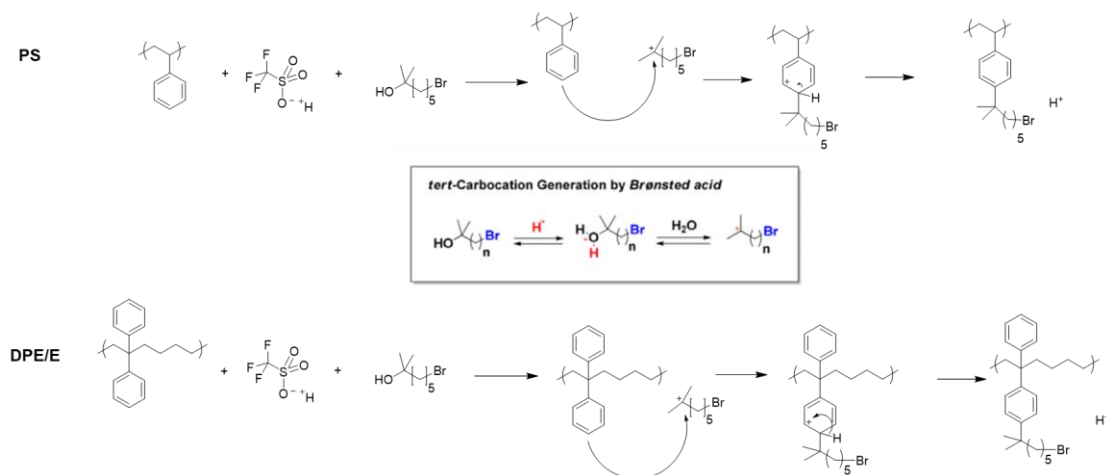


Figure 9. Friedel-Crafts bromoalkylation of DPE/E and PS, utilizing triflic acid as a Brønsted acid to generate *tert*-carbocation.

Polystyrene functionalization was carried out at 0°C with no issues. Decrease in polymer molecular weights was observed in DPE/E when the functionalization reaction was conducted at

0°C. Lowering the reaction temperature to -20°C, achieved by using a dry ice bath in 70% water and 30% methanol, gave successful functionalization reactions.

Vacuum and argon were cycled 5 times on an airfree flask containing polymer. Anhydrous dichloromethane to make a 1 wt% solution was injected into the airfree flask and the polymer was dissolved. The solution was then cooled to reaction temperature. The tertiary alcohol was diluted in ~5 mL anhydrous dichloromethane, collected in a syringe fitted with a long stainless-steel needle (Cadence Science, deflected point septum penetration needles 12" long, 20 gauge) and added by a syringe pump over 5 minutes. The triflic acid was injected by a glass syringe (Hamilton, luer tip gastight syringe, Model 1002 LT Syringe) using a stainless-steel needle (Cadence Science, deflected point septum penetration needles 4" long, 20 gauge) all at once, as soon as the first drop of diluted tertiary alcohol was added to the polymer solution. The reactions were terminated by precipitating into an excess of methanol. The polymer was dissolved in dichloromethane and washed with saturated aqueous sodium bicarbonate to remove residual triflic acid, then washed with distilled water to remove salts, and then the polymer solution was precipitated in an excess of methanol. The precipitated polymer was recovered using a Buchner glass frit filter funnel and fully dried under dynamic vacuum at 80°C.

2.6 Nuclear Magnetic Resonance (NMR)

Nuclear magnetic resonance (NMR) spectroscopy is a commonly used technique for evaluating the chemical structure of polymers. NMR utilizes the magnetic properties of atomic nuclei (their magnetic moments) and the fact that their energy states are quantized to examine the local chemical environments of atoms.¹⁴⁹

The relationship between energy (E) and frequency (ν) is written as $\Delta E = h\nu$, where h = Planck's constant. This means that when electromagnetic radiation with a frequency (ν) corresponding to the ΔE needed to change the energy state from its base energy state to a higher, excited energy state is applied, the electromagnetic radiation is absorbed and the higher energy state is achieved.

To align the spins of the atomic nuclei in an NMR experiment, a sample is placed in a strong magnetic field and a radio frequency (RF) pulse of frequencies is applied to reach nuclear excitation. The detector measures the free induction decay (FID) with time. The FID decays back to the baseline when the RF pulse ends, as the excited spin state of the atomic nucleus relaxes, by releasing energy to the environment as thermal energy, back to the baseline state, which is aligned with the applied magnetic field. The frequency spectrum of the individual resonance frequencies can be obtained by taking the Fourier Transform of the decaying FID.¹⁴⁹ Various reference nuclei can be used, including proton (^1H), carbon (^{13}C), and fluorine (^{19}F). This work only employs proton (^1H) NMR.

NMR spectra are all relative and are reported against a defined reference. For proton NMR, the reference is the compound tetramethylsilane (TMS); its signal is set as $\nu_{\text{standard}} = 0$. Other signals are described in terms of the difference between their frequency and the frequency of the standard, and normalized by dividing by the frequency of the spectrometer. The chemical shift, δ (in ppm), is defined as

$$\delta = \frac{\nu_{\text{sample}} - \nu_{\text{standard}}}{\nu_0} \quad (2.2)$$

Where ν_{sample} is the measured signal frequency, ν_{standard} is the reference frequency, and ν_0 is the frequency of the spectrometer (i.e. 500 MHz).

An atom's resonance frequency and excited state's decay rate back to baseline are affected by the chemical environment of the atom, specifically its electron density. An increase in electron density, which increases shielding and reduces the influence of the applied magnetization, shifts to lower frequency, which is observed as a low δ . The integration of the peaks of the NMR resonance signals gives a relative contribution. The peak area represents the relative number of nuclei that have that chemical environment. Combined, these allow for the assigning of resonance peaks to chemical structures, making NMR spectra maps of the chemical environments of polymers.¹⁴⁹

NMR spectra can be used with polymers in a variety of ways. NMR can check the purity of polymer samples, the degree of functionalization of a polymer, the microstructure of a polymer, and even the determine the stoichiometric ratio of monomer units in a copolymer.

2.7 Size Exclusion Chromatography (SEC)

A standard technique for the rapid analysis of polymer number-averaged molecular weight (M_n), weight-averaged molecular weight (M_w), and the dispersity ($D \equiv M_w/M_n$) is size exclusion chromatography (SEC). This technique is centered around liquid chromatography column or columns in series to increase the column path length; the columns are packed with rigid, porous media as the stationary phase and a liquid mobile phase that solubilizes the polymer. Initially the technique was known as gel-permeation chromatography (GPC) or gel filtration chromatography (GFC), however SEC has become the dominant term as gels are no longer the only column packing medium used. The solubilized polymer is sorted by size based on its hydrodynamic radius as it passes through the columns. Larger polymers are eluted sooner, that is, have a shorter retention time in the column, because they are too large to fit in the smaller, more tortuous porosity paths, thus bypass most pores.¹⁵⁰

The hydrodynamic volume of a polymer scales with the radius of gyration (R_g) cubed (*i.e.* R_g^3), and the radius of gyration of a polymer scales with molecular weight as $R_g \sim N^\nu$. ν is a proportionality constant based on the conformation of the polymer chain; $\nu = 1$ for a rod, $\nu = 1/2$ for an unperturbed coil, $\nu = 1/3$ for a dense globule, and $\nu \approx 3/5$ for a swollen coil in a good solvent.¹

The solution passes through the columns and is then analyzed by a detector. Commonly used detectors are refractive index (RI), light scattering, UV-Vis absorption, and viscometer. Among these, the RI detector is the most common. The RI detector measures the difference in refractive indices of the solubilized polymer eluted and pure solvent to determine the concentration of the solute.¹ The relationship to determine the concentration is:

$$n(c) = n_s + \left(\frac{\partial n}{\partial c}\right) + \dots \quad (2.3)$$

Where $n(c)$ is the refractive index of the solute with some concentration c , n_s is the refractive index of the pure solvent, and $(\partial n/\partial c)$ is the proportionality that relates $(n(c) - n_s)$ directly to c .

The intensity of the RI signal is plotted versus the retention time to show the concentration eluted with time, in arbitrary units, minutes, and number of polymer chains, respectively. The retention time is translated into the more relevant molecular weight through a calibration curve, which is created using a standard polystyrene reference that contains a range of known molecular weight polystyrene samples and relating their molecular weights to measured retention times. A SEC sample must be filtered (0.2 μm syringe filter) to remove contaminants and undissolved polymer that will clog the column and effect retention times of subsequent samples.

Factors that affect a polymer's hydrodynamic radius include solvent, temperature, and the polymer composition. To translate between different polymers and different solvents, Mark-

Houwink are used. Molecular weight of novel polymers, however, are often reported against a polystyrene standard, as their Mark-Houwink parameters are often not known.

In this work, an Agilent 1200 series SEC was used with a refractive index detector and PLGel Mixed-C columns as the stationary phase. Tetrahydrofuran was used as the mobile phase, at a flow rate of 1 mL/min. An injection volume of 50 μ L was used with two columns and a guard column.

2.8 Differential Scanning Calorimetry (DSC)

The thermal properties of polymer materials can be characterized by differential scanning calorimetry (DSC). DSC measures the heat flow into and out of a sample needed to change its temperature relative to a reference. A material's characteristic thermal transitions can be found and quantified by measuring its changes in heat capacity with changing temperature. DSC as a technique is capable of finding a polymer's chief thermal property, the glass transition polymer (T_g). The T_g is the point above which the polymer chains are able to slide by one another and the polymeric material can flow. The glass transition manifests in the thermogram as a step change as the material's heat capacity changes as the material transitions from a glassy state to a rubbery state.¹

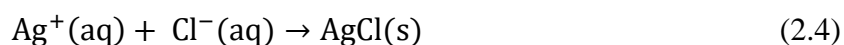
2.9 Ion Exchange Capacity (IEC)

An ion exchange membrane's ability to conduct ions is directly tied to its ion content. The ion content also impacts the water uptake as water molecules are attracted to the ionic sites by hydrogen bonding; this water uptake can foster the formation of water channels in the membrane and improve the conductivity of water solvated ions, because of this, it is needed to quantify the

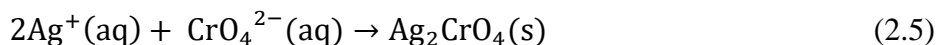
ion content of membranes to evaluate the water uptake and conductivity as functions of ion content.^{54, 83, 151}

There are two common ways of expressing the ion content of a material, as ion exchange capacity (IEC) or as equivalent weight (EW). IEC is expressed in millimoles (milliequivalents) per gram of polymer; EW is expressed as grams of polymer per moles of ions (equivalents). IEC and EW are reciprocals of each other: $EW = 1000 / IEC$. This work reports ion content as IEC.

Methods to determine ion content include NMR and titration, in this work Mohr titration was used.¹⁵² membranes with chloride counterions were dried overnight under dynamic vacuum at 80°C, weighed, and soaked in aqueous 0.5 M sodium nitrate (NaNO₃) for 24 hours. Immersion in aqueous NaNO₃ liberates the Cl⁻ counter ions into solution. After 24 hours, 3 drops of potassium chromate (K₂CrO₄), a bright yellow colorimetric indicator, were added to the aqueous NaNO₃ + Cl⁻ solution. The solution, while stirred with a magnetic stir bar, was titrated against a 0.1 M silver nitrate (AgNO₃) aqueous solution. As AgNO₃ is added dropwise, the Ag⁺ will react with available Cl⁻ ions to form silver chloride (AgCl), an insoluble white solid:



When all available Cl⁻ ions have reacted, Ag⁺ will react with CrO₄²⁻ ions to form silver chromate (Ag₂CrO₄), an insoluble rust-red solid:



Rust-colored precipitates indicate the completion of the titration. The amount of Cl⁻ counterions that were present in the membrane sample and membrane IEC is calculated as:

$$IEC = \frac{\text{ions [millimoles]}}{\text{mass of polymer membrane [g]}} \quad (2.6)$$

2.10 Ion Conductivity

The ion conductivity of an ion exchange membrane measures the ions moving through the membrane, measured in Siemens / centimeter. The ion conductivity is a crucial property of an ion exchange membrane, as the ion conductivity dictates the rate of electricity generated by the fuel cell. The working ions that pass through the ion exchange membrane enable the electricity generating reaction at the electrode. Good conductivity is the result of continuous, hydrated channels; microphase separation between the hydrophobic, glassy backbone and the hydrophilic ionic groups is driven by ionic association and water adsorbed to the ionic functional groups, which forms a continuous network of hydrated channels for the transportation of ions.³⁶⁻³⁷ Several factors, including polymer backbone architecture,¹⁰⁹⁻¹¹⁵ density and type of ionic groups,^{106, 116} and operating conditions, like humidity,¹¹⁷⁻¹¹⁹ dictate the formation of effective water channel networks. The precise mechanism of ion transport within these hydrated channels is still unknown, however ion transport is proposed to be a combination of diffusion of ions through the water filled ion conducting channels, convection and the Grotthus mechanism of ions to “hop” along through a network of hydrogen bonds by breaking and re-forming hydrogen bonds.^{36, 83, 120-122}

An Arrhenius dependence on temperature, that is linear dependence of $\log(\sigma)$ on T^{-1} , is often observed for ionic conductivity in classic liquid electrolytes, salts dissolved in low molecular weight solvents, as well as in water solvated polymer electrolytes with single ion conduction, where only the counter ion is mobile with one ion covalently bonded to the polymer.³¹

While operational electrochemical devices apply voltage across a membrane's thickness and the ions are conducted through-plane of the membrane, laboratories, for ease of measurement, generally employ a four-point probe electrode method that applies voltage across the surface of the membrane and measures in-plane conductivity to measure conductivity.¹⁵³

Chloride and hydroxide ion conductivities (σ in mS/cm) of ionomer membranes were measured using a four-point probe electrode method with BT-512 membrane conductivity test system (BekkTech LLC). Measurements were conducted in a fully hydrated condition where the cell was immersed in deionized water at 30°C, 60°C, and 80°C. The cell was equilibrated for at least 90 minutes before the conductivity measurement.

3. Anion Exchange Membranes Based on Poly(1,1-diphenylethylene-*alt*-butadiene)

3.1 Introduction

Polystyrene as a polymer has seen prevalent use in fields worldwide, including in anion exchange membranes, due to ease of synthesis and efficient costs. While polystyrene offers many beneficial properties in these fields, polystyrene comes up short in anion exchange membranes in several ways. Polystyrene's backbone chemistry leaves the backbone susceptible to free radical attack of the alpha hydrogen on the carbon with the pendant aromatic ring; additionally, polystyrene based AEMs tend to be extremely brittle and have excessive water uptake, all of which hinder the use of polystyrene for AEM applications.^{6, 23, 147, 154}

A monomer similar to styrene, 1,1-diphenylethylene (DPE), has garnered attention as a possible monomer for an AEM polymer system. However, due to steric hinderance, DPE cannot self-polymerize, thus a comonomer is required for a DPE based polymer system. With anionic polymerization under the right conditions, butadiene can make an alternating copolymer with DPE due to the reaction kinetics favoring butadiene adding to DPE and DPE's sterics prohibiting self-polymerization.¹⁴⁴ Poly(1,1-diphenylethylene-*alt*-butadiene) (DPE/B) is a polymer that holds multiple properties that make it an appealing candidate for AEM applications: an all carbon backbone resists hydroxide attack, multiple phenyl groups per repeat unit allow for greater functionalization, and no alpha hydrogen on the polymer backbone.^{90, 154} DPE/B offers a direct comparison to polystyrene, in that polystyrene has one phenyl ring per repeat unit (~100 g/mol), and that DPE/B has two phenyl ring per repeat unit (~200 g/mol); this allows for functionalization of a given percentage of phenyl rings on each polymer species to have a similar IEC, allowing for

better comparison between the two species. While DPE/B and polystyrene are similar, DPE/B offers characteristics that can improve on polystyrene's AEM properties: the two phenyl rings on one backbone carbon and the 5 carbons of space between carbons with pendant phenyls both offer more space between functional groups, which can allow for better aggregation of those functional groups.

3.2 Experimental Details

3.2.1 Materials

Butadiene (Sigma-Aldrich) was purified twice over *n*-butyllithium and vacuum distilled. 1,1-diphenylethylene (TCI) was purified over *n*-butyllithium and vacuum distilled. Styrene (Acros) was purified twice over di-*n*-butylmagnesium and vacuum distilled. Cyclohexane (Sigma-Aldrich) was purified by passing through activated alumina (BASF F-200) and activated copper catalyst (BASF Q-5). Tetrahydrofuran (Sigma-Aldrich) was purified by passing through activated alumina (BASF F-200). Naphthalene (TCI), potassium (Acros Organics), nickel(II) 2-ethylhexanoate (Aldrich), triethylaluminum (Aldrich), ethyl 6-bromohexanoate (Alfa Aesar), methyl magnesium bromide (Alfa Aesar), anhydrous dichloromethane (Honeywell), trifluoromethanesulfonic acid (Alfa Aesar), citric acid (VWR), sodium bicarbonate (EMD Millipore), dimethylsulfoxide (EMD Millipore), sodium chloride (Fisher), sodium nitrate (BDH), silver nitrate (Alfa Aesar), ethanol (Acros), *n*-butyllithium (Aldrich), di-*n*-butylmagnesium (Aldrich), and *sec*-butyllithium (Aldrich) were used as received.

3.2.2 Potassium Naphthalenide

Potassium metal was collected in a Chemglass Airfree flask and dried. Naphthalene was added under positive argon pressure. Tetrahydrofuran was cannulated in, and the reaction mixture

was stirred overnight. The potassium naphthalenide solution was used within two weeks to preserve the integrity of the electron transfer agent.

3.2.3 Polymerization

Polystyrene (PS) was synthesized via anionic polymerization. In a reactor containing cyclohexane under argon at 43°C, *sec*-butyllithium was added. Styrene monomer was slowly added. The reaction was allowed to proceed overnight to completion. The living polymer chains were terminated with argon-purged methanol. The synthesized PS polymer in cyclohexane was precipitated in methanol, recovered, and dried under vacuum. The synthesized PS was characterized by size exclusion chromatography using polystyrene standards, ¹H nuclear magnetic resonance, and differential scanning calorimetry.

Poly(1,1-diphenylethylene-*alt*-butadiene) (DPE/B) alternating copolymer was synthesized by anionic polymerization. In a reactor containing 1,1-diphenylethylene (DPE) in tetrahydrofuran under argon at 0°C, potassium naphthalenide was added to activate DPE. After enough time had passed to activate DPE, butadiene was added slowly. The reaction was allowed to proceed for 14 hours to ensure completion. The living polymer chains were terminated with argon-purged methanol. The synthesized DPE/B polymer in tetrahydrofuran was precipitated in methanol, recovered, and dried under vacuum. The synthesized DPE/B was characterized by size exclusion chromatography using polystyrene standards, ¹H nuclear magnetic resonance, and differential scanning calorimetry.

3.2.4 Selective Hydrogenation

Hydrogenated poly(1,1-diphenylethylene-*alt*-butadiene) alternating copolymer was prepared by selective hydrogenation of DPE/B alternating copolymer using nickel-aluminum catalyst.¹⁵⁵ The nickel-aluminum catalyst was prepared by slowly adding triethylaluminum under

argon to a 0.1M nickel(II) 2-ethylhexanoate solution in cyclohexane at 0°C. The solution was slowly warmed to room temperature with stirring for at least 2 hours before use. Selective hydrogenation was conducted in a Parr reactor under 600 psi of hydrogen at 90°C for 48 hours. The hydrogenated DPE/E polymer solution in cyclohexane was washed with 8 wt% aqueous citric acid solution, saturated sodium bicarbonate solution, and deionized water. The polymer was then precipitated in methanol, then fully dried in vacuum at 70°C.

3.2.5 Synthesis of Brominating Agent

7-bromo-2-methyl-2-heptanol was prepared based on a previous literature report.¹⁴⁷ Under argon atmosphere, ethyl 6-bromohexanoate (Alfa Aesar, 0.11 mmol) was diluted in dry tetrahydrofuran (120 ml), then cooled to 0 °C, and methyl magnesium bromide solution (Alfa Aesar, 0.3 mol) was slowly cannulated to the solution. The reaction mixture was stirred for overnight before quenching with saturated ammonium chloride (NH₄Cl) in deionized water (~60mL). Synthesized 7-bromo-2-methyl-2-heptanol was extracted with diethyl ether twice, dried over magnesium sulfate, rotary evaporated to collect diethyl ether, vacuum distilled, and stored in a freezer in a dry box.

3.2.6 Acid-Catalyzed Friedel-Crafts Bromoalkylation of DPE/E and PS

Acid-catalyzed Friedel-Crafts bromoalkylation reaction was used to functionalize the phenyl groups of DPE/E polymer with 7-bromo-2-methyl-2-heptanol to make alkylbromo-functionalized poly(1,1-diphenylethylene-*alt*-butadiene) (DPE/E-Br).¹⁴⁷ The following is a representative procedure. DPE/E polymer (0.5 g, 2.1 mmol polymer) was completely dissolved in anhydrous dichloromethane at room temperature. The polymer solution was chilled to -20°C using a dry ice bath with methanol and water (30% methanol, balance water). 7-bromo-2-methyl-2-heptanol (1.0g, 4.81 mmol) solution in anhydrous dichloromethane (5 ml) was slowly added to the

DPE/E polymer solution using a syringe pump over 5 minutes. As soon as the first drop of the diluted 7-bromo-2-methyl-2-heptanol solution was added to the reactor, triflic acid (0.53mL, 1.0 mmol. molar ratio of triflic acid to 7-bromo-2-methyl-2-heptanol = 1.1) was injected to the reaction flask using a glass syringe to catalyze the functionalization reaction. The reaction was terminated after 10 minutes by pouring the solution into methanol. The polymer was collected, redissolved in dichloromethane, washed with saturated sodium bicarbonate to remove and residual acid, then washed with distilled water to remove any salts. The polymer was then precipitated in methanol again, then dried under vacuum at 80°C. The same procedure was followed to functionalize PS to alkylbromo-functionalized polystyrene (PS-Br).

3.2.7 Homogeneous Quaternization

DPE/E-Br was dissolved in tetrahydrofuran to form a 2.5 wt% solution. The amount of polymer was determined by targeting 50 µm films in various casting dishes. A 3x excess of trimethylamine, 33 wt% in ethanol, was added and stirred for 24 hours. Dimethylsulfoxide was added such that the quaternized polymer would be 2.5 wt% in dimethylsulfoxide. The mixture was allowed to vent for at least four hours to allow the odorous excess trimethylamine to dissipate. The quaternized hydrogenated poly(1,1-diphenylethylene-*alt*-butadiene) (DPE/E(QA)) solution was then cast in a controlled airflow oven at 80°C overnight, then collected for characterization. The same procedure was followed for Br-PS to make quaternized polystyrene (PS(QA)) films.

3.2.8 Size Exclusion Chromatography (SEC)

The molecular weight and polydispersity of the synthesized DPE/B and PS polymers were characterized by a size exclusion chromatography system with a refractive index detector (SEC, Agilent). Three consecutive PLGel Mixed-C columns were used as the stationary phase, and tetrahydrofuran (30°C) at a flow rate of 1 mL/min was used as the mobile phase.

3.2.9 ¹H Nuclear Magnetic Resonance (¹H NMR)

The chemical composition and degree of functionalization were determined by ¹H NMR spectroscopy analysis (Agilent 500MHz spectrometer). Non-quaternized polymers were characterized at room temperature in either deuterated chloroform or deuterated tetrachloroethane and quaternized polymers were characterized using deuterated dimethylsulfoxide.

3.2.10 Differential Scanning Calorimetry

The glass transition temperatures of PS, Br-PS, DPE/E, and DPE/E-Br were characterized using differential scanning calorimetry (DSC) technique (TA instruments, Q2000) at a ramping rate 10 °C/min.

3.2.11 Ion Exchange Capacity (IEC) Measurements

IECs of membranes were determined by Mohr titration. The membranes with bromide or chloride counterions were dried under vacuum at 80°C, weighed, and immersed in an aqueous 0.5 M NaNO₃ solution for 48 hours. The NaNO₃ solution was titrated with a 0.1 M AgNO₃ aqueous solution using K₂CrO₄ as a colorimetric indicator.

3.2.12 Chloride Conductivity Measurements

Chloride ion conductivities (σ in mS/cm) of QA-PS and DPE/E(QA) membranes were measured using a four-point probe electrode method with BT-512 membrane conductivity test system (BekkTech LLC). Measurements were conducted in a fully hydrated condition where the cell was immersed in deionized water at 30°C, 60°C, and 80°C. The cell was equilibrated for at least 30 minutes before the conductivity measurement.

3.2.13 Chloride Water Uptake

Water uptake (WU) was calculated as

$$WU(\%) = [(W_{hydrated} - W_{dry}) \times 100] / W_{dry} \quad (3.1)$$

Where $W_{hydrated}$ and W_{dry} are the weights of the patted-dry water swollen and dry membranes, respectively. The dry membrane was prepared under dynamic vacuum at 80°C.

3.2.14 Hydroxide Counterion Exchange

While AEMs are used in applications, such as fuel cells or electrolyzers, with hydroxide (OH^-) counterions, they are rarely handled in hydroxide form during testing and characterization, due to hydroxide readily reacting with carbon dioxide to form carbonate species, which lower the performance of the membrane.¹⁵⁶ AEMs with chloride (Cl^-) counterions avoid this issue, making them easier to handle and characterize. However, since the OH^- form of membranes is what is used in application, it is valuable to characterize the membranes in hydroxide form as well as chloride form. In order to convert a membrane from chloride form to hydroxide form, the fully dried membrane is introduced to an argon filled glove box. There it is soaked in 1.0 M NaOH for 48 hours, rinsed with distilled water, then soaked in distilled water.

3.2.15 Hydroxide Water Uptake

Water uptake of the OH^- form of membranes was measured in an argon filled glovebox after exchanging the counter ion from chloride to hydroxide. Water uptake (WU) was calculated as $WU(\%) = [(W_{hydrated} - W_{dry}) \times 100] / W_{dry}$ where $W_{hydrated}$ and W_{dry} are the weights of the patted-dry water swollen and dry membranes, respectively. The dry membrane was prepared under dynamic vacuum at 80°C. The hydrated membrane was soaked in water overnight, patted dry to remove surface water, then weighed.

3.2.16 Hydroxide Conductivity

Hydroxide ion conductivities (σ in mS/cm) of QA-PS and DPE/E(QA) membranes were measured using a four-point probe electrode method with BT-512 membrane conductivity test system (BekkTech LLC). Measurements were conducted in a fully hydrated condition where the cell was immersed in deionized water at 30°C, 60°C, and 80°C. The cell was equilibrated for at least 30 minutes before the conductivity measurement. Since the hydroxide counterion rapidly reacts with carbon dioxide, replacing OH^- with CO_3^{2-} and HCO_3^- , the deionized water was bubbled with argon for an hour before adding the measurement and continued bubbling throughout.¹⁵⁷ The membrane was moved from the argon glovebox in a sealed bag and quickly placed in the argon bubbled water to limit CO_2 exposure.

3.3. Results

3.3.1 Polymerization of Poly(1,1-diphenylethylene-*alt*-butadiene)

Poly(1,1-diphenylethylene-*alt*-butadiene) ($M_n = 140$ kg/mol, $D = 1.15$), the precursor polymer to a selectively hydrogenated polymer backbone, was synthesized via anionic polymerization described in Experimental Details and visualized in Figure 10. Polystyrene used as a comparison was also synthesized via anionic polymerization ($M_n = 84$ kg/mol, $D = 1.19$)

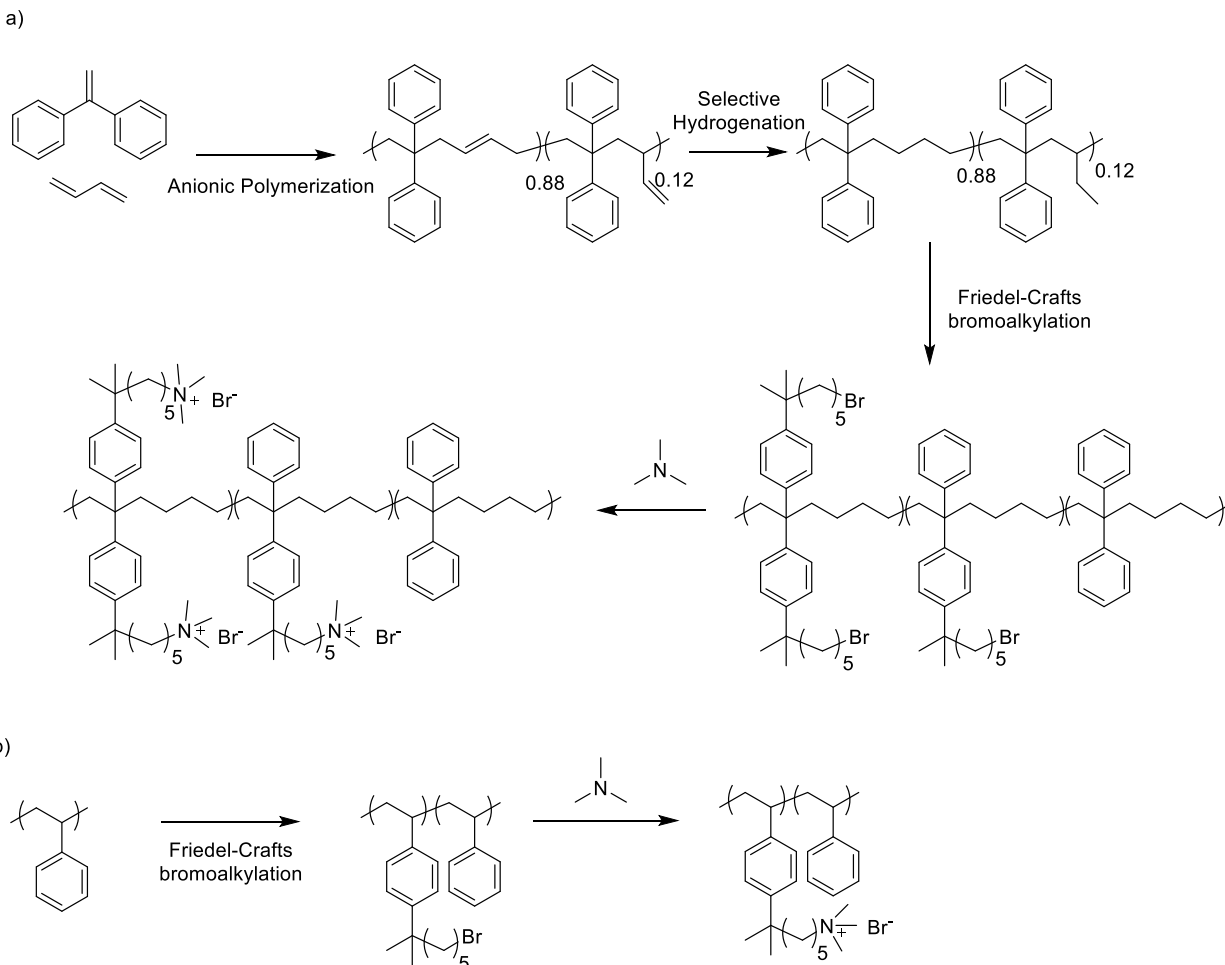


Figure 10. a) Polymerization, selective hydrogenation, bromoalkylation, and quaternization of DPE/B. b) Bromoalkylation and quaternization of PS.

The DPE/B polymer had a DPE to butadiene ratio of 1:1.08, and the butadiene was 88% 1,4 addition and 12% 1,2 addition, as measured by integration of peaks in the ^1H NMR (Figure 11). The reaction was found to have been run to completion by the lack of characteristic peaks of the 1,1-diphenylethylene monomer, with completion being the reaction of all present DPE. The GPC trace revealed a small peak prior to the main peak which can be attributed a negligible amount of coupling.

3.3.2 Selective Hydrogenation of Poly(1,1-diphenylethylene-*alt*-butadiene)

Upon the synthesis of the DPE/B precursor, the diene portions were selectively hydrogenated using a Ni/Al catalyst to convert it to hydrogenated poly(1,1-diphenylethylene-*alt*-butadiene) (DPE/E). Complete selective hydrogenation was confirmed by ^1H NMR, while the dispersity was measured by SEC. Complete hydrogenation of all 1,4 and 1,2-type butadiene units was confirmed by the complete disappearance of the alkene peaks in 5.5 – 4.0 ppm as well as the intensity ratio of alkane and aromatic hydrogens. The slight increase in M_n further corroborated the complete hydrogenation.

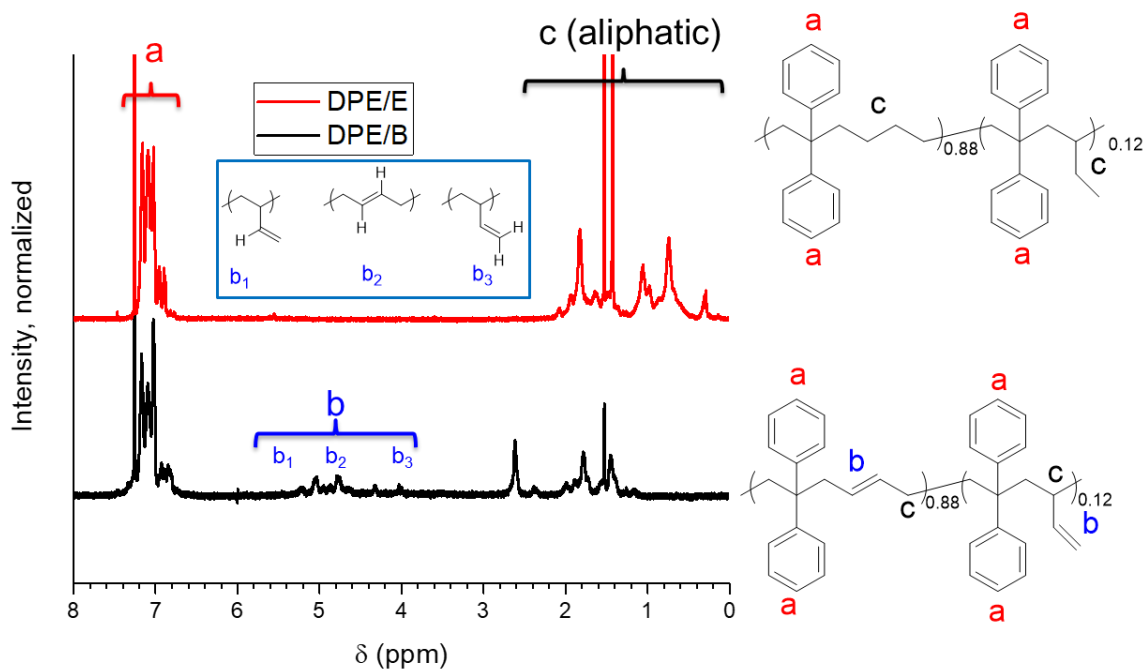


Figure 11. ^1H NMR of DPE/B and DPE/E. Selective hydrogenation of DPE/B was confirmed by the lack of alkene peaks (b) and the aromatic peaks (a) remaining.

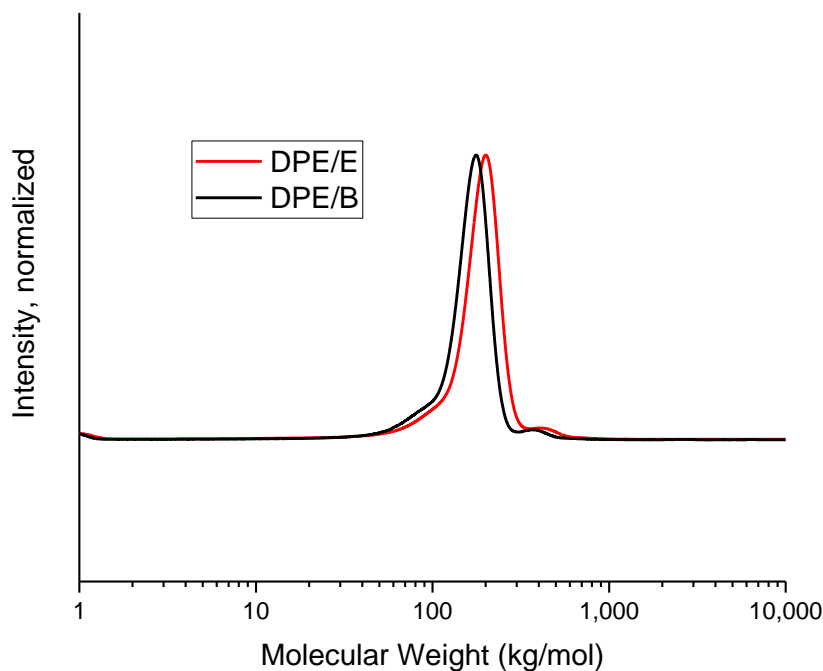


Figure 12. SEC chromatograph of DPE/B and DPE/E, showing no increase in dispersity after selective hydrogenation.

3.3.3 Acid Catalyzed Friedel-Crafts Bromoalkylation

The phenyl groups of DPE/E were functionalized via acid catalyzed Friedel-Crafts bromoalkylation with 7-bromo-2-methyl-2-heptanol.¹⁴⁷ The same procedure was also used to functionalize polystyrene as a baseline polymer for comparison. The reaction conditions are elaborated in the experimental details. Brominated polystyrene (PS-Br) showed very slight degradation under these conditions, whereas DPE/E-Br showed more evident degradation. Despite this, the DPE/E-Br still was nearly monodisperse, with \mathcal{D} equaling 1.7 at most. The degree of functionalization and efficiency of the reaction were determined by ^1H NMR.

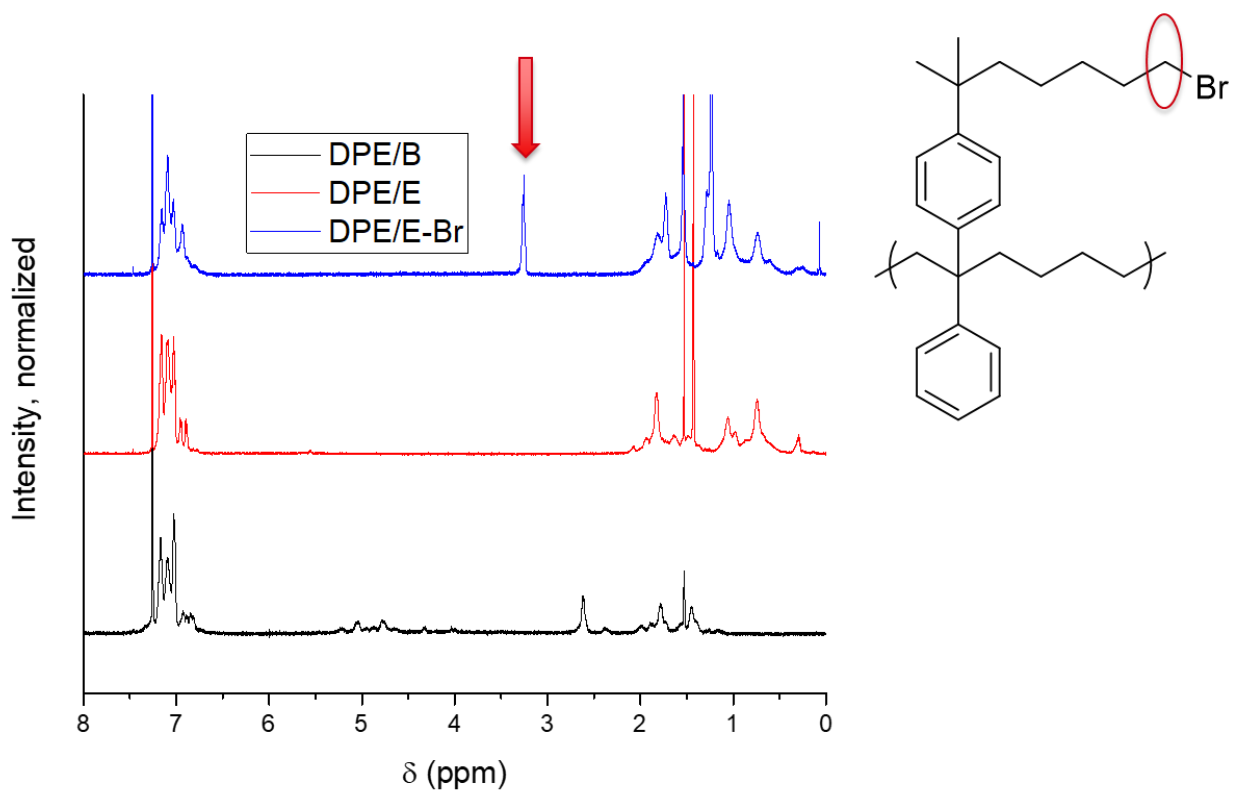


Figure 14. Representative ^1H NMR of DPE/E-Br, the arrow points to the peak from the hydrogens on the carbon adjacent to the bromine. The degree of functionalization was determined by the integration of this peak vs. the integration of the aromatic region.

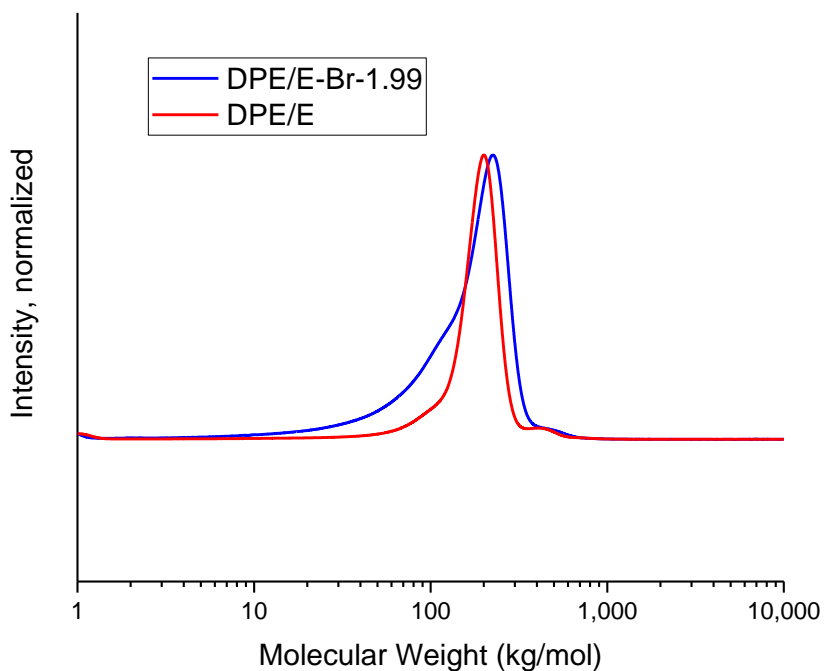


Figure 15. Representative SEC chromatogram of DPE/E-Br, showing a shift in the main peak to higher molecular weight as alkyl chains are added and an increase in lower molecular weight chains from unwanted degradation.

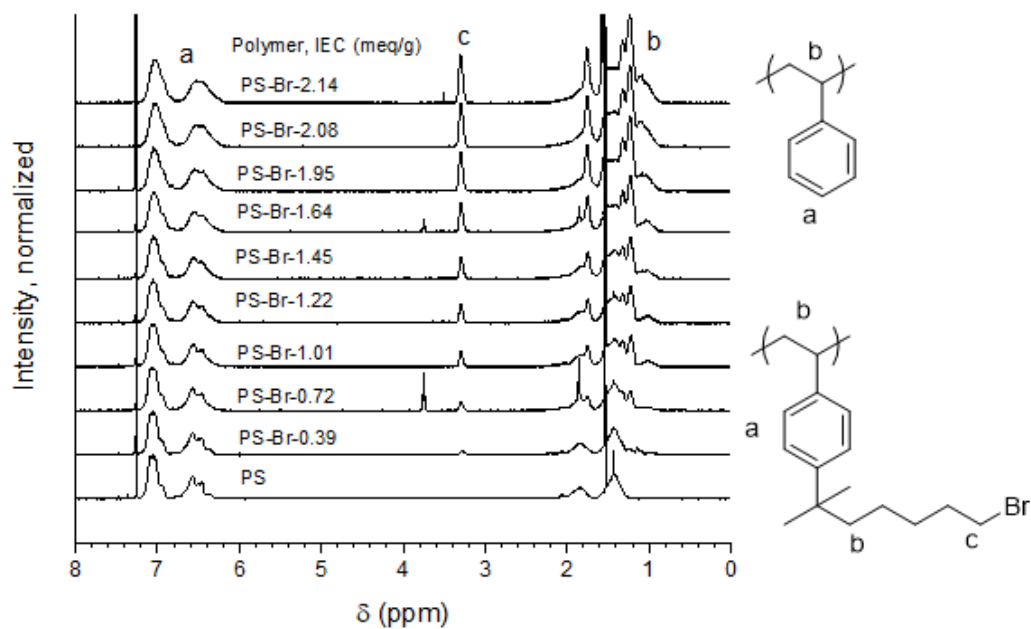


Figure 16. ^1H NMR of PS-Br of varying degrees of functionalization.

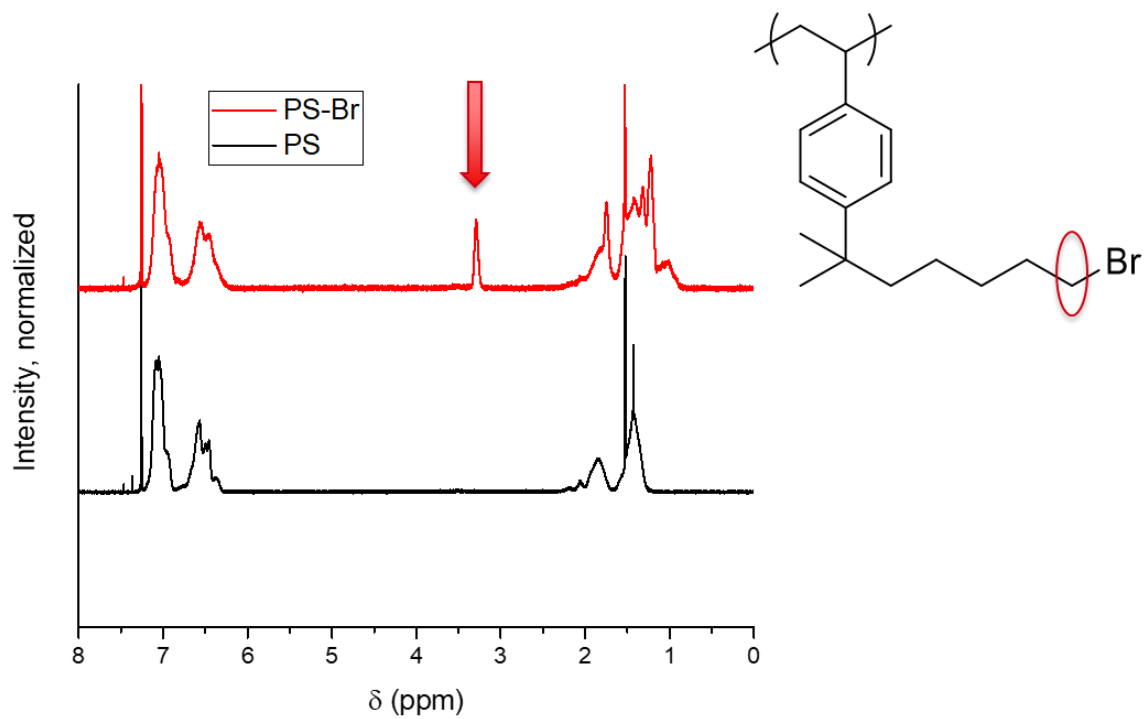


Figure 17. Representative ¹H NMR of PS-Br, the arrow points to the peak from the hydrogens on the carbon adjacent to the bromine. The degree of functionalization was determined by the integration of this peak vs. the integration of the aromatic region.

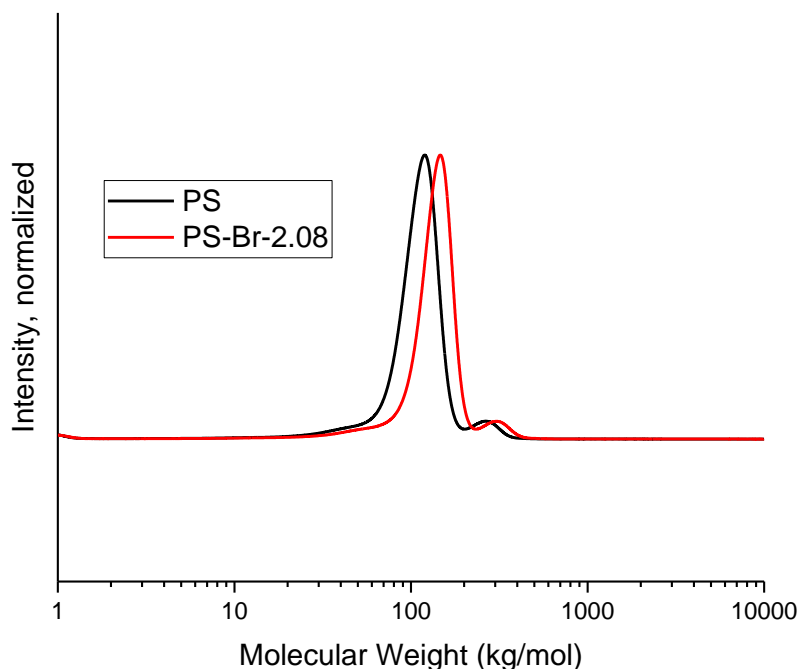


Figure 18. SEC chromatogram of PS-Br, showing a shift in the main peak to higher molecular weight as alkyl chains are added.

During the functionalization process, it was discovered that the functionalized DPE/E-Br polymer was bimodal in nature. That is, the SEC trace revealed two separate polymer species, one that had been functionalized, DPE/E-Br, and one that had not, DPE/E. This is a crucial issue, as the two-polymer species will phase separate if given the opportunity to reach equilibrium. The solvent casting method used to prepare AEMs allows polymers to reach equilibrium, as this allows homogenous polymer solutions to microphase separate and form ion conducting channels as the solvent evaporates. With a solution of two separate polymer species, the two species would also phase separate, leaving a heterogeneous film with a non-functionalized portion that has no ability to conduct ions. As such, optimization of the reaction solution was required to ensure that the reaction solution was one homogeneous phase rather than a two-phase mixture. This was done following the principals of a polymer phase diagram in solution.¹ In order to push the polymer

system from the heterogeneous, two phase mixture to a homogeneous mixture, it was required to either raise the temperature or decrease the concentration of polymer in solution. Since elevated temperature would make the reaction species more active, it would lead to greater degradation of the backbone; thus, it was determined the best way to get the homogeneous functionalization of the backbone polymer was to use a more dilute solution. SEC traces of DPE/E-Br at 5 wt% and 2.5 wt% confirmed that the more dilute solution led to homogeneous functionalization.

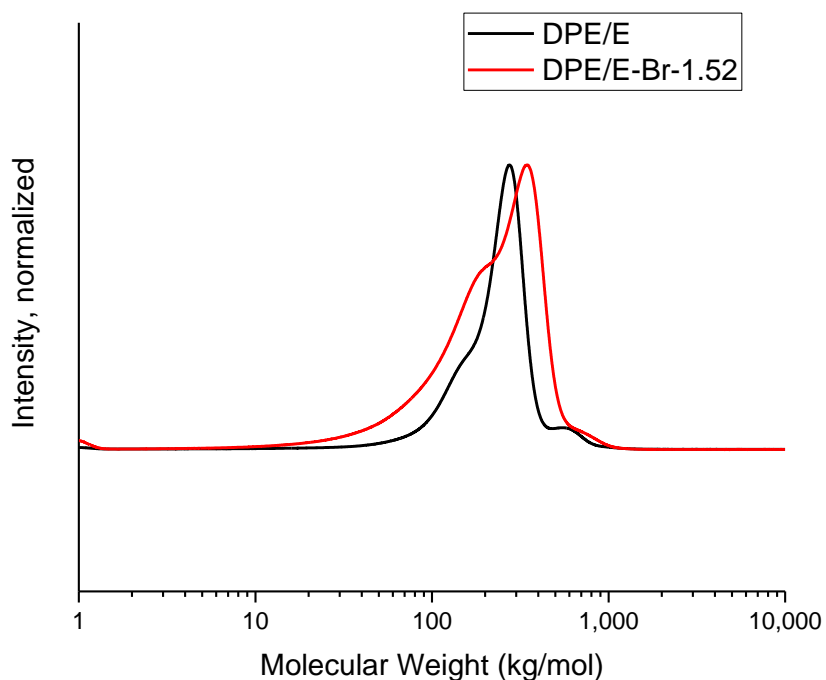


Figure 19. SEC chromatogram of bimodal DPE/E-Br, indicative of two different polymer species being present, a functionalized species and an unfunctionalized species.

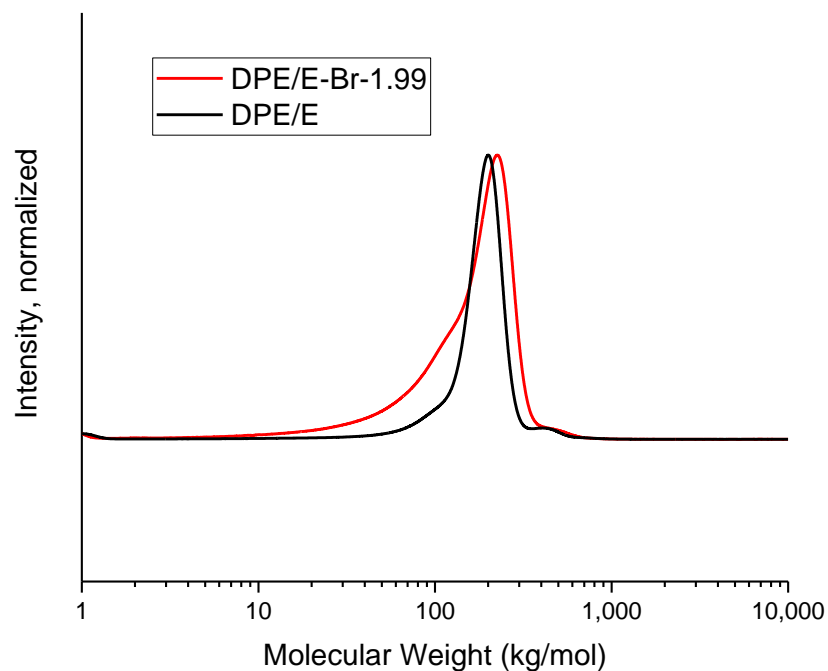


Figure 20. SEC chromatogram of monomodal DPE/E-Br, indicative of uniform functionalization across all chains.

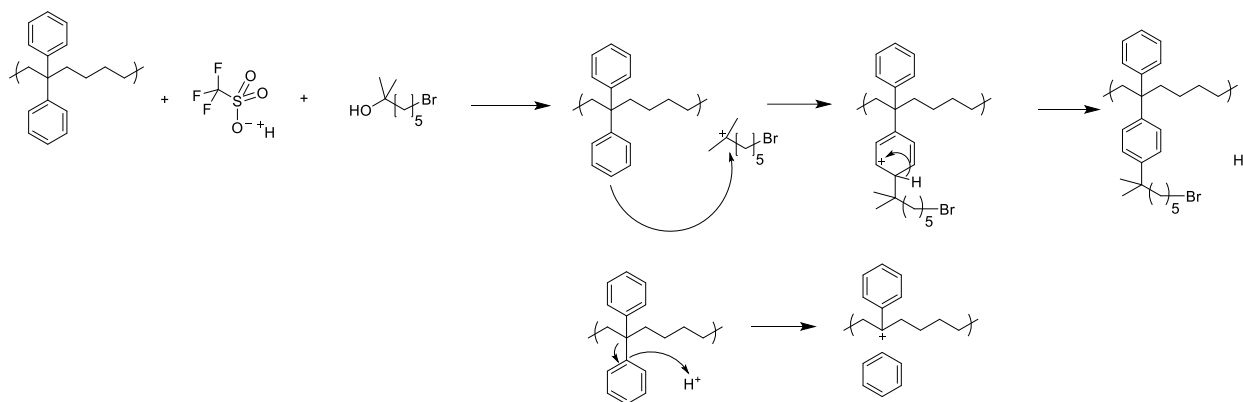


Figure 21. Mechanism of Friedel-Crafts bromoalkylation of DPE/E showing possible degradation mechanism of tertiary carbocation on polymer backbone stabilized by aromatic group.

The degree of functionalization was controlled by controlling the amount of brominating agent that was added; the reaction proceeded at 95-99% efficiency. The efficiency was determined by the degree of functionalization compared to the stoichiometric ratio of phenyls and brominated

agent added. The degree of functionalization was determined by the ratio of integrations of the aromatic hydrogens and the hydrogens on the carbon adjacent to the bromide.

3.3.4 Quaternization

After bromo-functionalization of the precursor polymers, the polymers were quaternized with trimethylammonium (TMA) in ethanol from PS-Br and DPE/E-Br to PS(QA) and DPE/E(QA), respectively. The quaternized forms of the polymers contain a quaternary ammonium with a positive charge, seen in Figure 22.

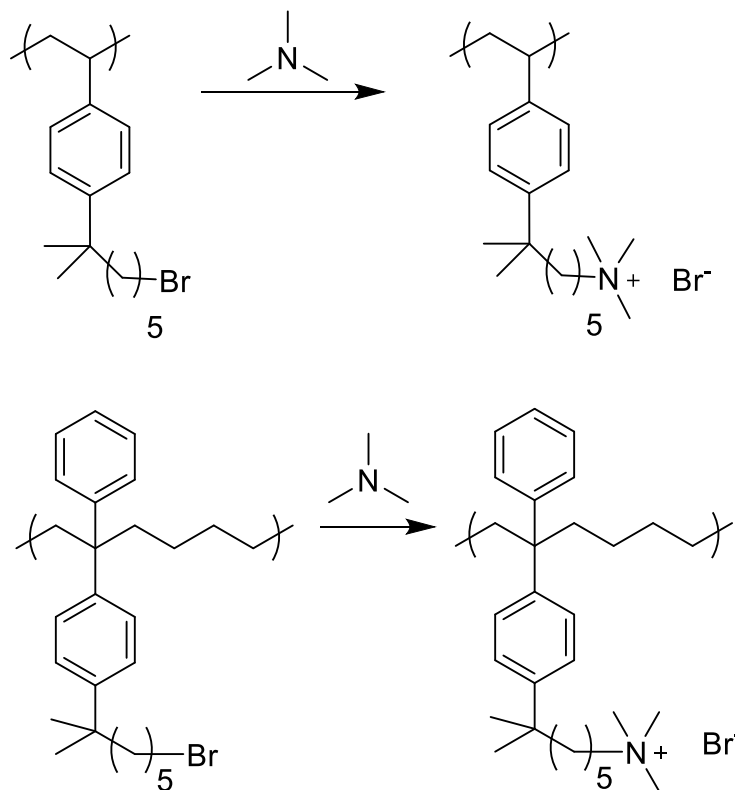


Figure 22. Quaternization of PS-Br and DPE/E-Br.

By dissolving the Br precursor in THF then added a stoichiometric excess of TMA solution, 100% quaternization was achieved. The exact conditions are detailed in the experimental sections. The difficulties of the homogeneous quaternization came in collecting the quaternized polymer. The quaternized polymer precipitated in several solvents, but was difficult to collect in order to

cast. To avoid the problem of collecting the quaternized polymer, DMSO was added to the homogeneous reaction mixture and the entire solution was solvent cast. The differences in boiling points of the solvents used, THF, ethanol, and DMSO, allowed for the evaporation of the volatile solvents so the quaternized polymer was only in the high boiling DMSO for the solvent casting. This allowed for slow casting which allows for the aggregation of the charged moieties and formation of ion conduction portions of the polymer.

3.3.5 Film Casting

Films were cast in conditions described in the experimental. A glass petri dish (Duroplan, DWK Life Sciences) was used due to the levelness of the dish. A perfectly level dish allows for an even membrane, which is ideal for practical use. However, when the quaternized polymers were cast in these glass dishes, they did not form a good film. The charged polymers aggregated on charged parts of the glass, leaving a broken scattering of polymer that stuck to the dish, rather than a uniform film that could be collected. To get a usable film, an aluminum weigh boat was used (Aluminum Smooth Weigh Dish, VWR). While this allowed for a usable film to be cast, it was far from ideal in several ways. First, the mass-produced weigh boats are not level like the glass petri dishes, so it is unable to produce a film with uniform thickness. Additionally, the weigh boats are easy to bend, so using one weigh boat for multiple castings is difficult. Using different weigh boats of varying degrees of levelness leads to films with differing amounts of uniformness in thickness. Several alternatives were tested, and the best was determined to be a petri dish made from PFA (perfluoroalkoxy alkane, Saint-Gobain Chemware). The dish is not uniformly level, so it does not provide films of uniform thickness, but using the same dish for each casting allows for the thickness to be consistent across samples. This was determined to be the most repeatable and consistent form of film casting, and was used to cast the films for this work.

The quaternized films were characterized by measuring the IECs using Mohr titration. Measuring the IEC confirmed that the homogeneous quaternization was successful in converting 100% of the Br groups to quaternary ammonium groups. After the IECs were confirmed, the films were ion exchanged to prepare for conductivity testing, detailed in 3.2.12. Ion Exchange Capacity (IEC) Measurements.

3.3.6 Differential Scanning Calorimetry

Prior to the quaternization of the Br-polymers, differential scanning calorimetry (DSC) was performed to find the T_g following the procedure detailed in the experimental. DSC was performed with the Br precursor rather than the final QA polymer because the charged group greatly lowers the T_g and the effect of the degree of functionalization is harder to determine. The T_g 's of the polymer series are listed in Table 1 and Table 2, and are plotted as a function of degree of functionalization in Figure 23. The T_g 's of the base, unfunctionalized polymers are within 5°C of each other and mirror each other as the IEC increases. This result is not surprising, given the similarity in structure, which leads to near identical IEC at the same degree of functionalization, and original T_g 's.

Table 1. T_g 's of DPE/E-Br at various degree of functionalizations.

Polymer	Degree of Functionalization (%)	IEC (meq./g)	T_g (°C)
DPE/E	0	0	103
DPE/E-Br-0.38	5	0.38	94
DPE/E-Br-0.83	12	0.83	90
DPE/E-Br-1.00	15	1.00	87
DPE/E-Br-1.43	24	1.43	77
DPE/E-Br-1.72	31	1.72	74
DPE/E-Br-1.99	39	1.99	65

Table 2. T_g 's of PS-Br at various degrees of functionalizations.

Polymer	Degree of Functionalization (%)	IEC (meq./g)	T_g (°C)
PS	0	0	100
PS-Br-0.72	10	0.72	89
PS-Br-1.01	15	1.01	83
PS-Br-1.22	19	1.22	86
PS-Br-1.45	24	1.45	76
PS-Br-1.95	37	1.95	64
PS-Br-2.08	41	2.08	59

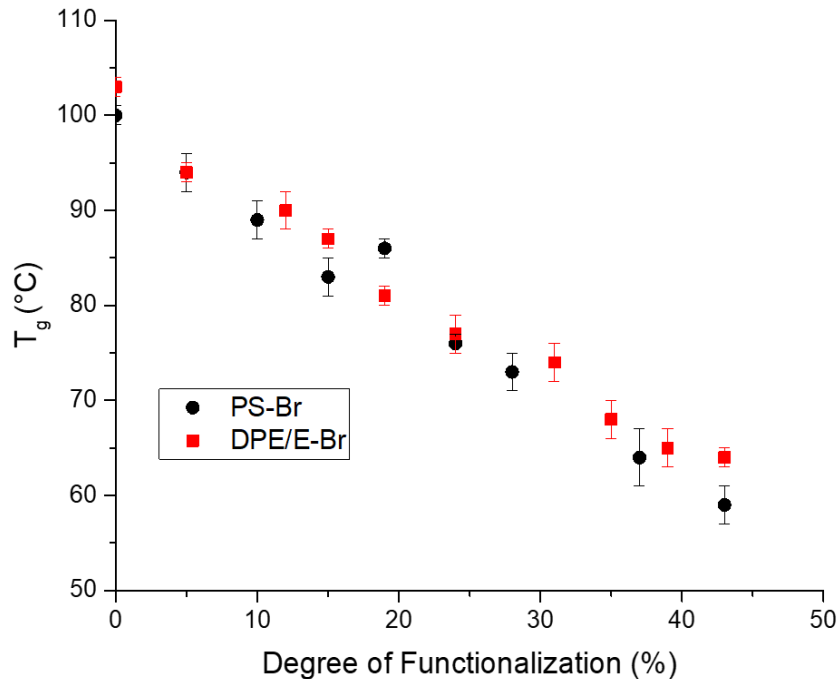


Figure 23. Glass transition temperatures (T_g 's) of PS-Br and DPE/E-Br, showing a decrease in T_g with increasing degree of functionalization.

3.3.7 Conductivity

Ion exchange capacities IEC of quaternized polymers was measured by Mohr titration, detailed in the experimental section, and compared with theoretical IEC from ^1H NMR of the brominated precursor. The titration IEC was found to be within experimental error of the theoretical IEC. Ion conductivity (σ) was measured with Cl^- counterions. Conductivity of DPE/E(QA) generally increased as IEC and temperature increased. The results are summarized in Table 3 and Table 4 and are depicted in Figure 24 through Figure 27 below.

Table 3. Cl⁻ conductivity of DPE/E(QA).

Polymer	Theoretical IEC (meq./g) ^a	Experimental IEC (meq./g) ^b	Cl ⁻ Conductivity (mS/cm)		
			30°C	60°C	80°C
DPE/E(QA)-0.38	0.38	0.40	0.5	0.5	0.4
DPE/E(QA)-0.83	0.83	0.87	0.6	1	1
DPE/E(QA)-1.00	1.00	1.08	0.5	1	4
DPE/E(QA)-1.43	1.43	1.46	5	18	38
DPE/E(QA)-1.72	1.72	1.74	8	22	36
DPE/E(QA)-1.99	1.99	2.05	12	37	38

^aCalculated from degree of bromination, reported in OH⁻ form. ^bMeasured via Mohr titration in Br⁻ or Cl⁻ form, converted and reported in OH⁻ form.

Table 4. Cl⁻ conductivity of PS(QA).

Polymer	Theoretical IEC (meq./g) ^a	Experimental IEC (meq./g) ^b	Cl ⁻ Conductivity (mS/cm)		
			30°C	60°C	80°C
PS(QA)-0.72	0.72	0.74	0.3	0.3	0.5
PS(QA)-1.01	1.01	1.05	1.5	6.1	15
PS(QA)-1.22	1.22	1.33	3.4	12	25
PS(QA)-1.45	1.45	1.50	5.9	25	30
PS(QA)-2.08	2.08	2.10	25	25	0.8

^aCalculated from degree of bromination, reported in OH⁻ form. ^bMeasured via Mohr titration in Br⁻ or Cl⁻ form, converted and reported in OH⁻ form.

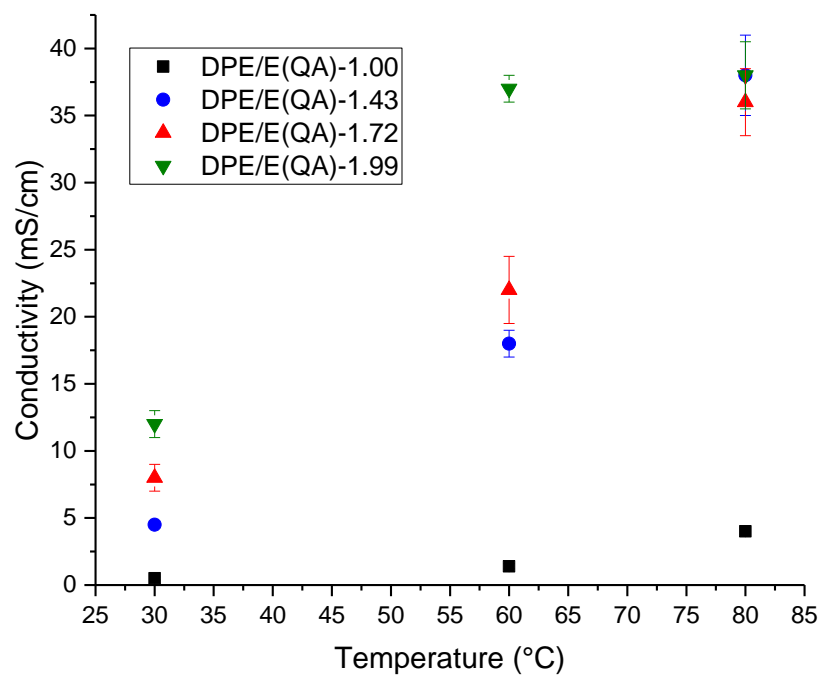


Figure 24. Cl⁻ conductivity of DPE/E(QA)-IEC.

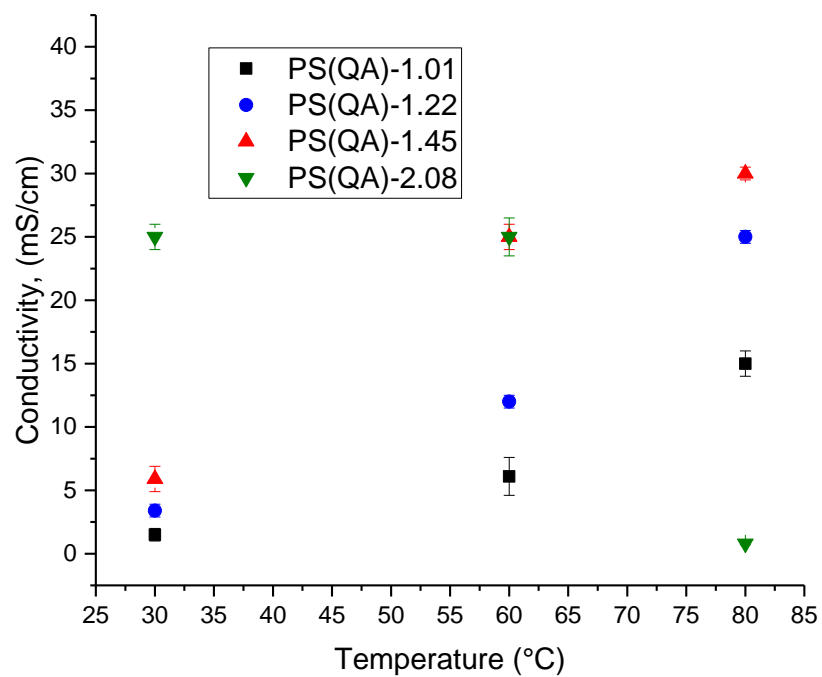


Figure 25. Cl⁻ conductivity of PS(QA)-IEC.

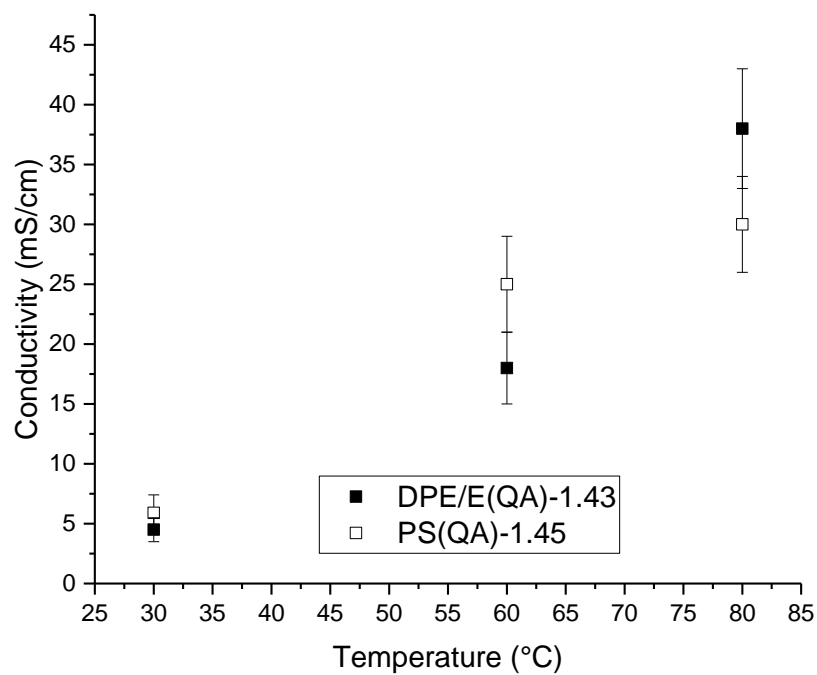


Figure 26. Cl⁻ conductivity of DPE/E(QA) and PS(QA) at IEC ~1.5 meq./g, showing nearly identical conductivity.

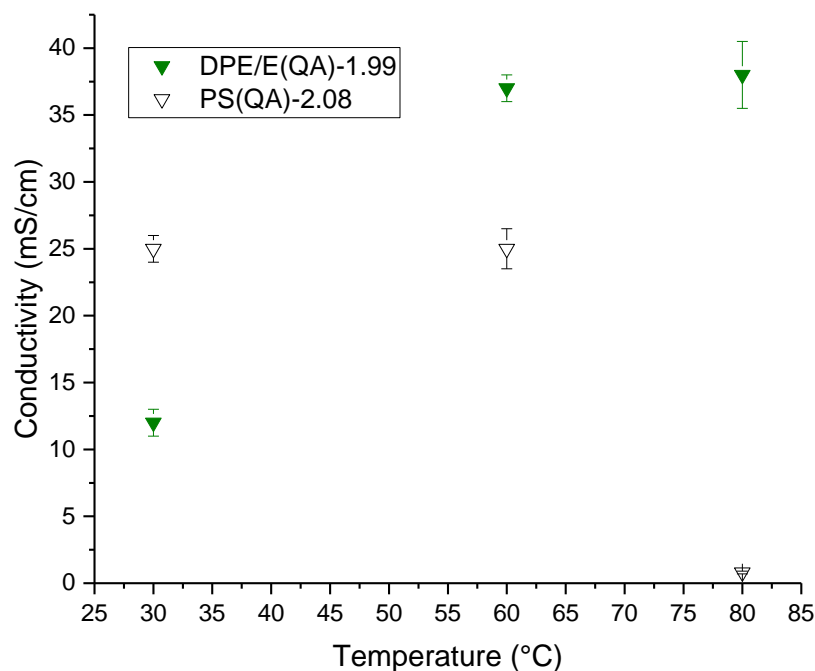


Figure 27. Cl⁻ conductivity of DPE/E(QA) and PS(QA) at IEC~2.0 meq./g, PS(QA)-2.08 conductivity drops to 0 mS/cm at high temperature (80°C) while DPE/E(QA)-1.99 maintains conductivity of 40 mS/cm.

At lower IECs, the conductivity of the DPE/E(QA) and PS(QA) series are nearly indistinguishable. As they have similar structures, IECs, and T_g 's, this is not unexpected. At higher IEC, approximately 2.0 meq./g, a major difference is observed. At 80°C, the operating temperature of a typical AEM fuel cell, PS(QA)-2.08 is no longer conductive. Upon removal from the conductivity setup, it is seen to be gel like, seen in Figure 28. DPE/E(QA)-1.99, however, withstood the elevated temperature and continued conducting.

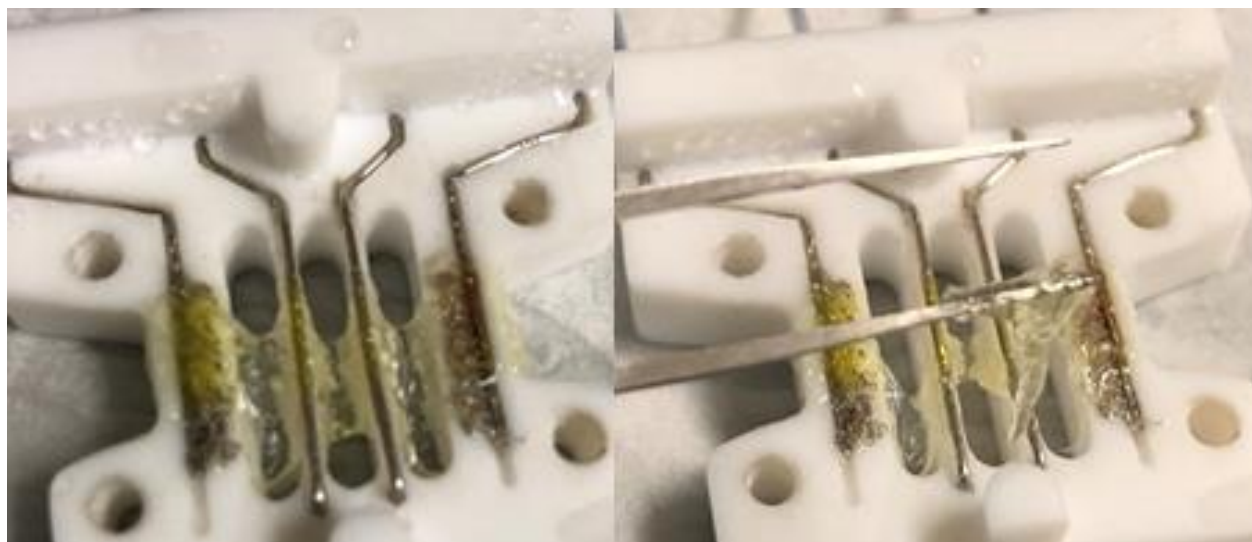


Figure 28. PS(QA)-2.08 after Cl⁻ conductivity measurement at 80°C, the film does not maintain its form, is very gel like, and is impossible to collect in one piece.

Table 5. OH⁻ conductivity of DPE/E(QA).

Polymer	Theoretical IEC (meq./g) ^a	Experimental IEC (meq./g) ^b	Cl ⁻ Conductivity (mS/cm)		
			30°C	60°C	80°C
DPE/E(QA)-1.50	1.50	1.46	10.64	22.54	40.06
DPE/E(QA)-2.02	1.99	2.05	8.26	14.60	19.92

^aCalculated from degree of bromination, reported in OH⁻ form. ^bMeasured via Mohr titration in Br⁻ or Cl⁻ form, converted and reported in OH⁻ form.

Table 6. OH⁻ conductivity of PS(QA).

Polymer	Theoretical IEC (meq./g) ^a	Experimental IEC (meq./g) ^b	Cl ⁻ Conductivity (mS/cm)		
			30°C	60°C	80°C
PS(QA)-1.50	1.50	1.52	10.12	22.09	35.00
PS(QA)-2.02	2.02	2.05	11.73	16.57	9.325

^aCalculated from degree of bromination, reported in OH⁻ form. ^bMeasured via Mohr titration in Br⁻ or Cl⁻ form, converted and reported in OH⁻ form.

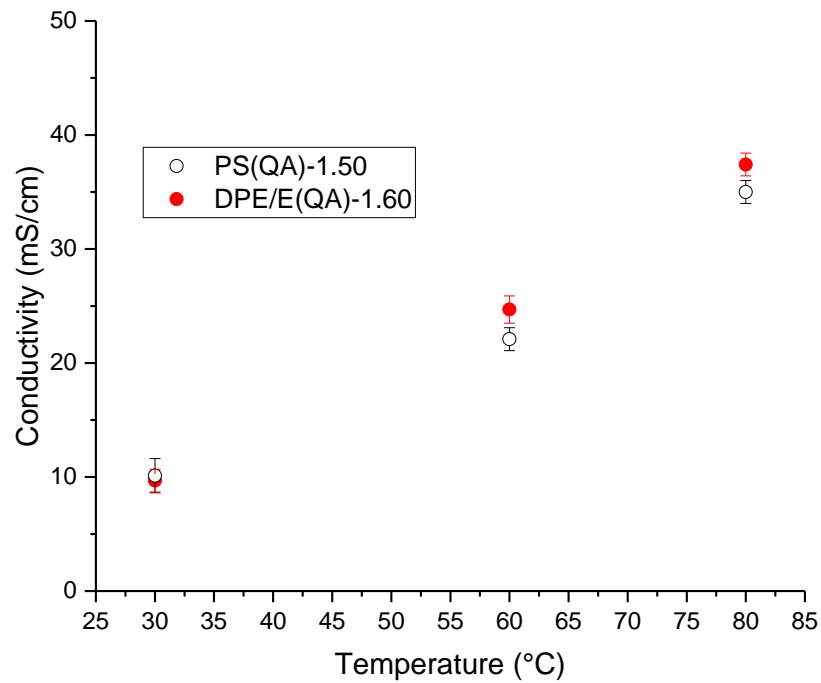


Figure 29. OH⁻ conductivity of DPE/E(QA) and PS(QA) at IEC~1.5 meq./g, showing no significant differences between the two species.

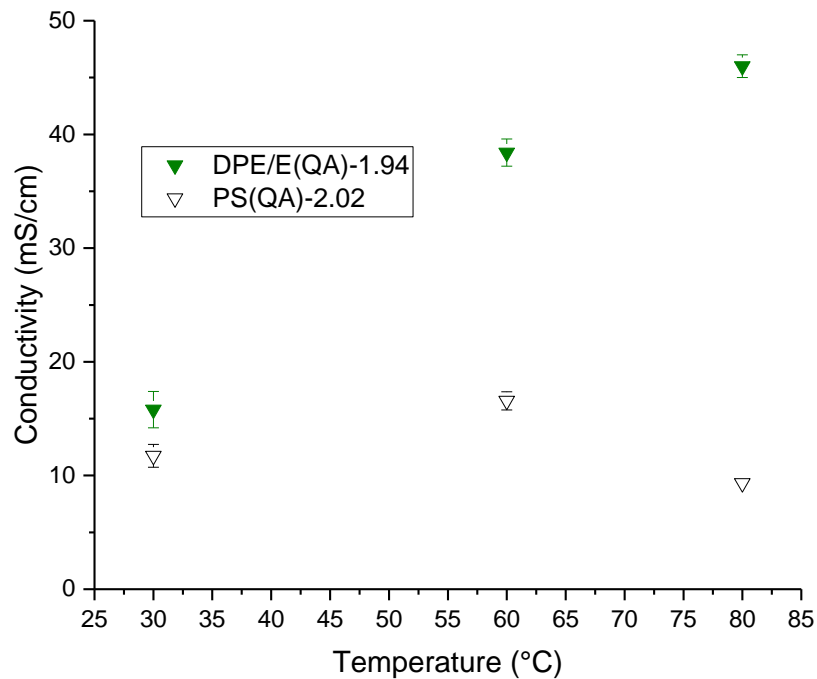


Figure 30. OH⁻ conductivity of DPE/E(QA) and PS(QA) at IEC~2.0 meq./g, PS(QA)-2.02 conductivity drops to 9 mS/cm at high temperature (80°C) while DPE/E(QA)-1.94 maintains conductivity of 46 mS/cm.



Figure 31. PS(QA)-2.02 after OH⁻ conductivity measurement at 80°C, the film does not maintain its form, is very gel like, and is impossible to collect in one piece.

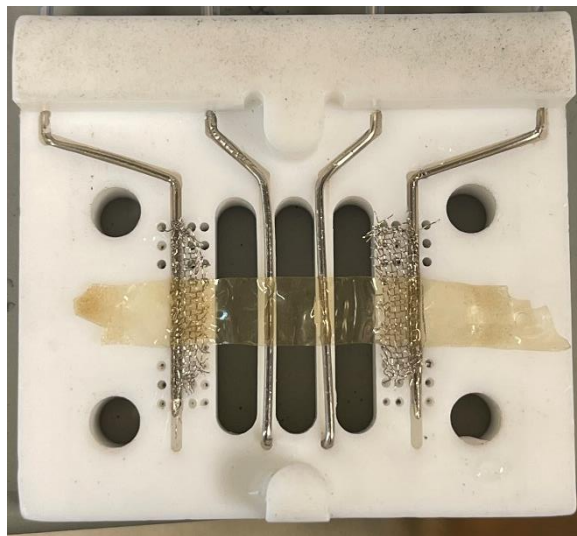


Figure 32. DPE/E(QA)-1.94 after OH⁻ conductivity measurement at 80°C, the film maintains its form with no noticeable difference after the measurement.

The hydroxide conductivity of DPE/E(QA) and PS(QA) showed similar trends to the chloride conductivity, seen in Figure 29 and Figure 30. At lower IEC, approximately 1.5 meq./g, conductivity was nearly identical between the two series. At higher IEC, near 2.0 meq./g, the two polymers were nearly identical in conductivity again, until the system was heated to 80°C. At 80°C, PS(QA)-2.08 steadily dropped in conductivity before levelling off at about 9 mS. When the conductivity cell was removed from the setup, the strip of PS(QA)-2.08 had lost all mechanical integrity, seen in Figure 31. Trying to remove the gel from the setup resulted in bits sticking to the tweezers and to the setup. Conversely, DPE/E(QA)-1.99 was able to withstand the elevated temperature and continue conducting, seen in Figure 32.

3.3.8 Water Uptake

To investigate the differences in conductivity observed between PS(QA) and DPE/E(QA), the water uptake of the two polymers were measured. The water uptake (WU) for both PS(QA) and DPE/E(QA) was calculated as: $WU(\%) = [(W_{hydrated} - W_{dry}) \times 100] / W_{dry}$

where $W_{hydrated}$ and W_{dry} are the weights of the patted-dry water swollen and dry membranes, respectively. Dry membranes were prepared under dynamic vacuum at 80°C. Hydrated membranes were prepared by soaking in deionized water overnight.

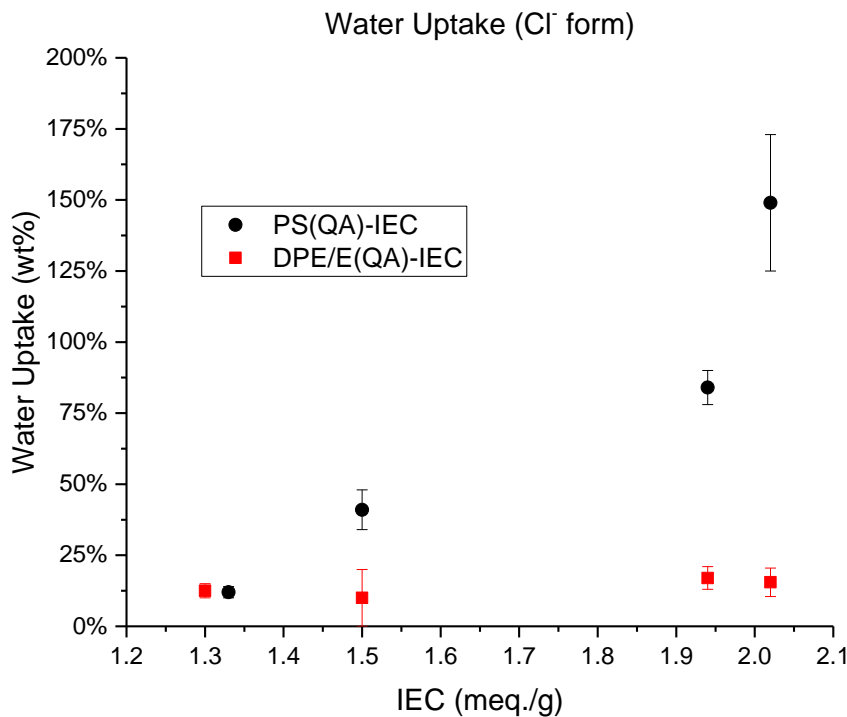


Figure 33. Water uptake of DPE/E(QA) and PS(QA) with Cl⁻ counterion, PS(QA) water uptake increases significantly with IEC while DPE/E(QA) maintains a water uptake of ~15% regardless of IEC.

The water uptakes of the polymer series in their chloride forms results show a stark contrast between the two polymer series, seen in Figure 33 and Figure 34. The PS(QA) polymer saw large amounts of water imbibed, whereas the DPE/E(QA) series did not absorb much water at all. The difference becomes more apparent at high ion content, where hydrated PS(QA) is doubling in mass over its dry form, but DPE/E(QA)'s mass increases by less than 20%. An interesting aspect of the water uptake of DPE/E(QA) is that as its IEC increased, its water uptake did not. This bucks the trend observed in anion exchange membranes of water uptake increasing as the ion content

increases, which can easily be seen in the PS(QA) series. This finding is incredibly fascinating, as a common obstacle for anion exchange membranes is detrimental water uptake at high IECs desired for improved conductivity.

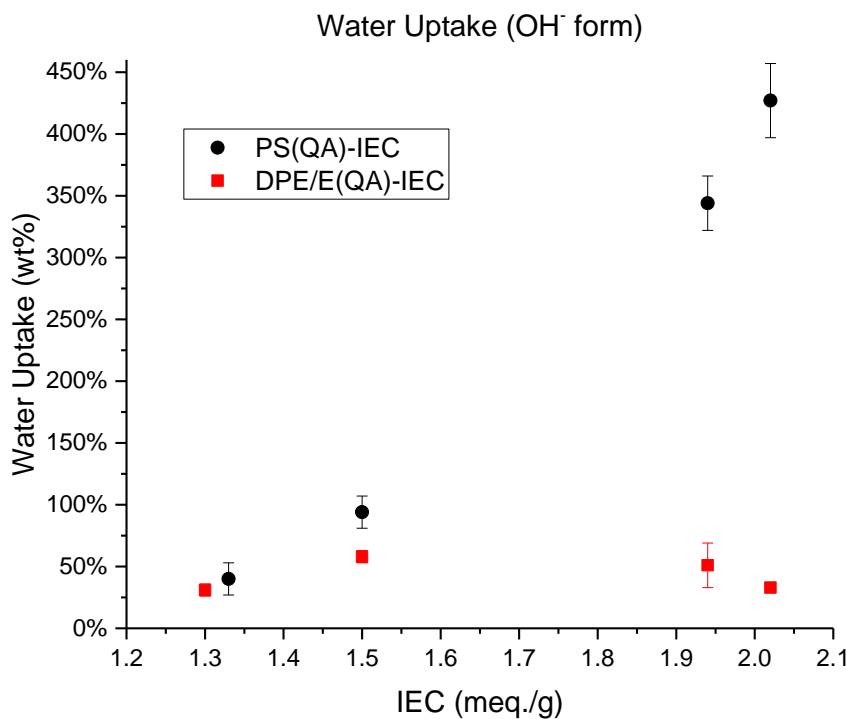


Figure 34. Water uptake of DPE/E(QA) and PS(QA) with OH⁻ counterion, PS(QA) water uptake increases significantly with IEC while DPE/E(QA) maintains a water uptake of ~50% regardless of IEC.

The polymers exhibit a similar trend in water uptake when the chloride counterion is replaced with a hydroxide counterion. As the ion content of PS(QA) increases, the water uptake increases significantly, absorbing over 300 wt% at IEC near 2.0 meq./g. Meanwhile, DPE/E(QA) with hydroxide counterions exhibited a similar water uptake trend as with chloride counterions, having much lower water uptake than its PS(QA) counterpart at high IEC and steady water uptake as IEC increased, bucking the trend of water uptake increasing with IEC. To explain this observation, one can look at the polymer backbones, seen in Figure 35.

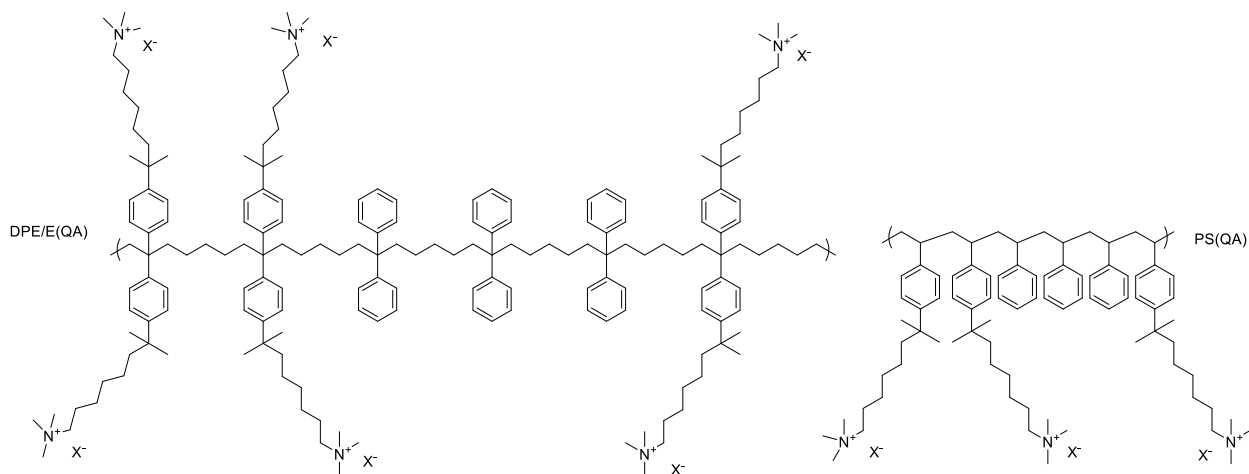


Figure 35. Potential backbone segments of DPE/E(QA) and PS(QA), both segments have functionalization of 50% and 3 consecutive repeat units without functionalization, DPE/E(QA), however, has a much longer chain segment between functionalized phenyls.

The DPE/E backbone offers two major differences in backbone structure from PS: two phenyl groups on the same carbon instead of one and five carbons between carbons with phenyl groups for DPE/E versus just one for PS. Both of these aspects of the DPE/E backbone can help improve the conductivity and water uptake of the DPE/E(QA) AEM; each allow for better ion aggregation.

Two phenyl groups on a single repeat unit allow for the possibility of two functional groups on a single repeat unit. We know bifunctional repeat units are possible with DPE/E without steric hinderance pushing the bromoalkyl groups to functionalize only one phenyl per repeat unit since 100% functionalization of poly(1,1-diphenylethylene-alt-tert-butyl-styrene) (DPE/tBS) is possible.¹⁵⁸ Seen in Figure 35, two functionalized phenyls on the same carbon allow for easier ionic aggregation, as the six-carbon spacer between the aromatic ring and the cation allow the cations the mobility to freely aggregate, while remaining close enough, by virtue of being bonded to the same carbon in the backbone, to easily find each other. Repeat units with multiple functional

groups are more ion rich and hydrophilic than repeat units with only one functional group. The possibility of two functional groups on a single repeat unit also increases the number of repeat units with no functional groups. More repeat units without functional groups create more polymer rich and hydrophobic regions in the polymer chain. Multiple of these unfunctionalized repeat units sequentially would especially contribute to the formation of thick polymer rich regions. Each of these aspects allow for better ion aggregation, allowing for better formation of ion rich (hydrophilic) regions and polymer rich (hydrophobic) regions.

Table 7. Properties of functionalized DPE/tBS copolymer, adapted from ¹⁵⁸.

	DoF^a	Projected IEC (OH⁻)^b	M_n (kg/mol)^c	M_w (kg/mol)^c	D^c	T_g (°C)^d
DPE/tBS	n/a	n/a	200	250	1.2	195
DPE/tBS(Br)-0.13	0.13	0.7	230	310	1.3	175
DPE/tBS(Br)-0.25	0.25	1.1	250	350	1.4	161
DPE/tBS(Br)-0.29	0.29	1.3	250	330	1.3	159
DPE/tBS(Br)-0.43	0.43	1.7	240	310	1.3	146
DPE/tBS(Br)-0.56	0.56	2.0	260	350	1.4	135
DPE/tBS(Br)-0.75	0.75	2.4	220	300	1.4	121
DPE/tBS(Br)-1.00	1.00	2.8	230	340	1.5	113

^aDegree of Functionalization, fraction of phenyls functionalized, determined from ¹H NMR. ^bDetermined from ¹H NMR. ^cMeasured by GPC. ^dMeasured by DSC.

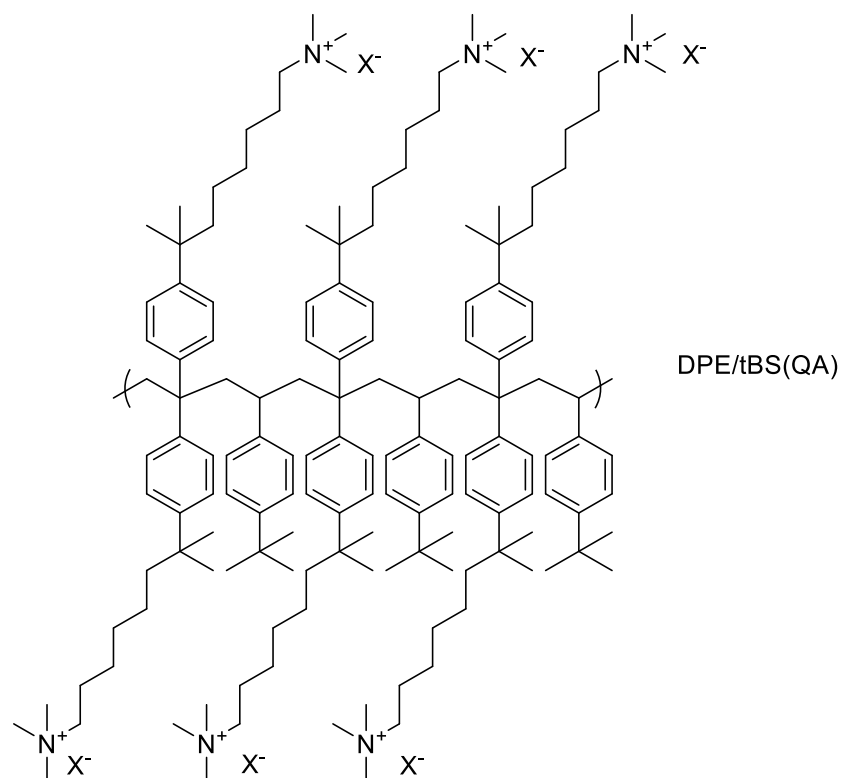


Figure 36. 100% functionalized DPE/tBS(QA), adapted from ¹⁵⁸.

Moreover, the five carbons of space between phenyl groups in the polymer backbone allow the backbone to orient itself more easily to facilitate the aggregation of cations much better than just one carbon in between aromatic groups in polystyrene. This, again, allows for better ion aggregation, allowing for better formation of ion rich (hydrophilic) regions and polymer rich (hydrophobic) regions. Combined, these allow for thicker hydrophobic regions; thicker hydrophobic limit the swelling of the hydrophilic regions, which in turn limits the water uptake. This aspect of the DPE/E backbone leads to better membrane properties, compared to membranes from a very similar backbone in PS.

3.4 Conclusions

We synthesized and characterized AEMs based on DPE/E polymer backbones analogous to AEMs based on PS backbones. Each polymer was modified via Friedel-Crafts bromoalkylation

to attach bromofunctional groups for quaternization. The DPE/E polymer backbones exhibited lower water uptake at higher IECs than its PS counterpart, while still conducting anions, something its PS counterpart was unable to match. The polymer backbone made this possible, as the DPE/E backbone allows for improved formation of both hydrophilic regions, which improve conductivity, and thicker hydrophobic regions, which limits water uptake. Polystyrene backbones could not achieve this kind of microphase separation, demonstrated by the catastrophic water uptake at IECs around 2.0. This decreased water uptake observed in DPE/E(QA) offers the potential for high conductivity, low water uptake AEMs. DPE/E(QA) can be used in polymer systems, which allow for improved morphologies in AEM applications, to improve on membrane properties over AEMs with polystyrene, which are commercially available.

Currently, DPE/E(QA) is not suitable to be used as a standalone anion exchange membrane due to its brittle nature and relatively low ion conductivity. It can, however, be used in a block copolymer system, specifically a triblock copolymer system utilizing DPE/E(QA) as symmetric outer blocks with a rubbery midblock of poly(ethylene-*co*-butylene) to improve on the mechanical properties as well as the conductivity due to more complex morphologies available to triblock copolymers as opposed to homopolymers. Polystyrene has been studied in such a system, polystyrene-*b*-poly(ethylene-*co*-butylene)-*b*-polystyrene (SEBS), and suffered from excessive water uptake and swelling.¹⁵⁹ Utilizing low water uptake DPE/E(QA) can mitigate the water uptake of the triblock AEM, leading to improved ion conductivity and membrane performance.

4. Cyclized Poly(1,1-diphenylethylene-*alt*-butadiene) with Glass Transition Temperature Above 200°C

4.1 Introduction

In order to optimize water uptake, that is to have enough water uptake to hydrate ion-conducting channels but not too much water that will cause mechanical failure, the drivers of water uptake in polymeric ion exchange membranes must be understood. Two commonly used strategies to combat the mechanical instabilities caused by excessive water uptake are physical and chemical crosslinking.¹⁵⁹⁻¹⁶⁵ Each strategy lowers the overall membrane IEC by adding non-ionic chain segments to improve mechanical strength. Furthermore, chemical crosslinking can lead to reduced membrane flexibility, excessively increased molecular weight that make the crosslinked polymer insoluble, and impede the formation of continuous ion-conducting channels which lowers conductivity.⁸⁶ Chemical crosslinking is used as a strategy because it improves membrane toughness by reducing the molecular weight between entanglements (M_e).¹⁶⁶⁻¹⁶⁷

An alternative means to avoid excessive water uptake is by using a backbone polymer with an elevated glass transition temperature to reduce the osmotic swelling. The free volume within a polymer controls its glass transition temperature (T_g); with low free volume, the polymer chains are packed closely and the resulting T_g is high, while polymers with more flexible backbones tend to have lower T_g 's.^{1, 168} Polymers with higher free volume tend to have higher segmental mobility, so the glass transition temperature is able to provide information about the local polymer segmental motion.^{1, 168-170}

Glassy polymers, while seen as solids, will flow when an applied stress supplies sufficient energy to the chains to rearrange into a more equilibrium configuration.¹ A higher T_g polymer will

more strongly resist this onset of chain flow, allowing for better accommodation of water uptake. Furthermore, a polymer's T_g impacts a polymer's mechanical recovery after it is deformed, impacting the performance of the membrane.^{1, 166, 171}

Another membrane property impacted by the glass transition temperature is membrane aging, where polymer chains gradually shift from their kinetically trapped state to their thermodynamic equilibrium configuration as they undergo structural relaxations in the glassy state.^{166, 172} Aging involves lowering the free volume and entropy, making the material stiffer and more brittle as it shifts to more glass-like and less rubber-like; as such, the polymer's T_g impacts the membrane aging process.^{166, 172} Aging is also impacted by the polymer's fractional free volume and chain stiffness.¹⁷²⁻¹⁷³ Stiffer polymers, polymers having a larger characteristic ratio (C_∞), are more brittle and have slower rates of aging and flow (creep), while more ductile polymers, due to their higher segmental mobility, have better ability to dissipate an applied force and thus age more quickly.¹⁷³⁻¹⁷⁵

High glass transition temperature polymers like poly(ether imide) (PEI, $T_g = 215^\circ\text{C}$),¹⁷⁶ poly(sulfone) (PSU, $T_g = 190 - 220^\circ\text{C}$),¹⁷⁷⁻¹⁸² and poly(phenylene oxide) (PPO, $T_g = 220^\circ\text{C}$)^{96, 113, 183-184} are common engineering thermoplastics and have been investigated as ion-exchange membrane backbones and have shown a high T_g backbone is valuable in resisting catastrophic water uptake.

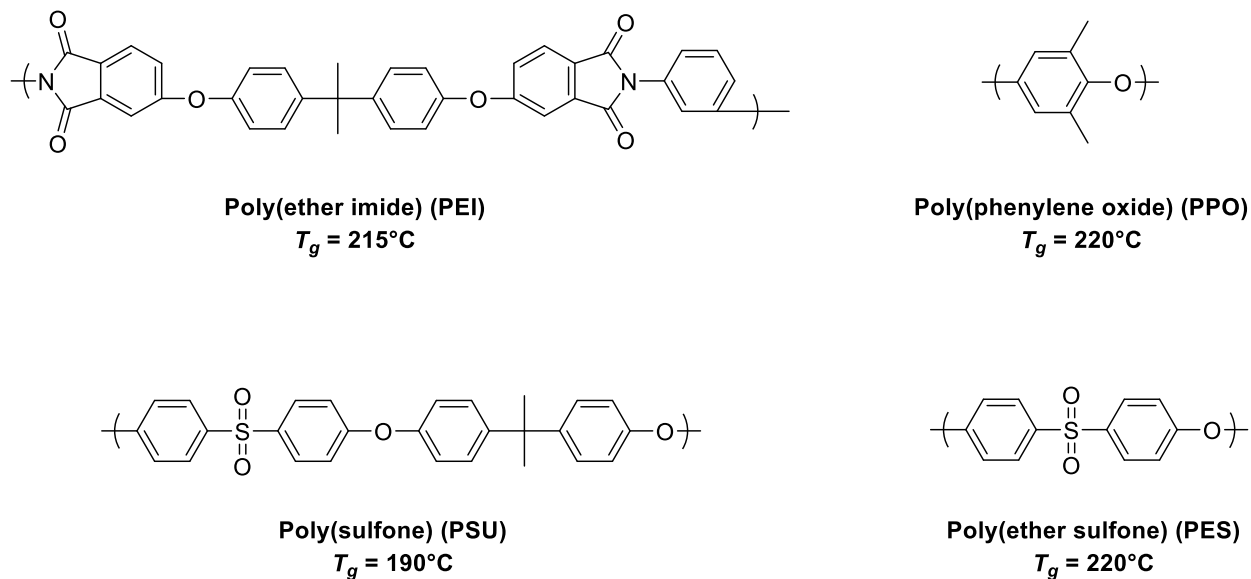


Figure 37. Various polymers with T_g 's around 200°C .

While the high glass transition temperature mitigates water uptake, the aryl ether bonds in the polymer backbone are vulnerable to degradation in alkaline environments.¹⁸⁵⁻¹⁸⁸ Thus, AEMs without these aryl-ether bonds are of the utmost interest, and AEMs with rigid polyphenylene backbones have been investigated as they exhibit less water uptake normalized against IEC than their polyolefin backbone counterparts.^{91, 93, 116, 189-195} For example, ionomers based on polystyrene ($T_g = 100^\circ\text{C}$) require block copolymer configuration as well as chemical crosslinking to produce mechanically stable AEMs.^{159, 161-162}

In the previous chapter, DPE/E(QA) was found to have improved conductivity over PS(QA) due to its ability to resist catastrophic water uptake at high IEC and temperature. This was despite the two precursor polymers, DPE/E and PS, having nearly identical glass transition temperatures. DPE/B can undergo intramolecular Friedel-Crafts cyclization to alkylate the double bonds present in the DPE/B backbone, forming 6 member rings into the backbone, making it much more rigid and increasing the glass transition temperature over 200°C .¹⁴⁶ In this work, cyclized

poly(1,1-diphenylethylene-*alt*-butadiene) (DPE/B-C) is synthesized, functionalized, and characterized for its AEM properties.

4.2. Experimental Details

4.2.1 Materials

Butadiene (Sigma-Aldrich) was purified twice over *n*-butyllithium and vacuum distilled. 1,1-diphenylethylene (TCI) was purified over *n*-butyllithium and vacuum distilled. Tetrahydrofuran (Sigma-Aldrich) was purified by passing through activated alumina (BASF F-200). Naphthalene (TCI), potassium (Acros Organics), ethyl 6-bromohexanoate (Alfa Aesar), methyl magnesium bromide (Alfa Aesar), anhydrous dichloromethane (Honeywell), trifluoromethanesulfonic acid (Alfa Aesar), sodium bicarbonate (EMD Millipore), dimethylsulfoxide (EMD Millipore), sodium chloride (Fisher), sodium nitrate (BDH), silver nitrate (Alfa Aesar), ethanol (Acros), and *n*-butyllithium (Aldrich), were used as received.

4.2.2 Potassium Naphthalenide

Potassium metal was collected in a Chemglass Airfree flask and dried. Naphthalene was added under positive argon pressure. Tetrahydrofuran was cannulated in, and the reaction mixture was stirred overnight. The potassium naphthalenide solution was used within two weeks to preserve the integrity of the electron transfer agent.

4.2.3 Polymerization

Poly(1,1-diphenylethylene-*alt*-butadiene) (DPE/B) alternating copolymer was synthesized by anionic polymerization.¹⁴⁴ In a reactor containing 1,1-diphenylethylene (DPE) in tetrahydrofuran under argon at 0°C, potassium naphthalenide was added to activate DPE. After enough time had passed to activate DPE, butadiene was added slowly. The reaction was allowed

to proceed for 14 hours to ensure completion. The living polymer chains were terminated with argon-purged methanol. The synthesized DPE/B polymer in tetrahydrofuran was precipitated in methanol, recovered, and dried under vacuum. The synthesized DPE/B was characterized by size exclusion chromatography using polystyrene standards, ^1H nuclear magnetic resonance, and differential scanning calorimetry.

4.2.4 Cyclization of DPE/B

Many reaction conditions were tested in optimizing the cyclization reaction, some of which can be seen in Table 8 in 4.3.1. Cyclization of Poly(1,1-diphenylethylene-*alt*-butadiene). The following is the reaction procedure that was used for the DPE/B-C that gave the best product and was used for the quaternized DPE/B-C(QA) that was characterized for its AEM properties.

DPE/B polymer (0.75g, 3.17 mmol repeat unit) was collected in an airfree flask, vacuum cycled with argon to remove moisture and atmospheric air, and dissolved in anhydrous dichloromethane at room temperature (2.5 wt% solution). The solution was cooled to -20°C using a dry ice bath with methanol and water (30% methanol, balance water), then trifluoroacetic acid (4.39 eq, 0.11 mL) was added to the solution. Triflic acid (0.25 equivalents, 0.07 mL) was added slowly. By diluting the triflic acid with trifluoroacetic acid (43 wt% triflic acid), the Hammett acidity function was lowered from 13.7 to 11.3.¹⁹⁶ This was done to curtail degradation observed in the reaction. The reaction was quenched by precipitating into methanol after 2 minutes. The polymer was collected, redissolved in dichloromethane, washed with saturated sodium bicarbonate to remove residual acid, then washed with distilled water to remove any salts. The polymer was then precipitated in methanol again, then dried under vacuum at 80°C .

4.2.5 Synthesis of Brominating Agent

7-bromo-2-methyl-2-heptanol was prepared based on a previous literature report.¹⁴⁷ Under argon atmosphere, ethyl 6-bromohexanoate (Alfa Aesar, 0.11 mmol) was diluted in dry tetrahydrofuran (120 ml), then cooled to 0°C, and methyl magnesium bromide solution (Alfa Aesar, 0.3 mol) was slowly cannulated to the solution. The reaction mixture was stirred for overnight before quenching with saturated ammonium chloride (NH₄Cl) in deionized water (~60mL). Synthesized 7-bromo-2-methyl-2-heptanol was extracted with diethyl ether twice, dried over magnesium sulfate, rotary evaporated to collect diethyl ether, vacuum distilled, and stored in a freezer in a dry box.

4.2.6 Acid-Catalyzed Friedel-Crafts Bromoalkylation of DPE/B-C

Acid-catalyzed Friedel-Crafts bromoalkylation reaction was used to functionalize the phenyl groups of DPE/B-C polymer with 7-bromo-2-methyl-2-heptanol to make alkylbromo-functionalized cyclized poly(1,1-diphenylethylene-*alt*-butadiene) (DPE/B-C-Br); the following is a representative procedure.¹⁴⁷ DPE/B-C polymer (0.5 g, 2.1 mmol repeat unit) was completely dissolved in anhydrous dichloromethane at room temperature. The polymer solution was chilled to -20°C using a dry ice bath with methanol and water (30% methanol, balance water). 7-bromo-2-methyl-2-heptanol (1.0g, 4.81 mmol) solution in anhydrous dichloromethane (5 ml) was slowly added to the DPE/B-C polymer solution using a syringe pump over 5 minutes. As soon as the first drop of the diluted 7-bromo-2-methyl-2-heptanol solution was added to the reactor, triflic acid (0.53mL, 1.0 mmol. molar ratio of triflic acid to 7-bromo-2-methyl-2-heptanol = 1.1) was injected to the reaction flask using a glass syringe to catalyze the functionalization reaction. The reaction was quenched after 10 minutes by precipitating the polymer in methanol. The polymer was collected, redissolved in dichloromethane, washed with saturated sodium bicarbonate to remove

and residual acid, then washed with distilled water to remove any salts. The polymer was then precipitated in methanol again, then dried under vacuum at 80°C.

4.2.7 Homogeneous Quaternization

DPE/B-C-Br was dissolved in tetrahydrofuran to form a 2.5 wt% solution. The amount of polymer was determined by targeting 50 µm films in various casting dishes. A 3x excess of trimethylamine, 33 wt% in ethanol, was added and stirred for 24 hours. Dimethylsulfoxide was added such that the quaternized polymer would be 2.5 wt% in dimethylsulfoxide. The mixture was allowed to vent for at least four hours to allow the odorous excess trimethylamine to dissipate. The quaternized cyclized poly(1,1-diphenylethylene-*alt*-butadiene) (DPE/B-C(QA)) solution was then cast in a controlled airflow oven at 80°C overnight, then collected for characterization.

4.2.8 Size Exclusion Chromatography (SEC)

The molecular weight and polydispersity of the synthesized DPE/B and PS polymers were characterized by a size exclusion chromatography system with a refractive index detector (SEC, Agilent). Three consecutive PLGel Mixed-C columns were used as the stationary phase, and tetrahydrofuran (30°C) at a flow rate of 1 mL/min was used as the mobile phase.

4.2.9 ¹H Nuclear Magnetic Resonance (¹H NMR)

The chemical composition and degree of functionalization were determined by ¹H NMR spectroscopy analysis (Agilent 500MHz spectrometer). Non-quaternized polymers were characterized at room temperature in either deuterated chloroform or deuterated tetrachloroethane and quaternized polymers were characterized using deuterated dimethylsulfoxide.

4.2.10 Differential Scanning Calorimetry

The glass transition temperatures of DPE/B-C and DPE/B-C-Br were characterized using differential scanning calorimetry (DSC) technique (TA instruments, Q2000) at a ramping rate 10 °C/min.

4.2.11 Ion Exchange Capacity (IEC) Measurements

IECs of membranes were determined by Mohr titration. The membranes with bromide or chloride counterions were dried under vacuum at 80°C, weighed, and immersed in an aqueous 0.5 M NaNO₃ solution for 48 hours. The NaNO₃ solution was titrated with a 0.1 M AgNO₃ aqueous solution using K₂CrO₄ as a colorimetric indicator.

4.2.12 Chloride Conductivity Measurements

Chloride ion conductivities (σ in mS/cm) of QA-PS and DPE/E(QA) membranes were measured using a four-point probe electrode method with BT-512 membrane conductivity test system (BekkTech LLC). Measurements were conducted in a fully hydrated condition where the cell was immersed in deionized water at 30°C, 60°C, and 80°C. The cell was equilibrated for at least 30 minutes before the conductivity measurement.

4.2.13 Chloride Water Uptake

Water uptake (WU) was calculated as $WU(\%) = [(W_{\text{hydrated}} - W_{\text{dry}}) \times 100] / W_{\text{dry}}$ where W_{hydrated} and W_{dry} are the weights of the patted-dry water swollen and dry membranes, respectively. The dry membrane was prepared under dynamic vacuum at 80°C.

4.2.14 Hydroxide Counterion Exchange

While AEMs are used in applications, such as fuel cells or electrolyzers, with hydroxide (OH⁻) counterions, they are rarely handled in hydroxide form during testing and characterization,

due to hydroxide readily reacting with carbon dioxide to form carbonate species, which lower the performance of the membrane.¹⁵⁶ AEMs with chloride (Cl⁻) counterions avoid this issue, making them easier to handle and characterize. However, since the OH⁻ form of membranes is what is used in application, it is valuable to characterize the membranes in hydroxide form as well as chloride form. In order to convert a membrane from chloride form to hydroxide form, the fully dried membrane is introduced to an argon filled glove box. There it is soaked in 1.0 M NaOH for 48 hours, rinsed with distilled water, then soaked in distilled water.

4.2.15 Hydroxide Water Uptake

Water uptake of the OH⁻ form of membranes was measured in an argon filled glovebox after exchanging the counter ion from chloride to hydroxide. Water uptake (WU) was calculated as $WU(\%) = [(W_{\text{hydrated}} - W_{\text{dry}}) \times 100] / W_{\text{dry}}$ where W_{hydrated} and W_{dry} are the weights of the patted-dry water swollen and dry membranes, respectively. The dry membrane was prepared under dynamic vacuum at 80°C. The hydrated membrane was soaked in water overnight, patted dry to remove surface water, then weighed.

4.2.16 Hydroxide Conductivity

Hydroxide ion conductivities (σ in mS/cm) of QA-PS and DPE/E(QA) membranes were measured using a four-point probe electrode method with BT-512 membrane conductivity test system (BekkTech LLC). Measurements were conducted in a fully hydrated condition where the cell was immersed in deionized water at 30°C, 60°C, and 80°C. The cell was equilibrated for at least 30 minutes before the conductivity measurement. Since the hydroxide counterion rapidly reacts with carbon dioxide, replacing OH⁻ with CO₃²⁻ and HCO₃⁻, the deionized water was bubbled with argon for an hour before adding the measurement and continued bubbling throughout.¹⁵⁷ The

membrane was moved from the argon glovebox in a sealed bag and quickly placed in the argon bubbled water to limit CO₂ exposure.

4.2.17 Mechanical Testing

Tensile stress-strain behavior of the membrane samples were obtained using a dynamic mechanical thermal analyzer (TA Q800) equipped with a temperature and humidity-controlled sample chamber. Membrane samples were equilibrated at 50 °C with 50% relative humidity (RH) over 1 h before testing. Rectangular test strips (5 mm × 15 mm) were strained at a load ramp of 0.5 N/min to a maximum of 18.0 N.

4.3 Results

4.3.1 Cyclization of Poly(1,1-diphenylethylene-*alt*-butadiene)

Poly(1,1-diphenylethylene-*alt*-butadiene) ($M_n = 240$ kg/mol, $D = 1.33$ for monodisperse, $M_n = 170$ kg/mol, $D = 1.25$ for bimodal) was synthesized via anionic polymerization described in the Experimental Details and visualized in Figure 38. The DPE/B polymer had a DPE to butadiene ratio of 1:1.08, and the butadiene was 88% 1,4 addition and 12% 1,2 addition, as measured by integration of peaks in the ¹H NMR. The reaction was found to have been run to completion by the lack of characteristic peaks of the 1,1-diphenylethylene monomer, with completion being the reaction of all present DPE. The SEC trace revealed a small peak prior to the main peak which can be attributed a negligible amount of coupling. Cyclization of the backbone was induced by the addition of triflic acid, detailed in the experimental details. In the optimizing of the cyclization reaction to mitigate or eliminate degradation of the polymer backbone, two different cyclized backbone species were observed. Cyclization was measured by ¹H NMR and DSC.

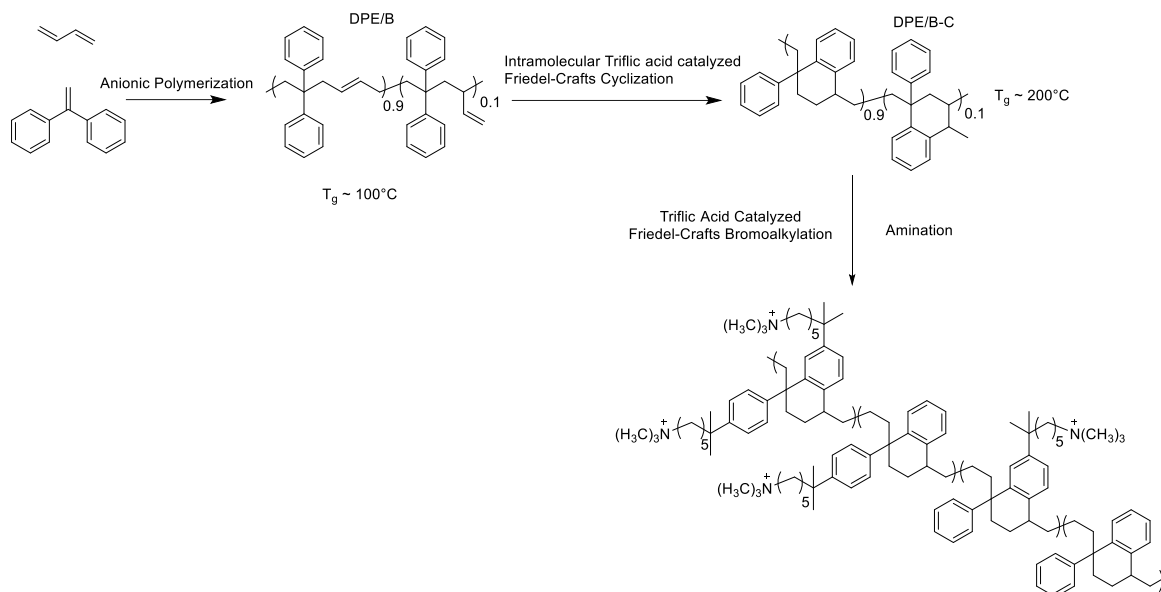


Figure 38. Anionic polymerization of DPE/B, followed by trific acid catalyzed intramolecular Friedel-Crafts cyclization, Friedel-Crafts bromoalkylation, and quaternization.

With a monodisperse backbone, the expected cyclization product was observed. In the ^1H NMR (Figure 39), cyclization was observed by the elimination of the characteristic double bond backbone peaks in the 5.5-6.5 region, the alkyl region grew in intensity and the aromatic peaks became much more broad, due to the formation of tetrahydronaphthyl bicyclic units¹⁴⁶.

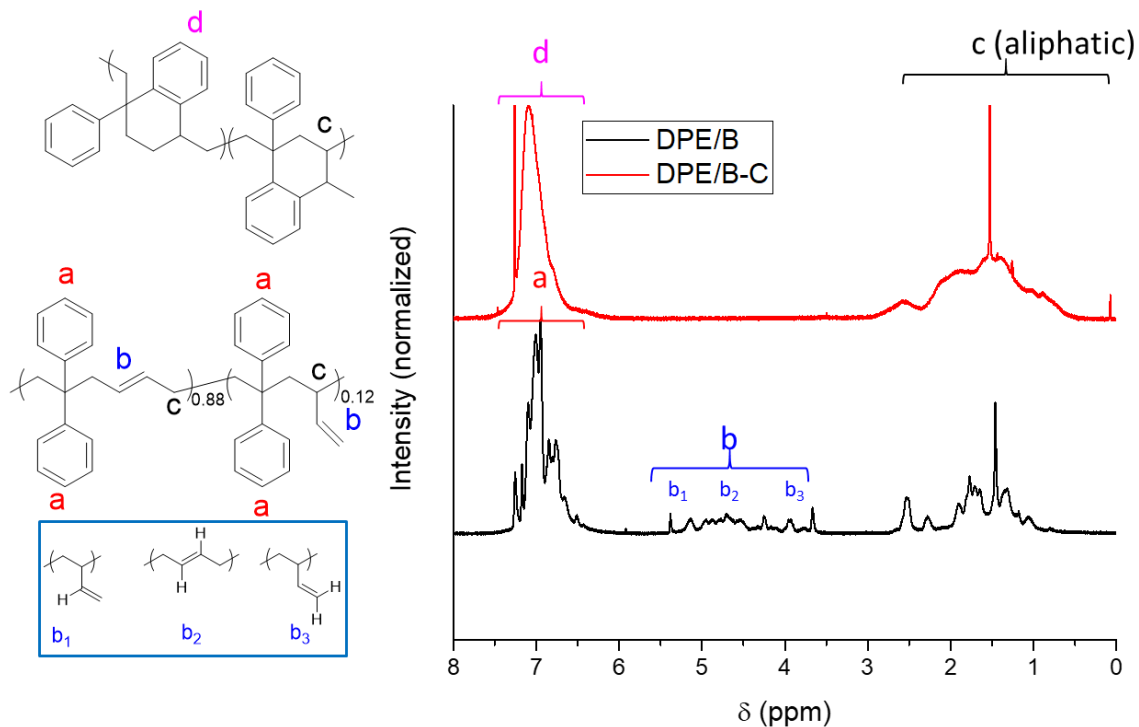


Figure 39. ^1H NMR of DPE/B and DPE/B-C from monodisperse DPE/B, cyclization was determined to have occurred by the loss of the alkene peaks (b) and the broadening of the aromatic region (a and d) and aliphatic region (c).

Cyclization was also confirmed by DSC. The DSC showed the T_g increased to around 210°C , seen in Figure 40. The increased T_g is indicative of a more rigid backbone, which comes from the cyclization of the backbone.

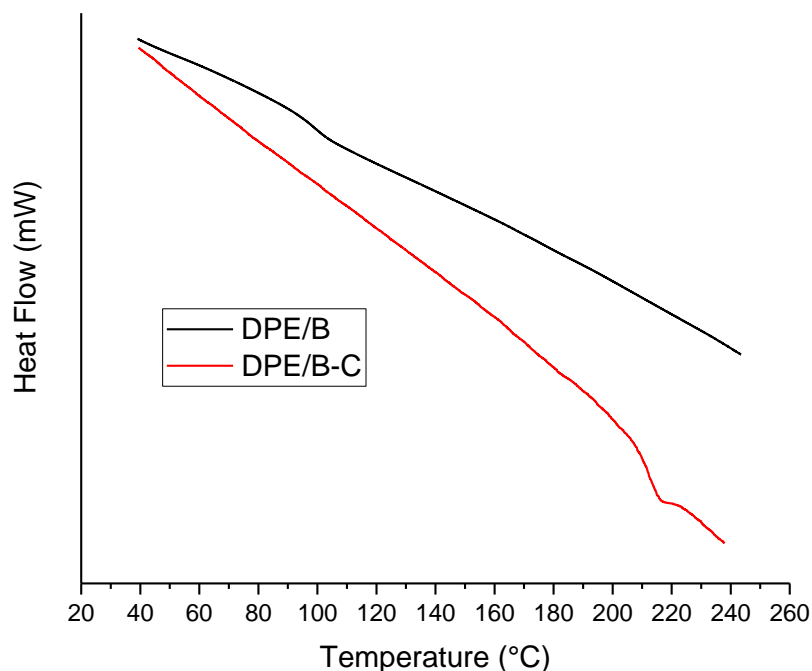


Figure 40. DSC of DPE/B-C from monodisperse DPE/B, compared to DPE/B.

The SEC trace of the cyclized product shows a shift in the retention time of the DPE/B-C in the SEC from DPE/B, when we do not expect a significant change in the molecular weight of the polymer after cyclization. This shift comes from the change in the hydrodynamic volume of the polymer backbone when it is cyclized, which dictates how long the polymer chains are retained in the column.¹ A change in the hydrodynamic volume alters the radius of gyration, changing the retention time of the polymer. The SEC chromatogram also shows degradation, indicated by the wider peak and the tail observed in the lower molecular weight region. To avoid this degradation, further optimization was pursued. The reaction was optimized by altering the polymer concentration, the acid concentration, and the reaction time and temperature, among other conditions. Table 8 shows some of the conditions used.

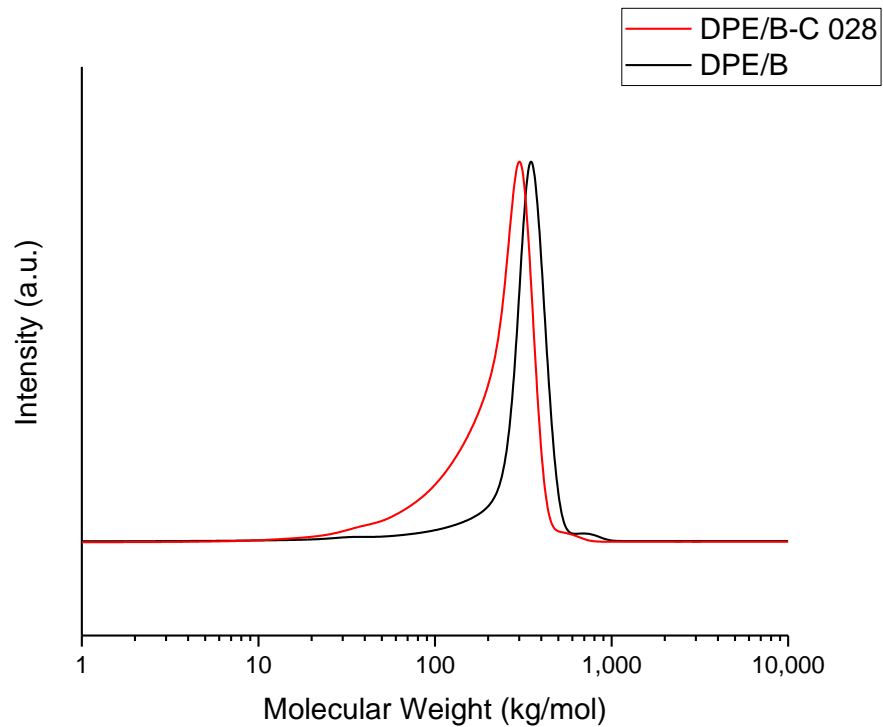


Figure 41. SEC chromatograms of DPE/B-C from monodisperse DPE/B, showing a shift in the molecular weight peak due to a change in hydrodynamic volume of the polymer backbone as well as an increase in dispersity from an increase in low molecular chains due to degradation.

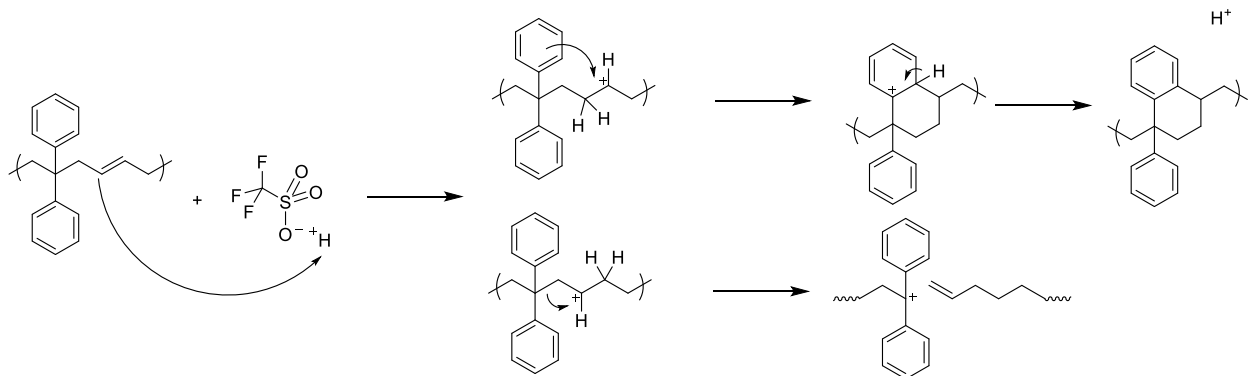


Figure 42. Cyclization mechanism and possible degradation mechanism of DPE/B. Reaction was optimized to get the cyclized product and avoid chain scission.

Table 8. Some reaction conditions tested in the optimization of the cyclization of DPE/B. Run DPE/B-028 was diluted with trifluoroacetic acid to reach a Hammett acidity function of -11.3, detailed in section 4.2.4., and was ultimately used as the optimized procedure.

Run	Temp. (°C)	Wt%	Eq. Triflic Acid	Reaction time (min)	Starting M_n (g/mol)	Final M_n (g/mol)	Starting \bar{D}	Final \bar{D}
DPE/B-C 001	0	5	2	30	145,000	29,000	1.74	2.28
DPE/B-C 008	0	2.5	0.5	10	145,000	62,000	1.74	2.13
DPE/B-C 013	-20	2.5	0.25	5	145,000	81,000	1.74	2.12
DPE/B-C 028	-20	2.5	0.25	2	238,000	136,000	1.33	1.69

In pursuing the optimization of the cyclization reaction of DPE/B, a bimodal DPE/B precursor was used. When cyclizing a bimodal DPE/B precursor, differences in the ^1H NMR were observed when compared to cyclized DPE/B from a monomodal DPE/B precursor. In the aromatic region, the peaks in DPE/B-C remained sharp, instead of broadening as expected and as seen in the ^1H NMR of the DPE/B-C from the monomodal precursor. The elimination of the characteristic double bond backbone peaks in the 5.5-6.5 region was consistent between cyclizations. The aromatic region retained sharp peaks when bimodal DPE/B is cyclized, whereas broadening of the aromatic region was observed for DPE/B-C from a monomodal DPE/B precursor.

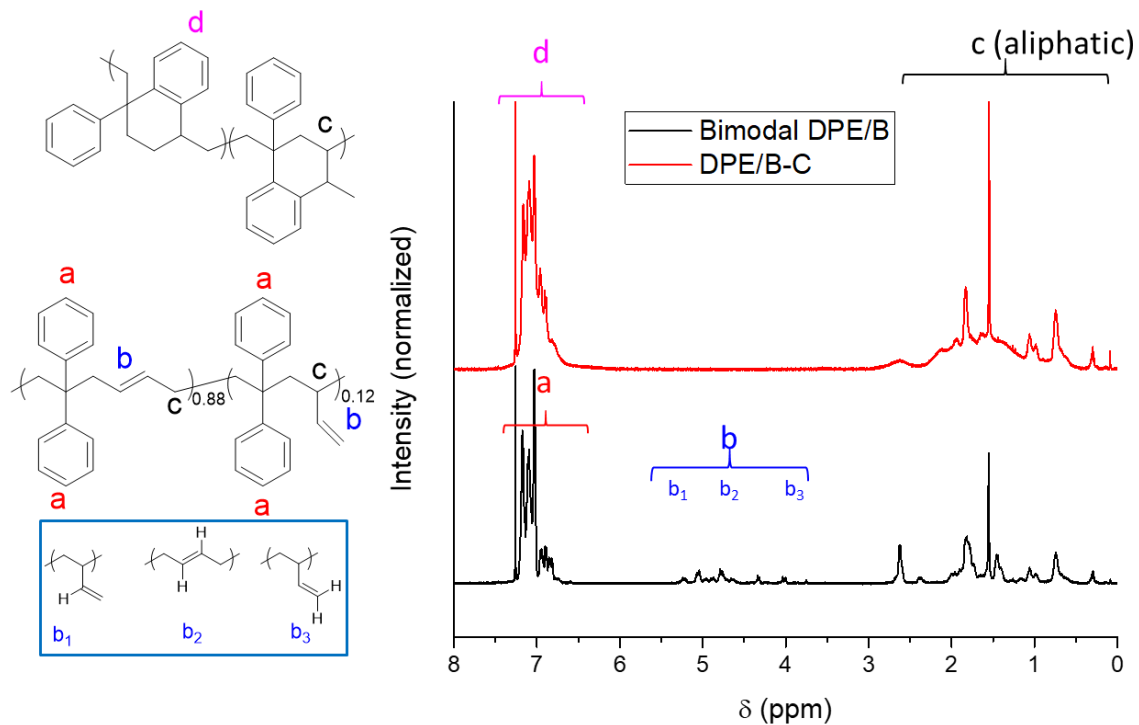


Figure 43. ^1H NMR of DPE/B and DPE/B-C from bimodal DPE/B, the loss of the alkene peaks (b) is indicative of cyclization but the expected broadening of the aromatic region (a and d) is not observed, while there is some broadening of the aliphatic region (c).

Despite these differences in the ^1H NMR, the DSC shows the DPE/B-C from a bimodal precursor still shows an elevated T_g , seen in Figure 44. The T_g of approximately 200°C is still a large increase from that of DPE/E, approximately 100°C .

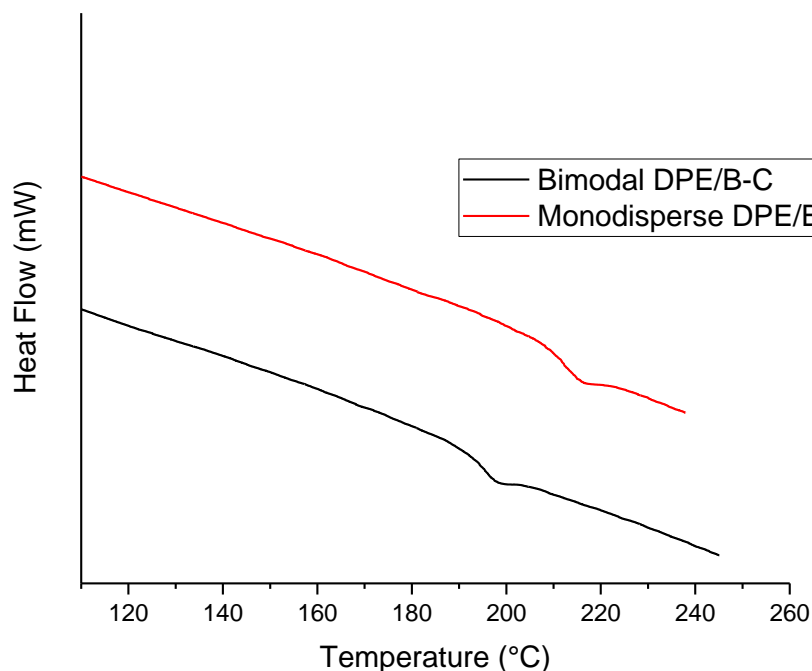


Figure 44. DSC of DPE/B-C from bimodal DPE/B, compared to DPE/B-C from monodisperse DPE/B-C, showing bimodal DPE/B-C has slightly lower T_g .

The SEC chromatogram of DPE/B-C from bimodal DPE/B, seen in Figure 45, shows less degradation than that of DPE/B-C from monomodal DPE/B. It also does not show a shift in the main peak, as expected and observed in the cyclization of monomodal DPE/B. This, combined with the lesser increase in T_g and the differences in ^1H NMR, supports that a different cyclized polymer has been made. The exact structure of this polymer is unknown; therefore, it is not used for further AEM characterization. Deeper investigation of the exact structure of the polymer backbone is ongoing to determine what is being made and whether if the reaction product is usable for AEM applications.

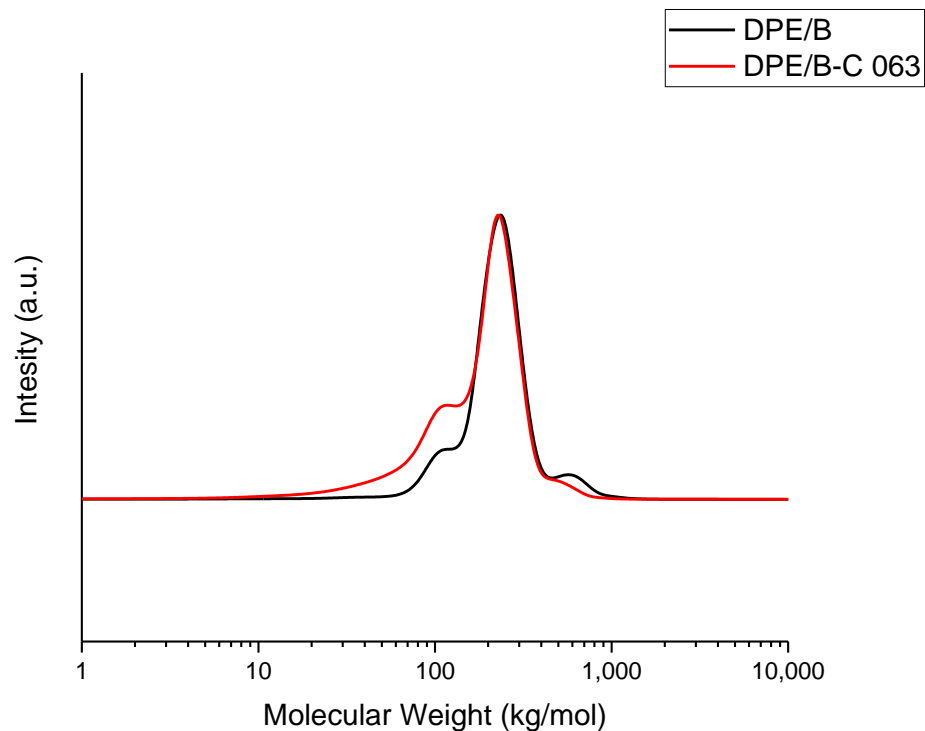


Figure 45. SEC chromatograms of DPE/B-C from monodisperse DPE/B, showing no shift in molecular weight, despite expecting one due to a change in the hydrodynamic volume of the polymer backbone.

To confirm that the differences observed in the ^1H NMR, DSC, and SEC traces were from the differences in the precursors, the same reaction conditions were used to cyclize both monodisperse and bimodal DPE/B. Using the same reaction conditions, differences in ^1H NMR were observed, seen in Figure 46.

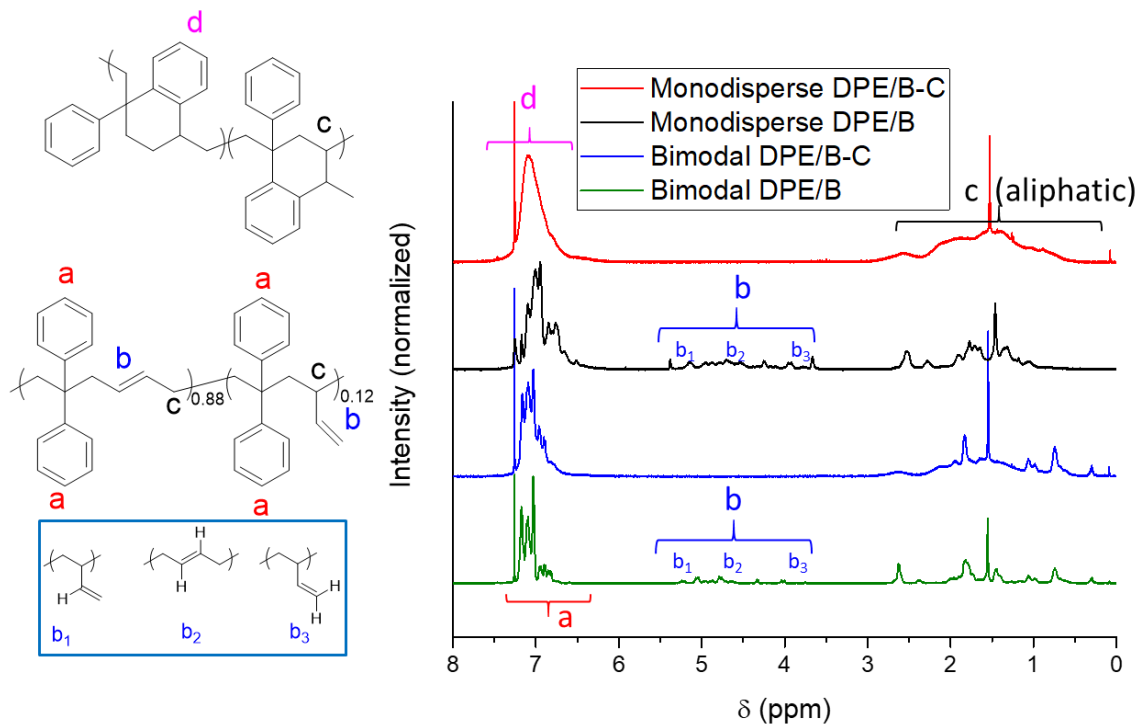


Figure 46. ^1H NMR of the cyclization product of different DPE/B precursors with the same reaction conditions, both precursors saw the disappearance of the alkene peaks (b), monodisperse DPE/B-C gave the expected ^1H NMR, seen in the broadening of the aromatic region (a and d) and in the aliphatic region (c), while bimodal DPE/B-C did not.

4.3.2 Acid Catalyzed Friedel-Crafts Bromoalkylation

The phenyl groups of DPE/B-C were functionalized via acid catalyzed Friedel-Crafts bromoalkylation with 7-bromo-2-methyl-2-heptanol.¹⁴⁷ The reaction conditions are elaborated in the experimental details. The degree of functionalization and efficiency of the reaction were determined by ^1H NMR. The degree of functionalization was controlled by controlling the amount of brominating agent that was added; the reaction proceeded at 95-99% efficiency. The efficiency was determined by the degree of functionalization compared to the stoichiometric ratio of phenyls and brominated agent added. The degree of functionalization was determined by the ratio of integrations of the aromatic hydrogens and the hydrogens on the carbon adjacent to the bromide.

The SEC chromatogram shows a significant increase in dispersity. This will ultimately need to be addressed, but should not have a major impact on the AEM properties to be measured.

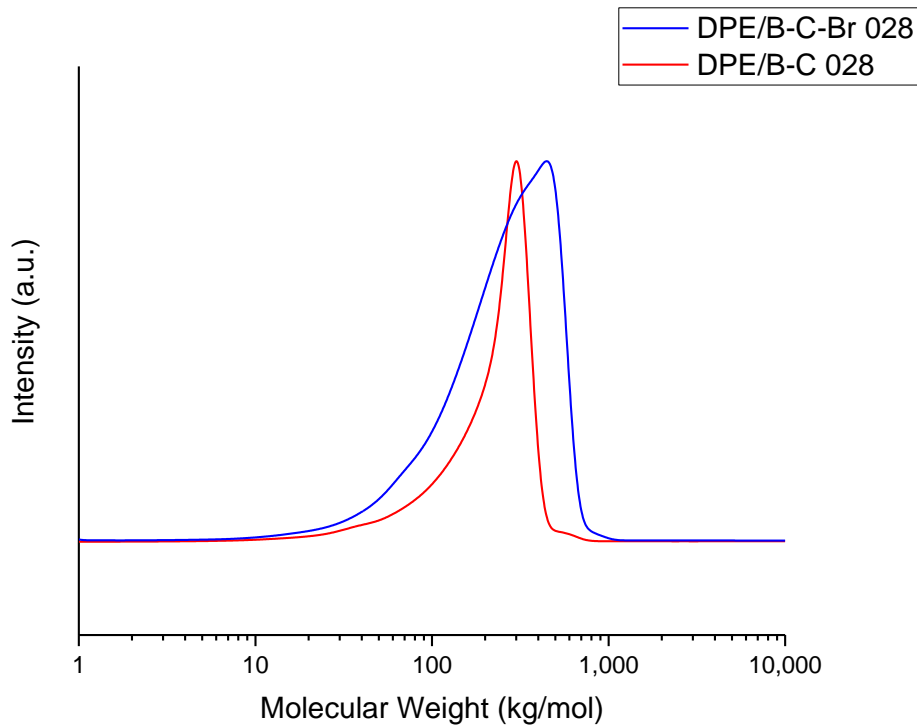


Figure 47. SEC chromatogram of bromofunctionalized DPE/B-C, showing an increase in molecular weight from the alkyl chains added as well as an increase in low molecular weight chains due to degradation.

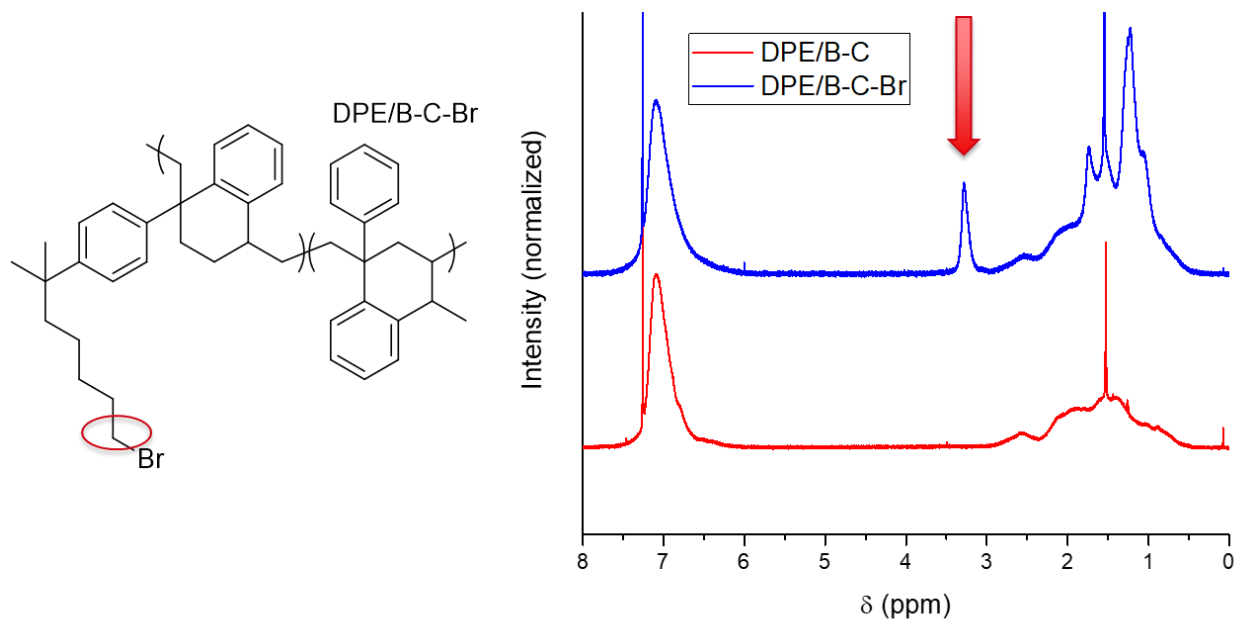


Figure 48. ^1H NMR of DPE/B-C-Br, the arrow points to the peak from the hydrogens on the carbon adjacent to the bromine. The degree of functionalization was determined by the integration of this peak vs. the integration of the aromatic region.

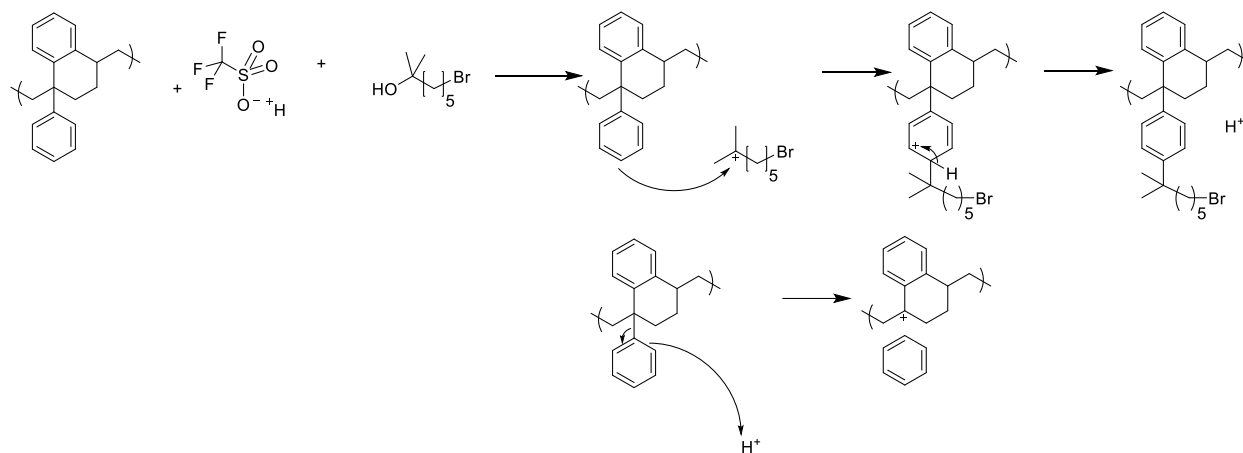


Figure 49. Functionalization mechanism of DPE/B-C, the ability to form a tertiary carbocation stabilized by an aromatic ring allows for easier degradation of the backbone.

4.3.3 Quaternization

After bromo-functionalization of the precursor DPE/B-C-Br, the polymers were quaternized with trimethylammonium (TMA) in ethanol to DPE/B-C(QA). The quaternized forms

of the polymers contain a quaternary ammonium with a positive charge, seen in Figure 50. By dissolving the DPE/B-C-Br precursor in THF then added a stoichiometric excess of TMA in solution, 100% quaternization was achieved. The exact conditions are detailed in the experimental sections. As the DPE/B-C-Br converted to DPE/B-C(QA), it became less soluble in THF. More polar and higher boiling point DMSO was added to return the mixture to a homogenous state and the entire solution was solvent cast. The differences in boiling points of the solvents used, THF, ethanol, and DMSO, allowed for the evaporation of the volatile solvents so the quaternized polymer was only in the high boiling DMSO for the solvent casting. This allowed for slow casting which allows for the aggregation of the charged moieties and formation of ion conduction portions of the polymer.

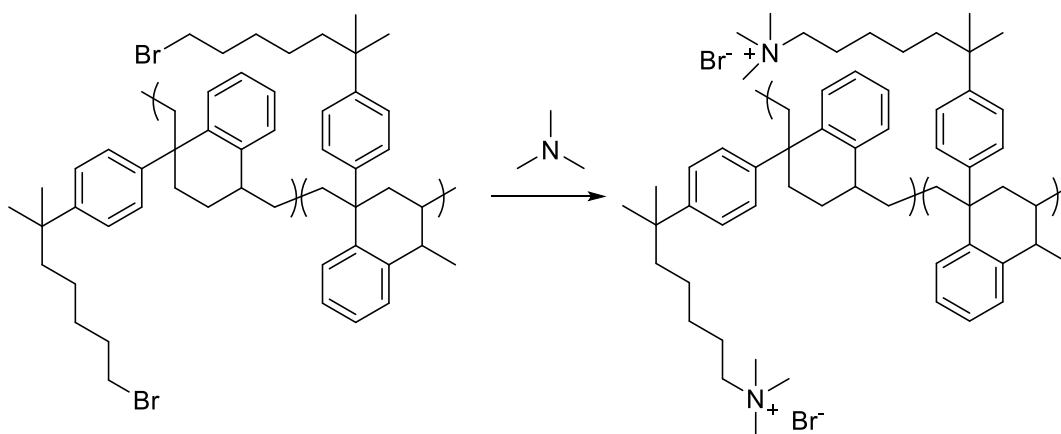


Figure 50. Quaternization of DPE/B-C-Br.

4.3.4 Film Casting

Films were cast in conditions described in 4.2.7. Homogenous Quaternization. By using a high temperature solvent and a controlled airflow oven, the polymer chains were able to reach an equilibrium conformation.

The quaternized films were characterized by measuring the IECs using Mohr titration. Measuring the IEC confirmed that the homogeneous quaternization was successful in converting 100% of the Br groups to quaternary ammonium groups. After the IECs were confirmed, the films were ion exchanged to prepare for conductivity testing, detailed in the experimental.

4.3.5 Differential Scanning Calorimetry

Prior to the quaternization of the DPE/B-C-Br precursors, differential scanning calorimetry (DSC) was performed to find the T_g following the procedure detailed in the experimental. DSC was performed with the Br precursor rather than the final QA polymer because the charged group greatly lowers the T_g and the effect of the degree of functionalization is harder to determine. The T_g 's of the polymer series are listed in Table 9 and plotted as a function of degree of functionalization. The unfunctionalized DPE/B-C had a T_g near 200°C, as expected. The elevated T_g is desirable for improved membrane properties and the impetus for cyclizing DPE/B.

Table 9. T_g 's of DPE/B-C-Br at various degree of functionalizations.

Polymer	Degree of Functionalization (%)	IEC (meq./g)	T_g (°C)
DPE/B-C	0	0	205
DPE/B-C-Br-0.75	20	1.23	171
DPE/B-C-Br-1.65	37	1.90	151
DPE/B-C-Br-2.06	42	2.06	136

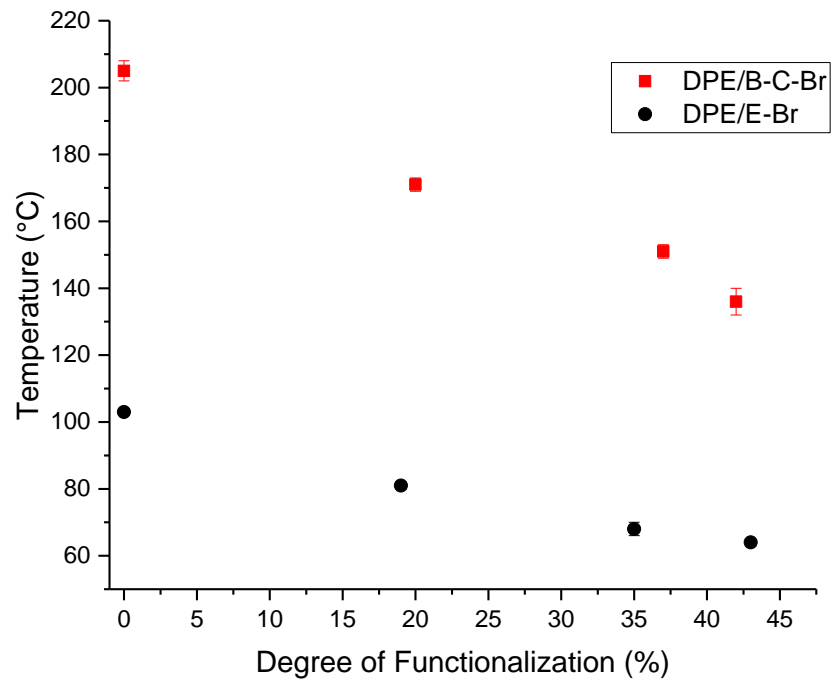


Figure 51. Glass transition temperatures (T_g 's) of DPE/B-C-Br and DPE/E-Br, each decrease with increasing degree of functionalization. DPE/B-C maintains $\sim 100^\circ\text{C}$ higher T_g than its DPE/E counterpart.

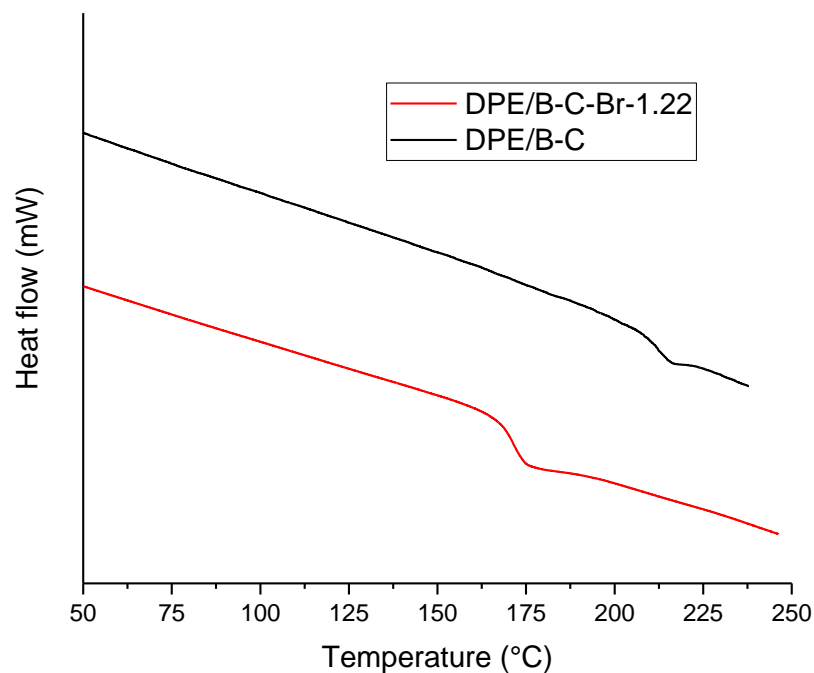


Figure 52. Example DSC of bromofunctionalized DPE/B-C.

4.3.6 Conductivity

Ion exchange capacities IEC of DPE/B-C(QA) was measured by Mohr titration, detailed in the experimental section, and compared with theoretical IEC from ^1H NMR of the brominated precursor. The titration IEC was found to be within experimental error of the theoretical IEC. Ion conductivity (σ) was measured with Cl^- counterions. Conductivity of the DPE/B-C(QA)-xx generally increased as IEC and temperature increased. The results are summarized in Table 10 and depicted in Figure 53 through Figure 55.

Table 10. Cl⁻ conductivity of DPE/B-C(QA).

Polymer	Theoretical IEC (meq./g) ^a	Experimental IEC (meq./g) ^b	Cl ⁻ Conductivity (mS/cm)		
			30°C	60°C	80°C
DPE/B-C(QA)-1.23	1.23	1.30	1.64	2.70	5.04
DPE/B-C(QA)-2.06	2.06	2.13	12.21	30.48	37.12

^aCalculated from degree of bromination, reported in OH⁻ form. ^bMeasured via Mohr titration in Br⁻ or Cl⁻ form, converted and reported in OH⁻ form.

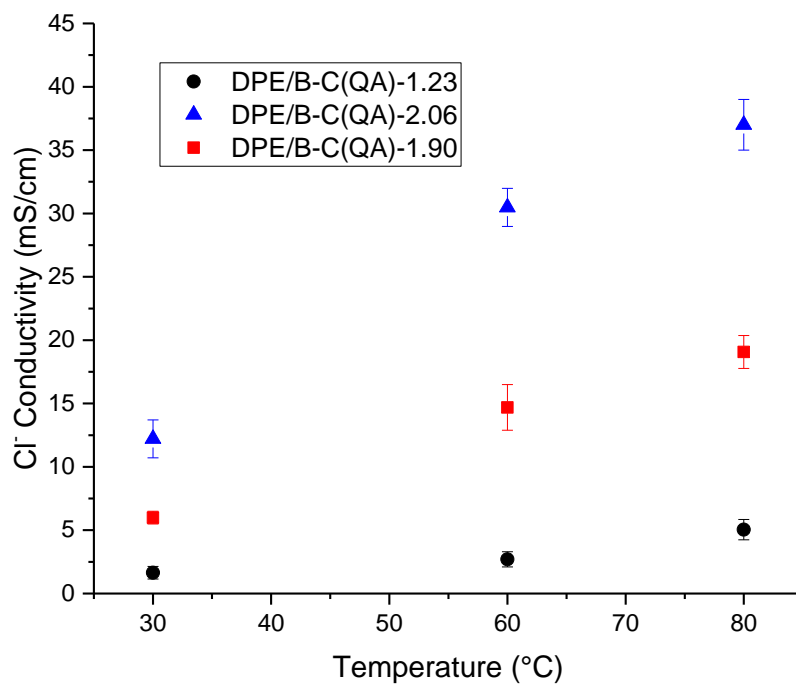


Figure 53. Cl⁻ conductivity of DPE/B-C(QA).

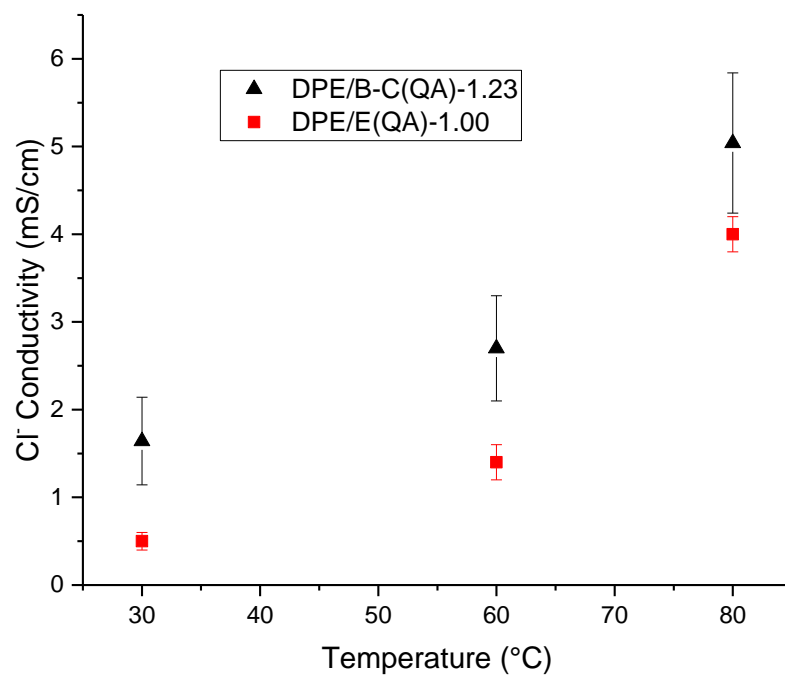


Figure 54. Cl⁻ conductivity of DPE/B-C(QA) and DPE/E(QA) at IEC~1, showing no significant difference in conductivity.

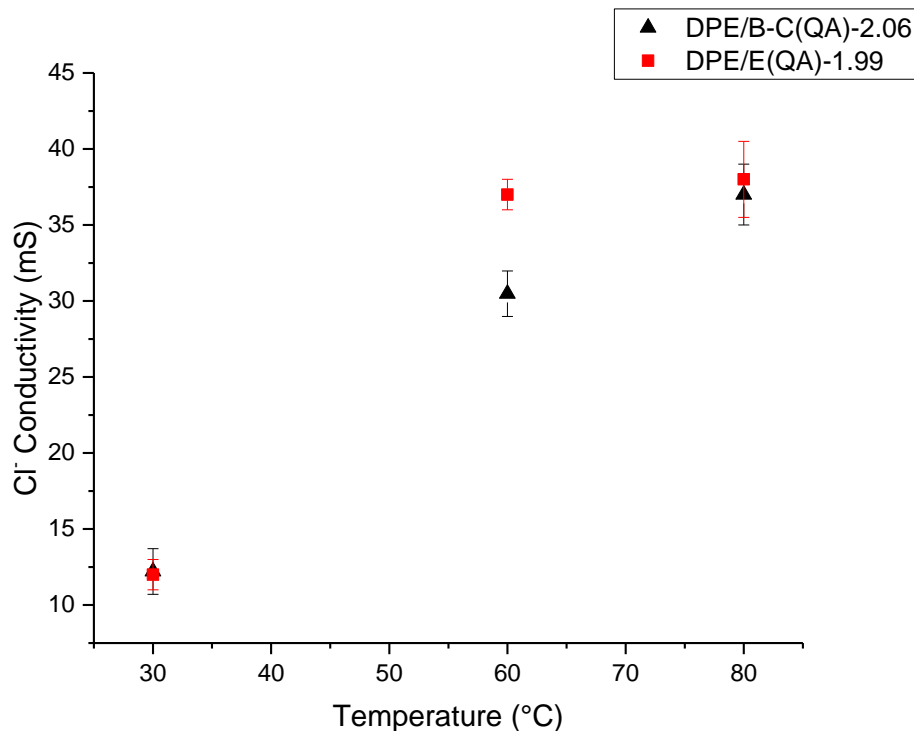


Figure 55. Cl⁻ conductivity of DPE/B-C(QA) and DPE/E(QA) at IEC~2, showing no significant difference in conductivity despite an elevated T_g for DPE/B-C(QA)-2.06

The DPE/B-C(QA) polymers were just as conductive as the DPE/E(QA) polymers at their respective IECs. This result is unsurprising, as merely increasing the polymer backbone's glass transition temperature does not necessitate an improved morphology. An improved glass transition temperature can, however, make the membrane more mechanically robust. The potential for adding mechanical strength to the membrane without sacrificing any conductivity offers a path forward for improvement and further research.

4.3.7 Water Uptake

The water uptake (WU) for both PS(QA) and DPE/E(QA) was calculated as:

$$WU(\%) = [(W_{hydrated} - W_{dry}) \times 100] / W_{dry}$$

where $W_{hydrated}$ and W_{dry} are the weights of the patted-dry water swollen and dry membranes, respectively. Dry membranes were prepared under dynamic vacuum at 80°C. Hydrated membranes were prepared by soaking in deionized water overnight.

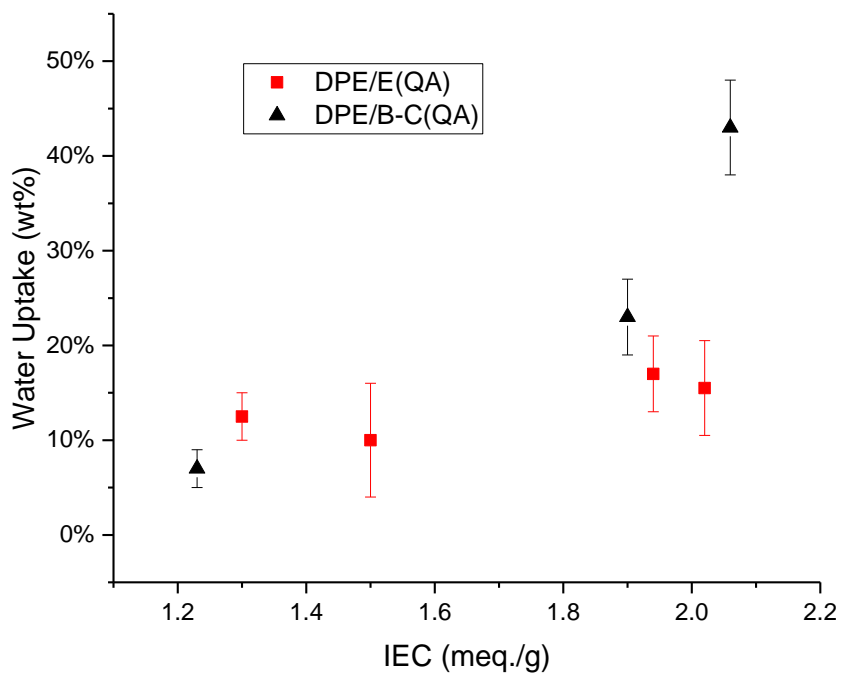


Figure 56. Water uptake of DPE/B-C(QA) and DPE/E(QA) in Cl⁻ form, DPE/B-C(QA) shows a higher water uptake than DPE/E(QA) despite having a higher T_g .

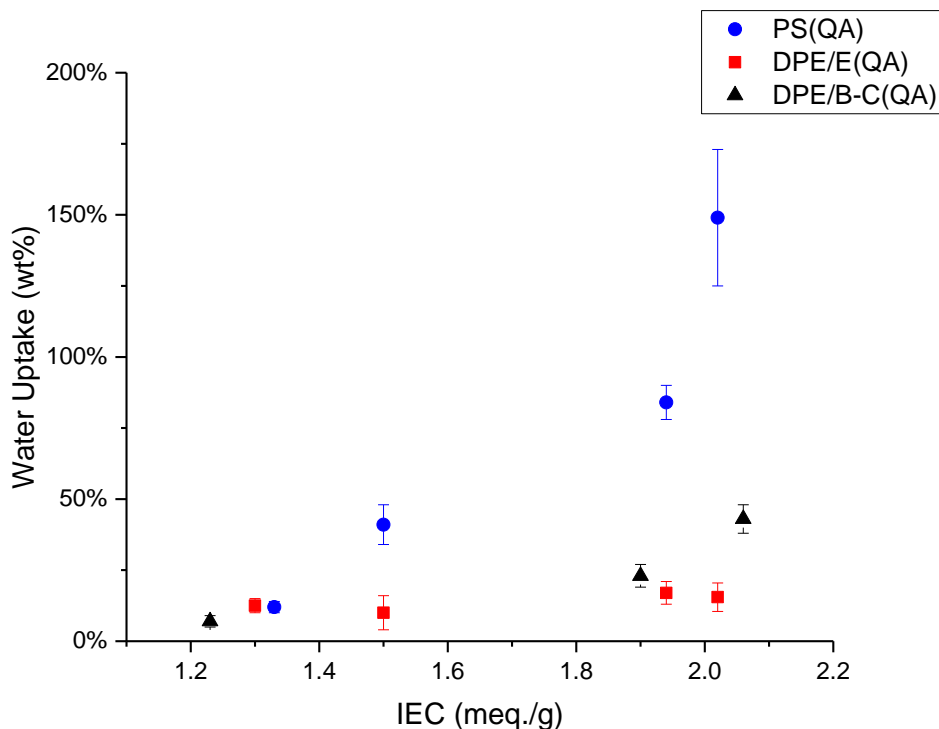


Figure 57. Water uptake of DPE/B-C(QA), DPE/E(QA), and PS(QA) in Cl⁻ form, DPE/B-C(QA) shows a higher water uptake than DPE/E(QA) despite having a higher T_g but still has a significantly lower water uptake than PS(QA).

The water uptake of the DPE/B-C(QA) series did not show any improvement over that of DPE/E(QA), seen in Figure 56. DPE/B-C(QA) did, however, avoid excessive water uptake observed in PS(QA), seen in Figure 57. This result, combined with the similar conductivities between DPE/E(QA) and DPE/B-C(QA) at IEC near 2.0, implies that DPE/B-C(QA) does not experience better ion aggregation than DPE/B(QA), despite its improved glass transition temperature.

4.3.8 Mechanical Strength

Dynamic mechanical analysis (DMA) of high IEC DPE/B-C(QA) and DPE/E(QA) was conducted at 50°C and 50% relative humidity (R.H.). The DMA results showed no significant difference between the two polymers, despite the significantly higher T_g for DPE/B-C(QA)-2.06.

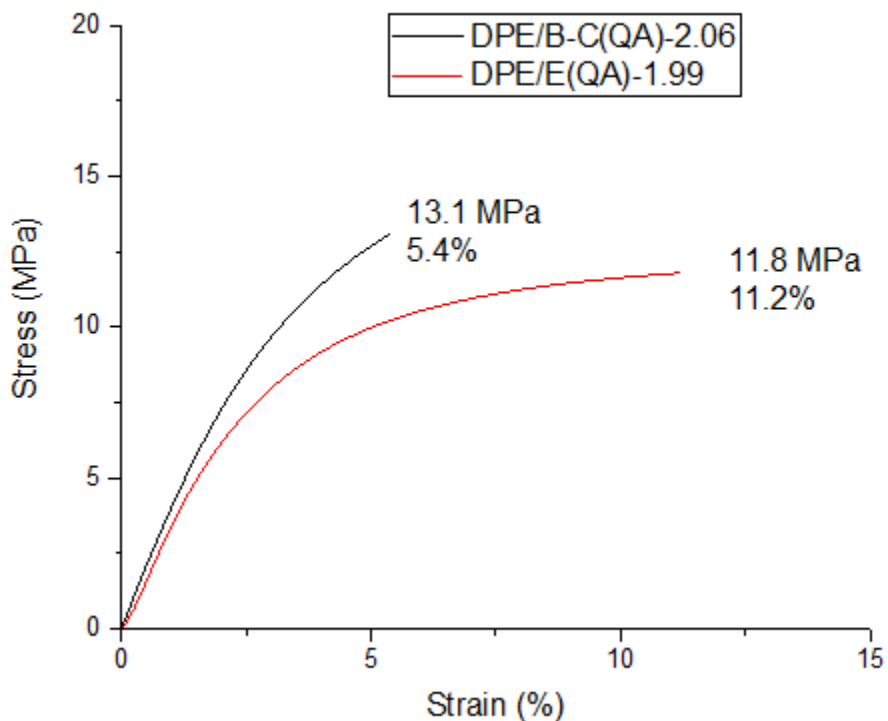


Figure 58. DMA characterization of DPE/B-C(QA) and DPE/E(QA) at IEC~2.0 at 50 °C and 50% R.H., no significant difference is observed in the mechanical properties with both polymers being brittle.

4.4 Conclusions

We synthesized and characterized AEMs based on high glass transition temperature DPE/B-C polymer backbones, comparing them to DPE/E based AEMs of similar ion content. Each polymer backbone was modified via Friedel-Crafts bromoalkylation to attach bromofunctional groups for quaternization. The DPE/B-C backbone and subsequent functionalized DPE/B-C-Br

boasted a T_g nearly 100°C greater than that of its DPE/E counterparts. Despite this, DPE/B-C(QA) did not show improved chloride conductivity or decreased water uptake; however, DPE/B-C(QA) did exhibit better properties compared to PS(QA). With these improvements over PS(QA), the potential for high conductivity, low water uptake AEMs can still be realized with DPE/B-C(QA). The elevated T_g did not manifest itself in a significant improvement in mechanical properties, either.

The future of this work is to incorporate the high T_g DPE/B-C(QA) into polymer systems to improve membrane properties. This can be done by copolymerization with a rubbery polymer that allows for a less brittle polymer system, similar to SEBS. Another route incorporating DPE/B-C(QA) into a polymer blend AEM system with a lower T_g polymer. Either route could afford the benefits of having a high T_g functional polymer with a rubbery polymer to impart improved overall mechanical properties and ion conductivity.

5. Thesis Summary

This research investigated structure-property relationships between polymer backbone, mechanical properties, and ion transport, providing insights to the research community at large that will help inform the design of future ion-exchange membranes.

In the first project, the backbone investigated was poly(1,1-diphenylethylene-alt-butadiene) (DPE/B). The bulky DPE monomer cannot self-polymerize, which lends itself to the precisely tailored synthesis of alternating copolymer backbones. The DPE/B alternating copolymer was selectively hydrogenated to saturate the polymer backbone (DPE/E), then functionalized via an acid-catalyzed Friedel-Crafts reaction to attach alkyl side chains containing bromofunctional groups for subsequent quaternization. The quaternized polymer was then compared to quaternized polystyrene of similar ion content for a baseline comparison to a well-known and used polymer for anion exchange membranes. This work revealed DPE/E(QA) to have extremely low water uptake without compromising conductivity, a finding that can be used in future work with block copolymer systems to make AEMs with high ion conductivity and low water uptake. A manuscript based on this work is in preparation to be submitted to a peer-reviewed journal.

Additionally, the DPE/B polymer was cyclized via an acid-catalyzed Friedel-Crafts reaction to increase the glass transition of the precursor polymer backbone. The cyclized DPE/B (DPE/B-C) had a glass transition temperature of 205°C, up from 103°C for DPE/E. DPE/B-C(QA) did not have higher ion conductivity, lower water uptake, and was not more mechanically robust, despite the increase in T_g . This work revealed DPE/B-C(QA) to not have better AEM properties

than DPE/E(QA), despite similar composition and a much higher backbone T_g . A manuscript based on this work is in preparation to be submitted to a peer-reviewed journal.

References

1. Hiemenz, P. C., Lodge, T. P., *Polymer Chemistry*. 2nd ed.; CRC Press, 2007.
2. Swager, T. M., 50th Anniversary Perspective: Conducting/Semiconducting Conjugated Polymers. A Personal Perspective on the Past and the Future. *Macromolecules* **2017**, *50* (13), 4867-4886.
3. Liang, Y.; Li, L.; Scott, R. A.; Kiick, K. L., 50th Anniversary Perspective: Polymeric Biomaterials: Diverse Functions Enabled by Advances in Macromolecular Chemistry. *Macromolecules* **2017**, *50* (2), 483-502.
4. Brinson, H. F.; Brinson, L. C., *Polymer Engineering Science and Viscoelasticity*. 2nd ed.; Springer, 2008.
5. Nicholson, J., *The Chemistry of Polymers*. 5th ed.; Royal Society of Chemistry: 2017.
6. Warshay, M.; Prokopius, P. R. The Fuel Cell in Space: Yesterday, Today and Tomorrow. In *Grove Anniversary (1839-1989) Fuel Cell Symposium*, London, Great Britain, September 18-21, 1989; pp 1-12.
7. MacArthur, D. E.; Waughray, D.; Stuchtey, M. R., *The New Plastics Economy, Rethinking the Future of Plastics*, World Economic Forum, 2016.
8. Geyer, R.; Jambeck Jenna, R.; Law Kara, L., Production, Use, and Fate of All Plastics Ever Made. *Sci. Adv.* **2017**, *3* (7), e1700782.
9. Grubbs, R. B.; Grubbs, R. H., 50th Anniversary Perspective: Living Polymerization—Emphasizing the Molecule in Macromolecules. *Macromolecules* **2017**, *50* (18), 6979-6997.
10. Brandrup, J.; Immergut, E. H.; Grulke, E. A.; Abe, A.; Bloch, D. R., *Polymer Handbook*. Vol. 89, Wiley, 1999.
11. Perkins, W. G., Polymer Toughness and Impact Resistance. *Polym. Eng. Sci.* **1999**, *39* (12), 2445-2460.
12. Strobl, G. R., *The Physics of Polymers*. Springer, 1997.
13. Bates, F. S.; Fredrickson, G. H., Block Copolymer Thermodynamics: Theory and Experiment. *Annu. Rev. Phys. Chem.* **1990**, *41* (1), 525-557.

14. Bates, F. S., Polymer-Polymer Phase Behavior. *Science* **1991**, 251 (4996), 898-905.
15. Ruzette, A.-V.; Leibler, L., Block Copolymers in Tomorrow's Plastics. *Nat. Mater.* **2005**, 4 (1), 19-31.
16. Iguchi, D.; Ohashi, S.; Abarro, G. J. E.; Yin, X.; Winroth, S.; Scott, C.; Gleydura, M.; Jin, L.; Kanagasegar, N.; Lo, C.; Arza, C. R.; Froimowicz, P.; Ishida, H., Development of Hydrogen-Rich Benzoxazine Resins with Low Polymerization Temperature for Space Radiation Shielding. *ACS Omega* **2018**, 3 (9), 11569-11581.
17. Mondal, R.; Pal, S.; Bhalani, D. V.; Bhadja, V.; Chatterjee, U.; Jewrajka, S. K., Preparation of polyvinylidene fluoride blend anion exchange membranes via non-solvent induced phase inversion for desalination and fluoride removal. *Desalination* **2018**, 445, 85-94.
18. Theato, P.; Klok, H.-A., *Functional Polymers by Post-Polymerization Modification: Concepts, Guidelines and Applications*. John Wiley & Sons, 2013.
19. Boasen, N. K.; Hillmyer, M. A., Post-Polymerization Functionalization of Polyolefins. *Chem. Soc. Rev.* **2005**, 34 (3), 267-275.
20. Mortier, J., *Arene Chemistry: Reaction Mechanisms and Methods for Aromatic Compounds*. John Wiley & Sons, 2015.
21. Schlüter, D. A.; Hawker, C.; Sakamoto, J., *Synthesis of Polymers: New Structures and Methods*. John Wiley & Sons, 2012.
22. Jaymand, M., Recent Progress in the Chemical Modification of Syndiotactic Polystyrene. *Polym. Chem.* **2014**, 5 (8), 2663-2690.
23. Jeon, J. Y. Mohanty, A. D.; Tian, D.; Bae, C., Ionic Functionalization of Polystyrene-b-poly (ethylene-co-butylene)-b-polystyrene via Friedel-Crafts Bromoalkylation and Its Application for Anion Exchange Membranes. *ECS Trans.* **2017**, 48 (19), 7085-7095.
24. Zhang, L.; Brostowitz, N. R.; Cavicchi, K. A.; Weiss, R. A., Perspective: Ionomer Research and Applications. *Macromol. React. Eng.* **2014**, 8 (2), 81-99.
25. Eisenberg, A.; Kim, J.-S., *Introduction to Ionomers*. Wiley, 1998.
26. Weiss, R. A.; Sen, A.; Pottick, L. A.; Willis, C. L., Block Copolymer Ionomers: 2. Viscoelastic and Mechanical Properties of Sulphonated Poly(styrene-ethylene/butylene-styrene). *Polymer* **1991**, 32 (15), 2785-2792.

27. Nyrkova, I. A.; Khokhlov, A. R.; Doi, M., Microdomains in Block Copolymers and Multiplets in Ionomers: Parallels in Behavior. *Macromolecules* **1993**, *26* (14), 3601-3610.
28. Eisenberg, A., Clustering of Ions in Organic Polymers. A Theoretical Approach. *Macromolecules* **1970**, *3* (2), 147-154.
29. Eisenberg, A.; Hird, B.; Moore, R., A New Multiplet-Cluster Model for the Morphology of Random Ionomers. *Macromolecules* **1990**, *23* (18), 4098-4107.
30. Zhang, Z.; Chen, Q.; Colby, R. H., Dynamics of Associative Polymers. *Soft Matter* **2018**, *14* (16), 2961-2977.
31. Hallinan, D. T.; Balsara, N. P., Polymer Electrolytes. *Annu. Rev. Mater. Res.* **2013**, *43* (1), 503-525.
32. Watanabe, M.; Sanui, K.; Ogata, N.; Kobayashi, T.; Ohtaki, Z., Ionic Conductivity and Mobility in Network Polymers from Poly(propylene oxide) Containing Lithium Perchlorate. *J. Appl. Phys.* **1985**, *57* (1), 123-128.
33. Boden, N.; Leng, S. A.; Ward, I. M., Ionic Conductivity and Diffusivity in Polyethylene Oxide/Electrolyte Solutions as Models for Polymer Electrolytes. *Solid State Ionics* **1991**, *45* (3), 261-270.
34. Kakihana, M.; Schantz, S.; Torell, L. M., Raman Spectroscopic Study of Ion–Ion Interaction and its Temperature Dependence in a Poly(propylene-oxide)-Based NaCF₃SO₃ –Polymer Electrolyte. *J. Chem. Phys.* **1990**, *92* (10), 6271-6277.
35. Andújar, J. M., Segura, F., Fuel cells: History and Updating. A Walk Along Two Centuries. *Renewable Sustainable Energy Rev.* **2009**, *13* (9), 2309-2322.
36. Kreuer, K.-D.; Paddison, S. J.; Spohr, E.; Schuster, M., Transport in Proton Conductors for Fuel-Cell Applications: Simulations, Elementary Reactions, and Phenomenology. *Chem. Rev.* **2004**, *104* (10), 4637-4678.
37. Kreuer, K. D., On the Development of Proton Conducting Polymer Membranes for Hydrogen and Methanol Fuel Cells. *J. Membr. Sci.* **2001**, *185* (1), 29-39.
38. Duan, Q.; Ge, S.; Wang, C.-Y., Water Uptake, Ionic Conductivity and Swelling Properties of Anion-Exchange Membrane. *J. Power Sources* **2013**, *243*, 773-778.
39. Zheng, Y.; Ash, U.; Pandey, R. P.; Ozioko, A. G.; Ponce-González, J.; Handl, M.; Weissbach, T.; Varcoe, J. R.; Holdcroft, S.; Liberatore, M. W.; Hiesgen, R.; Dekel, D. R.,

- Water Uptake Study of Anion Exchange Membranes. *Macromolecules* **2018**, *51* (9), 3264-3278.
40. Hsu, W. Y.; Barkley, J. R.; Meakin, P., Ion Percolation and Insulator-to-Conductor Transition in Nafion Perfluorosulfonic Acid Membranes. *Macromolecules* **1980**, *13* (1), 198-200.
 41. Zawodzinski, J. T. A., Springer, T. E., Davey, J., Jestel, R., Lopez, C., Valerio, J., Gottesfeld, S., A Comparative Study of Water Uptake By and Transport Through Ionomeric Fuel Cell Membranes. *J. Electrochem. Soc.* **1993**, *140* (7), 1981-1985.
 42. Zawodzinski, T. A., Water Uptake by and Transport Through Nafion® 117 Membranes. *J. Electrochem. Soc.* **1993**, *140* (4), 1041.
 43. Yeager, H. L. a. S., A., Cation and Water Diffusion in Nafion Ion Exchange Membranes: Influence of Polymer Structure. *J. Electrochem. Soc.* **1981**, *128* (9), 1880-1884.
 44. Okada, T. X., G.; Gorseth, O.; Kjelstrup, S.; Nakamura, N.; Arimura, T., Ion and Water Transport Characteristics of Nafion Membranes as Electrolytes. *Electrochim. Acta* **1998**, *43* (24), 3741-3747.
 45. Lai, Y.-H.; Mittelsteadt, C. K.; Gittleman, C. S.; Dillard, D. A., Viscoelastic Stress Model and Mechanical Characterization of Perfluorosulfonic Acid (PFSA) Polymer Electrolyte Membranes. In *3rd International Conference on Fuel Cell Science, Engineering and Technology*, Ypsilanti, Michigan, USA, May 23-25, 2005; pp 161-167.
 46. Mathias, M. F. M., R.; Gasteiger, H. A.; Conley, J. J.; Fuller, T. J.; Gittleman, C. J.; Kocha, S. S.; Miller, D. P.; Mittelsteadt, C. K.; Xie, T., Two Fuel Cell Cars in Every Garage. *Electrochem. Soc. Interface* **2005**, *14* (3), 24-35.
 47. Barragán, V. M.; Ruiz-Bauzá, C.; Villaluenga, J. P. G.; Seoane, B., Transport of Methanol and Water Through Nafion Membranes. *J. Power Sources* **2004**, *130* (1), 22-29.
 48. Sundmacher, K.; Scott, K., Direct Methanol Polymer Electrolyte Fuel Cell: Analysis of Charge and Mass Transfer in the Vapour–Liquid–Solid System. *Chem. Eng. Sci.* **1999**, *54* (13), 2927-2936.
 49. Inaba, M.; Kinumoto, T.; Kiriake, M.; Umebayashi, R.; Tasaka, A.; Ogumi, Z., Gas Crossover and Membrane Degradation in Polymer Electrolyte Fuel Cells. *Electrochim. Acta* **2006**, *51* (26), 5746-5753.

50. Evans, C. M.; Singh, M. R.; Lynd, N. A.; Segalman, R. A., Improving the Gas Barrier Properties of Nafion via Thermal Annealing: Evidence for Diffusion through Hydrophilic Channels and Matrix. *Macromolecules* **2015**, *48* (10), 3303-3309.
51. Alam, T. M.; Hibbs, M. R., Characterization of Heterogeneous Solvent Diffusion Environments in Anion Exchange Membranes. *Macromolecules* **2014**, *47* (3), 1073-1084.
52. Gebel, G., Structural Evolution of Water Swollen Perfluorosulfonated Ionomers From Dry Membrane to Solution. *Polymer* **2000**, *41* (15), 5829-5838.
53. Morozova, S.; Muthukumar, M., Elasticity at Swelling Equilibrium of Ultrasoft Polyelectrolyte Gels: Comparisons of Theory and Experiments. *Macromolecules* **2017**, *50* (6), 2456-2466.
54. Dekel, D. R., Review of Cell Performance in Anion Exchange Membrane Fuel Cells. *J. Power Sources* **2018**, *375*, 158-169.
55. Hickner, M. A., Strategies for Developing New Anion Exchange Membranes and Electrode Ionomers. *Electrochem. Soc. Interface* **2017**, *26* (1), 69-73.
56. Arges, C. G.; Zhang, L., Anion Exchange Membranes' Evolution toward High Hydroxide Ion Conductivity and Alkaline Resiliency. *ACS Appl. Energy Mater.* **2018**, *1* (7), 2991-3012.
57. Li, N.; Guiver, M. D., Ion Transport by Nanochannels in Ion-Containing Aromatic Copolymers. *Macromolecules* **2014**, *47* (7), 2175-2198.
58. Shibayama, M.; Tanaka, T., Volume Phase Transition and Related Phenomena of Polymer Gels. In *Advances in Polymer Science*, Vol. 109; Polymer, 1993; pp 1-62.
59. Dimitriyev, M. S.; Chang, Y.-W.; Goldbart, P. M.; Fernández-Nieves, A., Swelling Thermodynamics and Phase Transitions of Polymer Gels. *Nano Futures* **2019**, *3* (4), 042001.
60. Manning, G. S., A Bead-Spring Chain as a One-Dimensional Polyelectrolyte Gel. *Soft Matter* **2018**, *14* (20), 4074-4080.
61. Fennell, E.; Kamphus, J.; Huyghe, J. M., The Importance of the Mixing Energy in Ionized Superabsorbent Polymer Swelling Models. *Polymers* **2020**, *12* (3), 609.
62. Kreuer, K.-D., The Role of Internal Pressure for the Hydration and Transport Properties of Ionomers and Polyelectrolytes. *Solid State Ionics* **2013**, *252*, 93-101.

63. Nishiyama, Y.; Satoh, M., Solvent- and Counterion-Specific Swelling Behavior of Poly(acrylic acid) Gels. *J. Polym. Sci., Part B: Polym. Phys.* **2000**, *38* (21), 2791-2800.
64. Tanaka, T., Collapse of Gels and the Critical Endpoint. *Phys. Rev. Lett.* **1978**, *40* (12), 820-823.
65. Carle, G.; Axhausen, K. W.; Wokaun, A.; Keller, P., Opportunities and Risks During the Introduction of Fuel Cell Cars. *Transport Reviews* **2005**, *25* (6), 739-760.
66. Kreuer, K.-D., Proton Conductivity: Materials and Applications. *Chem. Mater.* **1996**, *8* (3), 610-641.
67. Miriyev, A.; Stack, K.; Lipson, H., Soft Material for Soft Actuators. *Nat. Commun.* **2017**, *8* (1), 596.
68. Maurya, S.; Shin, S.-H.; Kim, Y.; Moon, S.-H., A Review on Recent Developments of Anion Exchange Membranes for Fuel Cells and Redox Flow Batteries. *RSC Adv.* **2015**, *5* (47), 37206-37230.
69. Paidar, M.; Fateev, V.; Bouzek, K., Membrane Electrolysis—History, Current Status and Perspective. *Electrochim. Acta* **2016**, *209*, 737-756.
70. Larminie, J. D., A., *Fuel Cell Systems Explained*. John Wiley & Sons, 2000.
71. *Fuel Cells*. <https://www.energy.gov/eere/fuelcells/fuel-cells> (accessed 2020-03-10).
72. Zhao, T.; Kreuer, K.-D.; Van Van Nguyen, T., *Advances in Fuel Cells*. Elsevier, 2007.
73. Logan, B. E., Peer Reviewed: Extracting Hydrogen and Electricity from Renewable Resources. *Environ. Sci. Technol.* **2004**, *38* (9), 160A-167A.
74. Jacobson, M. Z.; Colella, W. G.; Golden, D. M., Cleaning the Air and Improving Health with Hydrogen Fuel-Cell Vehicles. *Science* **2005**, *308* (5730), 1901.
75. Schultz, M. G.; Diehl, T.; Brasseur, G. P.; Zittel, W., Air Pollution and Climate-Forcing Impacts of a Global Hydrogen Economy. *Science* **2003**, *302* (5645), 624.
76. Milewski, J.; Kupecki, J.; Szczeńniak, A.; Uzunow, N., Hydrogen Production in Solid Oxide Electrolyzers Coupled with Nuclear Reactors. *Int. J. Hydrogen Energy* **2021**, *46* (72), 35765-35776.

77. Dyer, C. K., Fuel Cells for Portable Applications. *J. Power Sources* **2002**, *106* (1), 31-34.
78. Holton, O. T., Stevenson, J. W., The Role of Platinum in Proton Exchange Membrane Fuel Cells. *Platinum Met. Rev.* **2013**, *57* (4), 259-271.
79. Zhang, S.; Yuan, X.-Z.; Hin, J. N. C.; Wang, H.; Friedrich, K. A.; Schulze, M., A Review of Platinum-Based Catalyst Layer Degradation in Proton Exchange Membrane Fuel Cells. *J. Power Sources* **2009**, *194* (2), 588-600.
80. Srinivasan, S.; Manko, D. J.; Koch, H.; Enayetullah, M. A.; Appleby, A. J., Recent Advances in Solid Polymer Electrolyte Fuel Cell Technology with Low Platinum Loading Electrodes. *J. Power Sources* **1990**, *29* (3), 367-387.
81. McLean, G. F.; Niet, T.; Prince-Richard, S.; Djilali, N., An Assessment of Alkaline Fuel Cell Technology. *Int. J. Hydrogen Energy* **2002**, *27* (5), 507-526.
82. Abdel Rahim, M. A.; Abdel Hameed, R. M.; Khalil, M. W., Nickel as a Catalyst for the Electro-Oxidation of Methanol in Alkaline Medium. *J. Power Sources* **2004**, *134* (2), 160-169.
83. Merle, G.; Wessling, M.; Nijmeijer, K., Anion Exchange Membranes For Alkaline Fuel Cells: A Review. *J. Membr. Sci.* **2011**, *377* (1), 1-35.
84. Varcoe, J. R.; Slade, R. C. T., Prospects for Alkaline Anion-Exchange Membranes in Low Temperature Fuel Cells. *Fuel Cells* **2005**, *5* (2), 187-200.
85. Hickner, M. A.; Herring, A. M.; Coughlin, E. B., Anion Exchange Membranes: Current Status and Moving Forward. *J. Polym. Sci., Part B: Polym. Phys.* **2013**, *51* (24), 1727-1735.
86. Varcoe, J. R.; Atanassov, P.; Dekel, D. R.; Herring, A. M.; Hickner, M. A.; Kohl, P. A.; Kucernak, A. R.; Mustain, W. E.; Nijmeijer, K.; Scott, K.; Xu, T.; Zhuang, L., Anion-Exchange Membranes in Electrochemical Energy Systems. *Energy Environ. Sci.* **2014**, *7* (10), 3135-3191.
87. Gottesfeld, S.; Dekel, D. R.; Page, M.; Bae, C.; Yan, Y.; Zelenay, P.; Kim, Y. S., Anion Exchange Membrane Fuel Cells: Current Status and Remaining Challenges. *J. Power Sources* **2018**, *375*, 170-184.
88. Lee, K. H.; Cho, D. H.; Kim, Y. M.; Moon, S. J.; Seong, J. G.; Shin, D. W.; Sohn, J.-Y.; Kim, J. F.; Lee, Y. M., Highly Conductive and Durable Poly (arylene ether sulfone)

- Anion Exchange Membrane with End-Group Cross-Linking. *Energy Environ. Sci.* **2017**, *10* (1), 275-285.
89. Guo, D.; Lai, A. N.; Lin, C. X.; Zhang, Q. G.; Zhu, A. M.; Liu, Q. L., Imidazolium-Functionalized Poly(arylene ether sulfone) Anion-Exchange Membranes Densely Grafted with Flexible Side Chains for Fuel Cells. *ACS Appl. Mater. Interfaces* **2016**, *8* (38), 25279-25288.
90. Tanaka, M.; Fukasawa, K.; Nishino, E.; Yamaguchi, S.; Yamada, K.; Tanaka, H.; Bae, B.; Miyatake, K.; Watanabe, M., Anion Conductive Block Poly(arylene ether)s: Synthesis, Properties, and Application in Alkaline Fuel Cells. *J. Am. Chem. Soc.* **2011**, *133* (27), 10646-10654.
91. Lee, W.-H.; Park, E. J.; Han, J.; Shin, D. W.; Kim, Y. S.; Bae, C., Poly(terphenylene) Anion Exchange Membranes: The Effect of Backbone Structure on Morphology and Membrane Property. *ACS Macro Lett.* **2017**, *6* (5), 566-570.
92. Mahmoud, A. M. A.; Elsaghier, A. M. M.; Otsuji, K.; Miyatake, K., High Hydroxide Ion Conductivity with Enhanced Alkaline Stability of Partially Fluorinated and Quaternized Aromatic Copolymers as Anion Exchange Membranes. *Macromolecules* **2017**, *50* (11), 4256-4266.
93. Park, E. J.; Maurya, S.; Hibbs, M. R.; Fujimoto, C. H.; Kreuer, K.-D.; Kim, Y. S., Alkaline Stability of Quaternized Diels–Alder Polyphenylenes. *Macromolecules* **2019**, *52* (14), 5419-5428.
94. Hibbs, M. R.; Fujimoto, C. H.; Cornelius, C. J., Synthesis and Characterization of Poly(phenylene)-Based Anion Exchange Membranes for Alkaline Fuel Cells. *Macromolecules* **2009**, *42* (21), 8316-8321.
95. Yang, Y.; Knauss, D. M., Poly(2,6-dimethyl-1,4-phenylene oxide)-b-poly(vinylbenzyltrimethylammonium) Diblock Copolymers for Highly Conductive Anion Exchange Membranes. *Macromolecules* **2015**, *48* (13), 4471-4480.
96. Pan, J.; Han, J.; Zhu, L.; Hickner, M. A., Cationic Side-Chain Attachment to Poly(phenylene oxide) Backbones for Chemically Stable and Conductive Anion Exchange Membranes. *Chem. Mater.* **2017**, *29* (12), 5321-5330.
97. Hossain, M. M.; Hou, J.; Wu, L.; Ge, Q.; Liang, X.; Mondal, A. N.; Xu, T., Anion Exchange Membranes with Clusters of Alkyl Ammonium Group for Mitigating Water Swelling but not Ionic Conductivity. *J. Membr. Sci.* **2018**, *550*, 101-109.

98. Meek, K. M.; Nykaza, J. R.; Elabd, Y. A., Alkaline Chemical Stability and Ion Transport in Polymerized Ionic Liquids with Various Backbones and Cations. *Macromolecules* **2016**, *49* (9), 3382-3394.
99. Zhu, L.; Yu, X.; Peng, X.; Zimudzi, T. J.; Saikia, N.; Kwasny, M. T.; Song, S.; Kushner, D. I.; Fu, Z.; Tew, G. N.; Mustain, W. E.; Yandrasits, M. A.; Hickner, M. A., Poly(olefin)-Based Anion Exchange Membranes Prepared Using Ziegler–Natta Polymerization. *Macromolecules* **2019**, *52* (11), 4030-4041.
100. Zhu, M.; Su, Y.; Wu, Y.; Zhang, M.; Wang, Y.; Chen, Q.; Li, N., Synthesis and Properties of Quaternized Polyolefins with Bulky Poly(4-phenyl-1-butene) Moieties as Anion Exchange Membranes. *J. Membr. Sci.* **2017**, *541*, 244-252.
101. Hu, E. N.; Lin, C. X.; Liu, F. H.; Yang, Q.; Li, L.; Zhang, Q. G.; Zhu, A. M.; Liu, Q. L., Cross-Linked Poly(vinylbenzyl chloride) Anion Exchange Membranes with Long Flexible Multihead for Fuel Cells. *ACS Appl. Energy Mater.* **2018**, *1* (7), 3479-3487.
102. Zeng, Q. H.; Liu, Q. L.; Broadwell, I.; Zhu, A. M.; Xiong, Y.; Tu, X. P., Anion Exchange Membranes Based on Quaternized Polystyrene-block-poly(ethylene-ran-butylene)-block-Polystyrene for Direct Methanol Alkaline Fuel Cells. *J. Membr. Sci.* **2010**, *349* (1), 237-243.
103. Elabd, Y. A., Ion Transport in Hydroxide Conducting Block Copolymers. *Mol. Syst. Des. Eng.* **2019**, *4* (3), 519-530.
104. Elabd, Y. A.; Hickner, M. A., Block Copolymers for Fuel Cells. *Macromolecules* **2011**, *44* (1), 1-11.
105. Li, Y.; Liu, Y.; Savage, A. M.; Beyer, F. L.; Seifert, S.; Herring, A. M.; Knauss, D. M., Polyethylene-Based Block Copolymers for Anion Exchange Membranes. *Macromolecules* **2015**, *48* (18), 6523-6533.
106. Mohanty, A. D.; Ryu, C. Y.; Kim, Y. S.; Bae, C., Stable Elastomeric Anion Exchange Membranes Based on Quaternary Ammonium-Tethered Polystyrene-b-poly(ethylene-co-butylene)-b-polystyrene Triblock Copolymers. *Macromolecules* **2015**, *48* (19), 7085-7095.
107. Wang, L.; Hickner, M. A., Highly Conductive Side Chain Block Copolymer Anion Exchange Membranes. *Soft Matter* **2016**, *12* (24), 5359-5371.
108. Nykaza, J. R.; Benjamin, R.; Meek, K. M.; Elabd, Y. A., Polymerized Ionic Liquid Diblock Copolymer as an Ionomer and Anion Exchange Membrane for Alkaline Fuel Cells. *Chem. Eng. Sci.* **2016**, *154*, 119-127.

109. Kuray, P.; Noda, T.; Matsumoto, A.; Jacob, C.; Inoue, T.; Hickner, M. A.; Runt, J., Ion Transport in Pendant and Backbone Polymerized Ionic Liquids. *Macromolecules* **2019**, *52* (17), 6438-6448.
110. Zhu, L.; Peng, X.; Shang, S.-L.; Kwasny, M. T.; Zimudzi, T. J.; Yu, X.; Saikia, N.; Pan, J.; Liu, Z.-K.; Tew, G. N.; Mustain, W. E.; Yandrasits, M.; Hickner, M. A., High Performance Anion Exchange Membrane Fuel Cells Enabled by Fluoropoly(olefin) Membranes. *Adv. Funct. Mater.* **2019**, *29* (26), 1902059.
111. Rodgers, M.; Yang, Y.; Holdcroft, S., A Study of Linear Versus Angled Rigid Rod Polymers for Proton Conducting Membranes Using Sulfonated Polyimides. *Eur. Polym. J.* **2006**, *42* (5), 1075-1085.
112. Lee, M.; Park, J. K.; Lee, H.-S.; Lane, O.; Moore, R. B.; McGrath, J. E.; Baird, D. G., Effects of Block Length and Solution-Casting Conditions on the Final Morphology and Properties of Disulfonated Poly(arylene ether sulfone) Multiblock Copolymer Films for Proton Exchange Membranes. *Polymer* **2009**, *50* (25), 6129-6138.
113. Dang, H.-S.; Jannasch, P., Exploring Different Cationic Alkyl Side Chain Designs for Enhanced Alkaline Stability and Hydroxide Ion Conductivity of Anion-Exchange Membranes. *Macromolecules* **2015**, *48* (16), 5742-5751.
114. Nguyen, H.-D.; Assumma, L.; Judeinstein, P.; Mercier, R.; Porcar, L.; Jestin, J.; Iojoiu, C.; Lyonnard, S., Controlling Microstructure–Transport Interplay in Highly Phase-Separated Perfluorosulfonated Aromatic Multiblock Ionomers via Molecular Architecture Design. *ACS Appl. Mater. Interfaces* **2017**, *9* (2), 1671-1683.
115. Chen, Y.; Rowlett, J. R.; Lee, C. H.; Lane, O. R.; VanHouten, D. J.; Zhang, M.; Moore, R. B.; McGrath, J. E., Synthesis and Characterization of Multiblock Partially Fluorinated Hydrophobic Poly(arylene ether sulfone)-Hydrophilic Disulfonated Poly(arylene ether sulfone) Copolymers for Proton Exchange Membranes. *J. Polym. Sci., Part A: Polym. Chem.* **2013**, *51* (10), 2301-2310.
116. Hibbs, M. R., Alkaline Stability of Poly(phenylene)-Based Anion Exchange Membranes with Various Cations. *J. Polym. Sci., Part B: Polym. Phys.* **2013**, *51* (24), 1736-1742.
117. Majsztrik, P. W.; Satterfield, M. B.; Bocarsly, A. B.; Benziger, J. B., Water Sorption, Desorption and Transport in Nafion Membranes. *J. Membr. Sci.* **2007**, *301* (1), 93-106.
118. Williams, M. V.; Kunz, H. R.; Fenton, J. M., Operation of Nafion®-Based PEM Fuel Cells with no External Humidification: Influence of Operating Conditions and Gas Diffusion Layers. *J. Power Sources* **2004**, *135* (1), 122-134.

119. Mochizuki, T.; Kakinuma, K.; Uchida, M.; Deki, S.; Watanabe, M.; Miyatake, K., Temperature- and Humidity-Controlled SAXS Analysis of Proton-Conductive Ionomer Membranes for Fuel Cells. *ChemSusChem* **2014**, *7* (3), 729-733.
120. Mauritz, K. A.; Moore, R. B., State of Understanding of Nafion. *Chem. Rev.* **2004**, *104* (10), 4535-4586.
121. Agmon, N., The Grotthuss Mechanism. *Chem. Phys. Lett.* **1995**, *244* (5), 456-462.
122. Kreuer, K.-D.; Rabenau, A.; Weppner, W., Vehicle Mechanism, A New Model for the Interpretation of the Conductivity of Fast Proton Conductors. *Angew. Chem., Int. Ed. Engl.* **1982**, *21* (3), 208-209.
123. Berrod, Q.; Lyonard, S.; Guillermo, A.; Ollivier, J.; Frick, B.; Manseri, A.; Améduri, B.; Gébel, G., Nanostructure and Transport Properties of Proton Conducting Self-Assembled Perfluorinated Surfactants: A Bottom-Up Approach toward PFSA Fuel Cell Membranes. *Macromolecules* **2015**, *48* (17), 6166-6176.
124. Siu, A.; Schmeisser, J.; Holdcroft, S., Effect of Water on the Low Temperature Conductivity of Polymer Electrolytes. *J. Phys. Chem. B* **2006**, *110* (12), 6072-6080.
125. Kusoglu, A.; Weber, A. Z., New Insights into Perfluorinated Sulfonic-Acid Ionomers. *Chem. Rev.* **2017**, *117* (3), 987-1104.
126. Mecheri, B.; Felice, V.; Zhang, Z.; D'Epifanio, A.; Licoccia, S.; Tavares, A. C., DSC and DVS Investigation of Water Mobility in Nafion/Zeolite Composite Membranes for Fuel Cell Applications. *J. Phys. Chem. C* **2012**, *116* (39), 20820-20829.
127. Peckham, T. J.; Holdcroft, S., Structure-Morphology-Property Relationships of Non-Perfluorinated Proton-Conducting Membranes. *Adv. Mater.* **2010**, *22* (42), 4667-4690.
128. *World of Change: Global Temperatures*. <https://earthobservatory.nasa.gov/world-of-change/global-temperatures> (accessed 2022-07-22).
129. *Global Climate Change: Vital Signs of the Planet*. <https://climate.nasa.gov/vital-signs/carbon-dioxide/> (accessed 2022-07-22).
130. *Electricity Explained: Electricity Generation, Capacity, and Sales in the United States*. <https://www.eia.gov/energyexplained/electricity/electricity-in-the-us-generation-capacity-and-sales.php> (accessed 2022-07-22).

131. *Hydrogen Production: Electrolysis*. <https://www.energy.gov/eere/fuelcells/hydrogen-production-electrolysis> (accessed 2022-07-22).
132. Sarkar, S.; SenGupta, A. K.; Prakash, P., The Donnan Membrane Principle: Opportunities for Sustainable Engineered Processes and Materials. *Environ. Sci. Technol.* **2010**, *44* (4), 1161-1166.
133. Zeng, L.; Zhao, T. S.; Wei, L.; Jiang, H. R.; Wu, M. C., Anion Exchange Membranes for Aqueous Acid-Based Redox Flow Batteries: Current Status and Challenges. *Appl. Energy* **2019**, *233-234*, 622-643.
134. Hsieh, H. Q., Roderic P., *Anionic Polymerization: Principles and Practical Applications*. 1 ed.; Marcel Dekker, Inc., 1996.
135. Webster, O. W., Living Polymerization Methods. *Science* **1991**, *251* (4996), 887.
136. Szwarc, M., 'Living' Polymers. *Nature* **1956**, *178* (4543), 1168-1169.
137. Glasse, M. D., Spontaneous Termination in Living Polymers. *Prog. Polym. Sci.* **1983**, *9* (2), 133-195.
138. Bywater, S.; Firat, Y.; Black, P. E., Microstructures of Polybutadienes Prepared by Anionic Polymerization in Polar Solvents. Ion-Pair and Solvent Effects. *J. Polym. Sci. Polym. Chem. Ed.* **1984**, *22* (3), 669-672.
139. Szwarc, M.; Levy, M.; Milkovich, R., Polymerization Initiated by Electron Transfer to Monomer. A New Method of Formation of Block Polymers¹. *J. Am. Chem. Soc.* **1956**, *78* (11), 2656-2657.
140. Ogle, C. A.; Strickler, F. H.; Gordon III, B., Reaction of Polystyryllithium with Tetrahydrofuran. *Macromolecules* **1993**, *26* (21), 5803-5805.
141. Stanetty, P.; Mihovilovic, M. D., Half-Lives of Organolithium Reagents in Common Ethereal Solvents. *J. Org. Chem.* **1997**, *62* (5), 1514-1515.
142. Bywater, S.; Worsfold, D., The Effect of Dielectric Constant on the Rate of Anionic Polymerization. *J. Phys. Chem.* **1966**, *70* (1), 162-166.
143. Hadjichristidis, N.; Iatrou, H.; Pispas, S.; Pitsikalis, M., Anionic Polymerization: High Vacuum Techniques. *J. Polym. Sci., Part A: Polym. Chem.* **2000**, *38* (18), 3211-3234.

144. Heime, Y.; Yoshio, O., Anionic Copolymerization of Butadiene and 1,1-Diphenylethylene. *Bull. Chem. Soc. Jpn.* **1970**, *43* (1), 148-151.
145. Choi, S.-H.; Bates, F. S.; Lodge, T. P., Structure of Poly(styrene-*b*-ethylene-*alt*-propylene) Diblock Copolymer Micelles in Squalane. *J. Phys. Chem. B* **2009**, *113* (42), 13840-13848.
146. Cai, Y.; Lu, J.; Jing, G.; Yang, W.; Han, B., High-Glass-Transition-Temperature Hydrocarbon Polymers Produced through Cationic Cyclization of Diene Polymers with Various Microstructures. *Macromolecules* **2017**, *50* (19), 7498-7508.
147. Jeon, J. Y. U., Z.; Kangovi, G.; Lee, S.; Bae, C., Functionalization of Syndiotactic Polystyrene via Superacid-Catalyzed Friedel-Crafts Alkylation. *Top. Catal.* **2018**, *61*, 610-615.
148. Trant, C.; Hwang, S.; Bae, C.; Lee, S., Synthesis and Characterization of Anion-Exchange Membranes Using Semicrystalline Triblock Copolymers in Ordered and Disordered States. *Macromolecules* **2020**, *53* (19), 8548-8561.
149. Günther, H., *NMR Spectroscopy: Basic Principles, Concepts and Applications in Chemistry*. John Wiley & Sons, 2013.
150. Yau, W. W.; Kirkland, J. J.; Bly, D. D.; Striegel, A., *Modern Size-Exclusion Liquid Chromatography: Practice of Gel Permeation and Gel Filtration Chromatography*. John Wiley & Sons, 2009.
151. Hickner, M. A.; Ghassemi, H.; Kim, Y. S.; Einsla, B. R.; McGrath, J. E., Alternative Polymer Systems for Proton Exchange Membranes (PEMs). *Chem. Rev.* **2004**, *104* (10), 4587-4612.
152. Skoog, D.; West, D.; Holler, F., Gas-Liquid Chromatography. In *Fundamentals of Analytical Chemistry*, 7th ed.; Saunders College Publishing, 1996, pp 686-700.
153. Cooper, K. R., Progress Toward Accurate Through-Plane Ion Transport Resistance Measurement of Thin Solid Electrolytes. *J. Electrochem. Soc.* **2010**, *157* (11), B1731.
154. Jeon, J. Y.; Tian, D.; Pagels, M. K.; Bae, C., Efficient Preparation of Styrene Block Copolymer Anion Exchange Membranes via One-Step Friedel-Crafts Bromoalkylation with Alkenes. *Org. Process Res. Dev.* **2019**, *23* (8), 1580-1586.

155. Fauq, A. H.; Kache, R.; Khan, M. A.; Vega, I. E., Synthesis of Acid-Cleavable Light Isotope-Coded Affinity Tags (ICAT-L) for Potential Use in Proteomic Expression Profiling Analysis. *Bioconjugate Chem.* **2006**, *17* (1), 248-254.
156. Adams, L. A.; Poynton, S. D.; Tamain, C.; Slade, R. C. T.; Varcoe, J. R., A Carbon Dioxide Tolerant Aqueous-Electrolyte-Free Anion-Exchange Membrane Alkaline Fuel Cell. *ChemSusChem* **2008**, *1* (1-2), 79-81.
157. Ziv, N.; Dekel, D. R., A Practical Method for Measuring the True Hydroxide Conductivity of Anion Exchange Membranes. *Electrochem. Commun.* **2018**, *88*, 109-113.
158. Trant, C. The Impact of Microstructured Morphology on Macroscale Properties of Anion Exchange Membranes. Ph.D. Dissertation, Rensselaer Polytechnic Institute, Troy, NY, 2021.
159. Jeon, J. Y.; Park, S.; Han, J.; Maurya, S.; Mohanty, A. D.; Tian, D.; Saikia, N.; Hickner, M. A.; Ryu, C. Y.; Tuckerman, M. E.; Paddison, S. J.; Kim, Y. S.; Bae, C., Synthesis of Aromatic Anion Exchange Membranes by Friedel–Crafts Bromoalkylation and Cross-Linking of Polystyrene Block Copolymers. *Macromolecules* **2019**, *52* (5), 2139-2147.
160. Lin, X.; Liu, Y.; Poynton, S. D.; Ong, A. L.; Varcoe, J. R.; Wu, L.; Li, Y.; Liang, X.; Li, Q.; Xu, T., Cross-Linked Anion Exchange Membranes for Alkaline Fuel Cells Synthesized Using a Solvent Free Strategy. *J. Power Sources* **2013**, *233*, 259-268.
161. Hao, J.; Gao, X.; Jiang, Y.; Zhang, H.; Luo, J.; Shao, Z.; Yi, B., Crosslinked High-Performance Anion Exchange Membranes Based on Poly(styrene-*b*-(ethylene-co-butylene)-*b*-styrene). *J. Membr. Sci.* **2018**, *551*, 66-75.
162. Dai, P.; Mo, Z.-H.; Xu, R.-W.; Zhang, S.; Wu, Y.-X., Cross-Linked Quaternized Poly(styrene-*b*-(ethylene-co-butylene)-*b*-styrene) for Anion Exchange Membrane: Synthesis, Characterization and Properties. *ACS Appl. Mater. Interfaces* **2016**, *8* (31), 20329-20341.
163. Ertem, S. P.; Tsai, T.-H.; Donahue, M. M.; Zhang, W.; Liu, Y.; Seifert, S.; Herring, A. M.; Coughlin, E. B., Photo-Cross-Linked Anion Exchange Membranes with Improved Water Management and Conductivity. *Macromolecules* **2016**, *49* (1), 153-161.
164. Zhu, L.; Zimudzi, T. J.; Li, N.; Pan, J.; Lin, B.; Hickner, M. A., Crosslinking of Comb-Shaped Polymer Anion Exchange Membranes via Thiol–Ene Click Chemistry. *Polym. Chem.* **2016**, *7* (14), 2464-2475.
165. Wang, L.; Hickner, M. A., Low-Temperature Crosslinking of Anion Exchange Membranes. *Polym. Chem.* **2014**, *5* (8), 2928-2935.

166. Meijer, H. E. H.; Govaert, L. E., Mechanical Performance of Polymer Systems: The Relation between Structure and Properties. *Prog. Polym. Sci.* **2005**, *30* (8), 915-938.
167. Wu, S., Control of Intrinsic Brittleness and Toughness of Polymers and Blends by Chemical Structure: A Review. *Polym. Int.* **1992**, *29* (3), 229-247.
168. Shrivastava, A., *Introduction to Plastics Engineering*. William Andrew, 2018.
169. Ruan, D.; Simmons, D. S., Glass Formation near Covalently Grafted Interfaces: Ionomers as a Model Case. *Macromolecules* **2015**, *48* (7), 2313-2323.
170. Ruan, D.; Simmons, D. S., Roles of Chain Stiffness and Segmental Rattling in Ionomer Glass Formation. *J. Polym. Sci., Part B: Polym. Phys.* **2015**, *53* (20), 1458-1469.
171. Wang, X.; Jian, W.; Lu, H.; Lau, D.; Fu, Y.-Q., Modeling Strategy for Enhanced Recovery Strength and a Tailorable Shape Transition Behavior in Shape Memory Copolymers. *Macromolecules* **2019**, *52* (16), 6045-6054.
172. Struik, L. C. E., Physical Aging in Plastics and Other Glassy Materials. *Polym. Eng. Sci.* **1977**, *17* (3), 165-173.
173. Levita, G.; Struik, L. C. E., Physical Ageing in Rigid Chain Polymers. *Polymer* **1983**, *24* (8), 1071-1074.
174. Frieberg, B. R.; Glynos, E.; Sakellariou, G.; Tyagi, M.; Green, P. F., Effect of Molecular Stiffness on the Physical Aging of Polymers. *Macromolecules* **2020**, *53* (18), 7684-7690.
175. Grigoriadi, K.; Putzeys, T.; Wübbenhorst, M.; van Breemen, L. C. A.; Anderson, P. D.; Hütter, M., Effect of Low-Temperature Physical Aging on The Dynamic Transitions of Atactic Polystyrene in the Glassy State. *J. Polym. Sci., Part B: Polym. Phys.* **2019**, *57* (20), 1394-1401.
176. Wang, G.; Weng, Y.; Chu, D.; Xie, D.; Chen, R., Preparation of Alkaline Anion Exchange Membranes Based on Functional Poly(ether-imide) Polymers for Potential Fuel Cell Applications. *J. Membr. Sci.* **2009**, *326* (1), 4-8.
177. Mohanty, A. D.; Lee, Y.-B.; Zhu, L.; Hickner, M. A.; Bae, C., Anion Exchange Fuel Cell Membranes Prepared from C-H Borylation and Suzuki Coupling Reactions. *Macromolecules* **2014**, *47* (6), 1973-1980.

178. Yan, J.; Zhu, L.; Chaloux, B. L.; Hickner, M. A., Anion Exchange Membranes by Bromination of Tetramethylbiphenol-Based Poly(sulfone)s. *Polym. Chem.* **2017**, *8* (16), 2442-2449.
179. Zschocke, P.; Quellmalz, D., Novel Ion Exchange Membranes Based on an Aromatic Polyethersulfone. *J. Membr. Sci.* **1985**, *22* (2), 325-332.
180. Yan, J.; Hickner, M. A., Anion Exchange Membranes by Bromination of Benzylmethyl-Containing Poly(sulfone)s. *Macromolecules* **2010**, *43* (5), 2349-2356.
181. Wang, J.; Li, S.; Zhang, S., Novel Hydroxide-Conducting Polyelectrolyte Composed of an Poly(arylene ether sulfone) Containing Pendant Quaternary Guanidinium Groups for Alkaline Fuel Cell Applications. *Macromolecules* **2010**, *43* (8), 3890-3896.
182. Hibbs, M. R.; Hickner, M. A.; Alam, T. M.; McIntyre, S. K.; Fujimoto, C. H.; Cornelius, C. J., Transport Properties of Hydroxide and Proton Conducting Membranes. *Chem. Mater.* **2008**, *20* (7), 2566-2573.
183. Tongwen, X.; Weihua, Y., Fundamental Studies of a New Series Of Anion Exchange Membranes: Membrane Preparation and Characterization. *J. Membr. Sci.* **2001**, *190* (2), 159-166.
184. Li, N.; Leng, Y.; Hickner, M. A.; Wang, C.-Y., Highly Stable, Anion Conductive, Comb-Shaped Copolymers for Alkaline Fuel Cells. *J. Am. Chem. Soc.* **2013**, *135* (27), 10124-10133.
185. Fujimoto, C.; Kim, D.-S.; Hibbs, M.; Wroblewski, D.; Kim, Y. S., Backbone Stability of Quaternized Polyaromatics for Alkaline Membrane Fuel Cells. *J. Membr. Sci.* **2012**, *423-424*, 438-449.
186. Arges Christopher, G.; Ramani, V., Two-Dimensional NMR Spectroscopy Reveals Cation-Triggered Backbone Degradation in Polysulfone-Based Anion Exchange Membranes. *Proc. Natl. Acad. Sci. U. S. A.* **2013**, *110* (7), 2490-2495.
187. Choe, Y.-K.; Fujimoto, C.; Lee, K.-S.; Dalton, L. T.; Ayers, K.; Henson, N. J.; Kim, Y. S., Alkaline Stability of Benzyl Trimethyl Ammonium Functionalized Polyaromatics: A Computational and Experimental Study. *Chem. Mater.* **2014**, *26* (19), 5675-5682.
188. Mohanty, A. D.; Tignor, S. E.; Krause, J. A.; Choe, Y.-K.; Bae, C., Systematic Alkaline Stability Study of Polymer Backbones for Anion Exchange Membrane Applications. *Macromolecules* **2016**, *49* (9), 3361-3372.

189. Adhikari, S.; Pagels, M. K.; Jeon, J. Y.; Bae, C., Ionomers for Electrochemical Energy Conversion & Storage Technologies. *Polymer* **2020**, *211*, 123080.
190. Noh, S.; Jeon, J. Y.; Adhikari, S.; Kim, Y. S.; Bae, C., Molecular Engineering of Hydroxide Conducting Polymers for Anion Exchange Membranes in Electrochemical Energy Conversion Technology. *Acc. Chem. Res.* **2019**, *52* (9), 2745-2755.
191. Lee, W.-H.; Kim, Y. S.; Bae, C., Robust Hydroxide Ion Conducting Poly(biphenyl alkylene)s for Alkaline Fuel Cell Membranes. *ACS Macro Lett.* **2015**, *4* (8), 814-818.
192. Wang, J.; Zhao, Y.; Setzler, B. P.; Rojas-Carbonell, S.; Ben Yehuda, C.; Amel, A.; Page, M.; Wang, L.; Hu, K.; Shi, L.; Gottesfeld, S.; Xu, B.; Yan, Y., Poly(aryl piperidinium) Membranes and Ionomers for Hydroxide Exchange Membrane Fuel Cells. *Nat. Energy* **2019**, *4* (5), 392-398.
193. Olsson, J. S.; Pham, T. H.; Jannasch, P., Tuning Poly(arylene piperidinium) Anion-Exchange Membranes by Copolymerization, Partial Quaternization and Crosslinking. *J. Membr. Sci.* **2019**, *578*, 183-195.
194. Fan, J.; Willdorf-Cohen, S.; Schibli, E. M.; Paula, Z.; Li, W.; Skalski, T. J. G.; Sergeenko, A. T.; Hohenadel, A.; Frisken, B. J.; Magliocca, E.; Mustain, W. E.; Diesendruck, C. E.; Dekel, D. R.; Holdcroft, S., Poly(bis-arylimidazoliums) Possessing High Hydroxide Ion Exchange Capacity and High Alkaline Stability. *Nat. Commun.* **2019**, *10* (1), 2306.
195. Akiyama, R.; Yokota, N.; Miyatake, K., Chemically Stable, Highly Anion Conductive Polymers Composed of Quinquephenylene and Pendant Ammonium Groups. *Macromolecules* **2019**, *52* (5), 2131-2138.
196. Saito, S.; SAITO, S.-i.; Ohwada, T.; Shudo, K., The Hammett Acidity Function H_0 of Trifluoromethanesulfonic Acid-Trifluoroacetic Acid and Related Acid Systems. A Versatile Nonaqueous Acid System. *Chem. Pharm. Bull.* **1991**, *39* (10), 2718-2720.